A Computational Strategy for Organic Photochemistry

Michael A. Robb, Marco Garavelli, Massimo Olivucci, and Fernando Bernardi

A Computational Strategy for Organic Photochemistry

Michael A. Robb*, Marco Garavelli*, Massimo Olivucci‡ and Fernando Bernardi †

Department of Chemistry, King's College London , Strand, London WC2R 2LS, United Kingdom, ‡ Istituto di Chimica Organica, Università degli Studi di Siena, Via Aldo Moro, I-53100 Siena, Italy, and †Dipartimento di Chimica "G. Ciamician" dell'Università di Bologna, Via Selmi 2, 40126 Bologna, Italy

INTRODUCTION

Modeling Photochemical Reactions

The aim of this tutorial is to provide an introduction to the practical computational investigation of photochemical reaction mechanisms. During the last decade or so, the speed of the computers has grown considerably and the computational investigation of realistic models of organic compounds is becoming a standard practice. Current applications range from the investigation of the mechanism of synthetically useful reactions to the study of short lived organic intermediates detected in the interstellar medium. For thermal reactions, standard state-of-the-art ab initio quantum chemical methods are already capable of providing a complete description of what happens at the molecular level during bond-breaking and bond-forming processes. In particular, it is

possible to compute the transition structure which connects a reactant to a product and the associated energy barrier with almost chemical accuracy (ca. 1 kcal mol^{-1} error). Furthermore the reaction path, i.e., the progression of the molecular structure towards the transition state and the product, can be determined, in a completely unbiased way, by computing the minimum energy path (MEP)[1] connecting the reactant to the product on the 3N-6 dimensional potential energy surface of the system.

A detailed understanding of the reaction pathway in the excited state manifold will increase our ability to design new and to control known photochemical reactions. As an example, the conversion of light into chemical energy in plants and animals involves extended conjugated molecules - carotenoids and retinals - bound in protein complexes. The use of such extended systems in optical data storage and processing technology is now being investigated. Photobiological systems exploit the ability of these chromophores to undergo cis-trans isomerization and to transduce radiative energy into thermal energy on picosecond or shorter timescales. Recent advances in time-resolved spectroscopy (e.g., the use of ultrafast laser pulses) has provided a powerful tool to monitor reaction dynamics on the femtosecond timescale[2] and made direct observation of these processes possible, increasing our understanding of the excited state structures and dynamics for model systems. Ultrafast (femtosecond) radiationless decay has been observed, for example, for simple dienes[3], cyclohexadienes[4,5], hexatrienes[6], and in both free[7] and opsin-bound[8] retinal protonated Schiff bases. However a complete understanding of molecular dynamics on multiple electronic states is required to interpret these laser experiments with confidence and to understand the principles involved in the design of optical devices.

Until recently, reaction path computations were mainly limited to the investigation of thermal reactions and thus to reactions occurring on a single potential energy surface. Photochemical processes, where the reactant resides on an excited state potential energy surface and the products accumulate on the ground state, could not be easily investigated. In photochemistry, the reaction path must have at least two branches: one located on the

excited state and the other located on the ground state energy surface. The main difficulty associated with such computations lies in the correct definition and practical computation of the "funnel" region where the excited state reactant or intermediate is delivered to the ground state. Thus, while the progression on excited state energy surface (i.e., the excited state "branch" of the reaction path) may be investigated with the same methods used for thermal reactions, there was no general way of defining the "locus" where the excited state branch of the reaction path was connected to the ground state branch. During the last decade, computational tools have been developed and strategies discovered to explore electronically excited state reaction paths[9-12]. The goal of such computational approaches, in the study of photochemical mechanisms, is the complete description of what happens at the molecular level *from energy absorption to product formation*. This review will focus on some of these new theoretical tools, with case studies to show how they can be applied.

Modern textbooks on photochemistry with a good theoretical treatment include Refs. 9-11. We shall begin with some simple ideas that are the main focus of the theoretical study of excited state processes. A very schematic view of the course of a photochemical reaction is given in Figure 1. Following light absorption, the system is promoted to an excited state ($\mathbf{R} \rightarrow \mathbf{R}^*$). Photoproduct formation can then occur by adiabatic reaction ($\mathbf{R}^* \rightarrow \mathbf{P}'^*$) on the excited state (a photochemical process) followed by emission ($\mathbf{P}'^* \rightarrow \mathbf{P}'$) or by internal conversion to the ground state (a photophysical process). However, the most common mechanism involves a *non-adiabatic radiationless decay* process which either regenerates the reactant **R** (a photophysical process) or generates new products **P** or **P'** (a photochemical process). Whether a photochemical reaction occurs, thus depends upon the relative rates of photochemical processes that generate new molecular structures versus competing photophysical processes that convert between electronic states at the same nuclear geometry. The competition between photochemical and photophysical processes may occur via two different mechanisms: branching at a same decay channel (see left side of

Figure 1) or competition between two different decay channels (see right side of Figure 1).

Understanding the mechanism of this non-adiabatic radiationless decay is central to explaining excited state processes. There are two possible mechanisms (see non-adiabatic reactions in Figure 1). When real surface crossings exist (conical intersection, see left side of Figure 1) and are accessible, the Landau-Zener model[11,13] (which we will discuss in more detail subsequently) provides a semi-classical model for fast radiationless decay. By 'accessible', we mean that there is a reaction co-ordinate with a sufficiently low energy barrier that leads from the initial excited state geometry to the crossing region. In this case, internal conversion can take place within a single vibrational oscillation through, or near, the surface crossing ($\mathbf{R}^* \rightarrow \mathbf{P}$ or $\mathbf{R}^* \rightarrow \mathbf{R}$) and radiationless decay occurs on a scale of ps (picosecond) to fs (femtosecond). If surface crossings are not present, or are present but not easily accessible, the process of radiationless decay is better described as the transformation of electronic energy into a manifold of vibronic states associated with the lower electronic state (see right side of Figure 1). This process is governed by the density of vibrational states and Franck-Condon factors (overlap of ground and excited state vibrational wavefunctions) according to the Fermi Golden rule formalism (Ref. 11, pp. 257). The Fermi Golden rule type decay occurs at a local minimum on the excited state (which might be either an avoided crossing, as shown in Figure 1, or the minima $\mathbf{R}^*$ or $\mathbf{P'}^*$). This process is much slower than decay at a surface crossing and typical internal conversion rates for aromatic hydrocarbons are found to be 10^5-10^6 s^{-1}.

Figure 1

Recently it has been shown that certain photochemical radiationless reactions are extremely fast. For example, the *cis* to *trans* isomerization of the retinal chromophore in the vision process occurs in ca. 200 fs. This demonstrates that these reactions are likely to

occur via real surface crossings since they can be faster than processes such as fluorescence and internal conversion via avoided crossings or at local minima which take place on a μs (microsecond) to ns (nanosecond) timescale. *Recent complementary theoretical computations have shown that low-lying intersections (real crossings) between the photochemically relevant excited state and the ground state occur with a previously unsuspected frequency*[14,15]. Such crossings, i.e., *conical intersections* in the case of two singlet (or two triplet) states, or *singlet-triplet intersections*, provide a very efficient "funnel" for radiationless deactivation[9,11,13,14-17] (internal conversion and intersystem crossing) and, in turn, prompt photoproduct formation.

To summarise, the decay probability (i.e., the internal conversion rate) at an avoided crossing or a local excited state minimum is controlled by the interaction between the vibrational energy levels of the ground and excited state potential energy surfaces by using the Fermi Golden Rule, and thus radiationless decay and fluorescence can occur on competitive timescales. On the other hand, radiationless decay at a conical intersection implies that the internal conversion process can approach 100% efficiency[13] so that any observed retardation in the internal conversion or reaction rate (i.e., the competition with fluorescence) must reflect the presence of some excited state energy barrier which separates $\mathbf{R}^*$ from the intersection structure. Finally, in the case where the radiationless decay leads to a chemical reaction, the molecular structure at the intersection must be related to the structure of the photoproducts.

The traditional view of deactivation of an electronically excited intermediate by internal conversion, mainly due to the work of Van der Lugt and Oosteroff[18] on the ring-opening of cyclobutene, was formulated in terms of avoided crossing funnels. Thus internal conversion rates were predicted to be slow as in aromatic hydrocarbons because of the finite gap at the avoided crossing (energy gap law). Because it was impossible to compute real reaction paths in the 1960s, the real nature of the funnel was missed. In Figure 2 we show the relation between an avoided crossing (a section of a cone along **R**-

P) and the double cone topology of a real conical intersection. In two dimensions, the Van der Lugt and Oosteroff model is refined by replacing the "avoided crossing" with an "unavoided crossing", i.e., a conical intersection as shown in Figure 2[15]. The Van der Lugt and Oosteroff model reaction avoided crossing path **R** ¾→ **P** is replaced by a path involving a real surface crossing **R** ¾→ **CI** ¾→ **P**. In the subsequent discussion we will use the acronym **CI** (in bold) to refer to conical intersections, while the acronym CI (plain text) is used for Configuration Intersection.

Figure 2

Teller[19] was the first to point out that in a polyatomic molecule the non-crossing rule, which is rigorously valid for diatomics, fails. Rather, two electronic states, even if they have the same symmetry, are allowed to cross at a conical intersection. Accordingly, radiationless decay from the upper to the lower intersecting state can occur within a single vibrational period when the system travels in the vicinity of such intersection points. In the field of photochemistry, Zimmerman[20] and Michl[21] were the first to suggest, independently, that certain photoproducts originate from internal conversion at a conical intersection. Zimmerman and Michl used the term "funnel" for this feature.

We can now suggest a theoretical basis for the computational modeling of photochemical reactions. We shall call this method the *pathway approach*, following the suggestion of Fuss et al.[22] According to this approach, the excited state motion is determined by the structure of the relevant excited and ground state potential energy surfaces. In simple terms, information on the excited state lifetime and on the type of photoproducts generated is obtained by following the detailed relaxation and reaction paths of the molecule along the potential energy surfaces *from the Franck-Condon (**FC**) point (i.e., vertically excited geometery) , or excited state intermediate, to the ground state*. This approach is part of a more general way of considering photochemistry which is already employed in one recent textbook[11]: it follows the pathway on the

potential energy surfaces and pays attention to local details such as slopes, barriers, saddle points, collecting funnels, etc. One key element of the pathway approach is the existence of low lying real crossings or excited state products preceded by a transition state which control the rate of transformation or decay of the excited state reactant. This feature has been suggested by experimental observations. Experiments on isolated molecules in cold-matrices, expanding-jets and in solution have revealed the presence of thermally activated fast radiationless decay channels in polyenes, such as hexatrienes and octatetraenes[23,24], and in aromatic compounds, such as benzene, azulene and azoalkanes[25,26]. In particular, recent spectroscopic low-temperature investigations of isolated polyene molecules have provided evidence that photoinduced double-bond *trans* → *cis* isomerization may occur via a *non-adiabatic* reaction path where the excited state intermediate decays to the ground state at a highly twisted molecular geometry. The original suggestions of Teller[19], Zimmerman[20] and Michl[21] have now been fully verified by recent computational results[25-40], which provide a particularly clear illustration of the application of the *pathway approach* to the study of organic photochemistry.

In Figure 3 we illustrate the results of two different experiments on *all-trans* octa-1,3,5,7-tetraene (*all-trans* OT).

Figure 3 (From Ref. 14.)

The first experiment (Figure 3a) is due to Kohler and co-workers[23] who recorded the fluorescence lifetime of S_1 ($2A_g$) *all-trans* OT as a function of the temperature. In this experiment the *all-trans* OT molecules are isolated in a molecular cavity of frozen n-hexane and do not interact with each other. From Figure 3a, one can see that, at temperatures above 200 K, the fluorescence lifetime drops dramatically indicating fast decay of the excited state molecules to the ground state. This event was assigned to the opening of a thermally activated efficient radiationless decay channel with a barrier height of ~1500 cm^{-1} (4.3 kcal mol^{-1})[11,14]. The second experiment (Figure 3b) is due to

Christensen, Yoshihara, Petek and co-workers[24], who reported the fluorescence decay rate of S_1 *all-trans* OT molecules measured in free jet expansion as a function of the excitation energy. These authors propose that (under isolated conditions in a cool-jet) *trans* → *cis* motion in *all-trans* OT is responsible for the observed radiationless decay channel on S_1 ($2A_g$) which opens up at ~2100 cm^{-1} (~6 kcal mol^{-1}) excess energy.

These experimental results can be rationalised using the potential energy profiles shown in Figure 4. In both experiments referred to above, the fluorescence lifetime decreases slowly and almost linearly by increasing the S_1 excess vibrational energy until an energy threshold is reached and a dramatic decrease in excited state lifetime is observed. Quantum chemical computations of the S_1 reaction path of *all-trans* OT[28] have revealed that the energy threshold corresponds to a transition state which connects an excited state intermediate to a conical intersection funnel. This result is schematically illustrated in Figure 4a. The computation predicts a 7.5 kcal mol^{-1} barrier in good agreement with the experiment. In the absence of a barrier, the reaction becomes ultrafast (see Figure 4b) and no fluorescence can be observed.

Figure 4

Features such as excited state intermediates and funnels are conveniently optimised [25-40], using gradient optimisation methods, as critical points on the potential energy surface associated with the photochemically relevant excited state (usually the first singlet or triplet excited state). The computation of the excited state potential energy surface per se can be carried out using standard quantum chemical methods. However, in excited state chemistry, it is clear that the knowledge of the molecular structure of the funnel appears to be of vital importance for the rationalisation and prediction of the observed photoproduct distribution. We expect the photoproduct molecular structure to be related to the molecular structure of the decay channel more or less in the same way in which the structure of a thermal product is related to that of the corresponding transition

state. Similarly, the detailed knowledge of the energetic stability of the decay channel relative, for instance, to the excited state equilibrium structure of the reactant is expected to be related to the excited state lifetime. In other words, *excited state energy barriers may control the time taken by the system to reach the decay channel.* Thus, the new feature that occurs in the quantum chemistry of photochemical reactions is the characterisation of the conical intersection and its relation to other features on the ground and excited state potential energy surface.

Aims and Objectives

The remainder of this tutorial is divided into three parts. The first two parts are theoretical while the third illustrates the application of these theoretical concepts via some case studies drawn mainly from our own work. Our objective is to outline a computational approach to photochemistry. We aim for a complete description of what happens along the reaction co-ordinate *from absorption to photoproduct formation*. We shall show how this can be achieved by mapping of the photochemical reaction path computed by following the MEP from the excited state intermediate (or from the Franck-Condon structure) to the ground state photoproduct *through* a conical intersection. This method (*pathway approach* [22]), discussed previously, pays attention to local details and properties like slopes, saddle points, barriers and funnels (such as conical intersections) and has an intimate connection to the approach using the motion of wavepackets or semi-classical trajectories on potential surfaces to describe ultrafast photochemical processes. This description is becoming increasingly important because of recent advances in femtosecond spectroscopy and ultrafast laser techniques[2-8,23,24].

The first theoretical subsection is conceptually oriented. We shall discuss the special "features" occurring when more than one energy surface is involved in the chemical reaction (e.g., avoided and real crossings) as well as the general structure of the

"photochemical reaction path" that connects the excited state reactant and the photoproducts through the funnel.

The second theoretical subsection is more practically oriented. Here we shall illustrate the computational tools and strategies which are being used to compute a photochemical reaction path. This discussion will include the computation of the excited state branch of the reaction path, how to study the branching at a conical intersection and computation of the "competing" ground state relaxation paths and a brief discussion of semi-classical trajectories. We will focus on the special techniques that are required for the study of excited state processes. In principle these can be implemented in a variety of computational algorithms as long as they can produce analytical gradients and hessians and give a balanced description of the energetics. It is not our purpose to discuss the details of particular algorithms that have been implemented. Rather we will focus on the conceptual background that is necessary to use such methods effectively. Thus we will limit ourselves mainly to some general remarks about current quantum chemical methods and algorithms that are suitable for computational organic photochemistry.

Finally, in the last subsection, we illustrate a few general results, via case studies, which have been obtained in the field of mechanistic organic photochemistry and compare them with modern (time resolved)[3-8,14,15,23,24] and traditional[41] experimental data. We shall concentrate on the following points: (a) the funnel structure; (b) the existence of chemically or stereochemically distinct competing paths, i.e., funnels, on the excited state energy surface; and (c) the reaction path branching, i.e., the competing ground state relaxation paths, at a specific funnel. Our objective is to illustrate how the observed photoproduct stereochemistry and distribution in a photochemical organic reaction must depend on radiationless decay via a conical intersection (i.e., a real surface crossing).

CHARACTERIZATION OF CONICAL INTERSECTIONS

The way the energy of a molecular system varies with small changes in its structure is specified by its *potential energy surface* (PES). A potential energy surface is a mathematical relationship linking molecular structure and the resultant energy. The concepts of energy surfaces for molecular motion, equilibrium geometries, transition structures and reaction paths depend on the Born-Oppenheimer approximation to treat the motion of the nuclei separately from the motion of the electrons. Minima on the potential energy surface for the nuclei can then be identified with the classical picture of equilibrium structures of molecules (i.e., reactant, product and intermediates); saddle points can be related to transition states and reaction rates (see Refs. 42 and 43 and Refs. cited therein). Minima, maxima and saddle points can be characterised by their first (i.e., the gradient) and second (i.e., the Hessian) derivatives of the energy[42,43].

If the Born-Oppenheimer approximation is not valid, for example in the vicinity of surface crossings, non-adiabatic coupling effects (that couple nuclear and electronic motion) need to be taken in account to correctly describe the motion of the molecular system. This is done, for instance, when one needs to describe a jump between two different PES. In this case, one uses semi-classical theories and the surface-hopping method which we discuss subsequently. We now discuss in some detail how the region where non-adiabatic effects become important can be characterised topologically.

"Non-Crossing Rule" and Conical Intersections

In photochemistry one must deal with a new type of potential surface feature (surface crossings and conical intersections), and we now introduce this subject. In diatomic molecules the PES of two states (e.g., the ground state and the first excited state) will only intersect if the states have a different (spatial or spin) symmetry.

However, this statement is *not true* in polyatomic systems[19,44,45]. Rather the correct statement is: *two PES of a polyatomic molecule can in principle intersect even if they belong to states of the same symmetry and spin multiplicity*.

The preceding sentence leaves open the question of whether such intersections actually occur in polyatomic systems. We now give a quantitative analysis of this situation[45]. If we suppose we have all but two of the solutions for the electronic part of the Schrödinger equation, and ϕ_1 and ϕ_2 are any two functions which, together with the known solutions, constitute a complete orthonormal set (the two missing solutions correspond to the two states whose energies are E_1 and E_2 respectively, and whose crossings we are interested in), then it must be possible to express each of the two remaining electronic eigenfunctions (which describes the states we want to examine) in the form

$$\Psi = \mathbf{c}_1\phi_1 + \mathbf{c}_2\phi_2 \qquad [1]$$

The resulting secular equation is then

$$\begin{bmatrix} H_{11} - E & H_{12} \\ H_{21} & H_{22} - E \end{bmatrix} \begin{bmatrix} c_1 \\ c_2 \end{bmatrix} = 0 \qquad [2]$$

and we can write down the expressions for the energies E_1 and E_2 of the two states as

$$E_1 = \frac{1}{2}\left[(H_{11} + H_{22}) - \sqrt{(H_{11} - H_{22})^2 + 4H_{12}^2}\right]$$
$$E_2 = \frac{1}{2}\left[(H_{11} + H_{22}) + \sqrt{(H_{11} - H_{22})^2 + 4H_{12}^2}\right] \qquad [3]$$

where the matrix elements are defined as

$$
\begin{aligned}
H_{11} &= \langle \phi_1 | H | \phi_1 \rangle \\
H_{22} &= \langle \phi_2 | H | \phi_2 \rangle \\
H_{12} &= \langle \phi_1 | H | \phi_2 \rangle = H_{21}
\end{aligned}
\qquad [4]
$$

Now, in order to have degenerate solutions (i.e., an unavoided crossing) the discriminant must vanish, and it is necessary to satisfy two independent conditions

$$
\begin{aligned}
H_{11} &= H_{22} \\
H_{12} (= H_{21}) &= 0
\end{aligned}
\qquad [5]
$$

This *requires the existence of at least two independently variable nuclear co-ordinates*. In a diatomic molecule there is only one variable co-ordinate - the interatomic distance - so the non-crossing rule can be stated as:

For states of different (spatial or spin) symmetry, H_{12} *is always zero and the two surfaces cross when* $H_{11} = H_{22}$. This is possible for a suitable value of the single variable co-ordinate. *Otherwise, if the two states have the same symmetry, they will not intersect*.

However in a system of three or more atoms (N is the number of atoms) there are enough degrees of freedom for the rule to break down: the two conditions (Eq. [5]) can be simultaneously satisfied by choosing suitable values for two independent variables, while the other n-2 degrees of freedom (n = 3N - 6) are free to be varied without leaving the crossing region.

If we denote these two independent co-ordinates by $\mathbf{x_1}$ and $\mathbf{x_2}$, and take the origin at the point where $H_{11} = H_{22} = W$ and $H_{12} (= H_{21}) = 0$, in the hypothesis of the first order (i.e., linear)[46] approximation, the secular equations may be cast in the form

$$\begin{bmatrix} \tilde{H}_{11} - E & \tilde{H}_{12} \\ \tilde{H}_{21} & \tilde{H}_{22} - E \end{bmatrix} \begin{bmatrix} c_1 \\ c_2 \end{bmatrix} = \begin{bmatrix} W + h_1\mathbf{x}_1 - E & l\mathbf{x}_2 \\ l\mathbf{x}_2 & W + h_2\mathbf{x}_1 - E \end{bmatrix} \begin{bmatrix} c_1 \\ c_2 \end{bmatrix} = 0 \qquad [6]$$

(i.e., $\tilde{H}_{11} = W + h_1\mathbf{x}_1$, etc.)

or

$$\begin{bmatrix} W + (m+k)\mathbf{x}_1 - E & l\mathbf{x}_2 \\ l\mathbf{x}_2 & W + (m-k)\mathbf{x}_1 - E \end{bmatrix} \begin{bmatrix} c_1 \\ c_2 \end{bmatrix} = 0 \qquad [7]$$

where $m = \frac{1}{2}(h_1 + h_2), k = \frac{1}{2}(h_1 - h_2)$. The eigenvalues are

$$E = W + m\mathbf{x}_1 \pm \sqrt{k^2\mathbf{x}_1^2 + l^2\mathbf{x}_2^2} \qquad [8]$$

Eq. 8 is the equation of an *elliptic double cone* (i.e., with different axes) with vertex at the origin (it will be a circular cone only for the case k = l). For this reason, such crossing points are called *conical intersections*. Indeed, if we plot the energies of the two intersecting states against the two internal co-ordinates $\mathbf{x}_1$ and $\mathbf{x}_2$ [whose values at the origin satisfy the two conditions $H_{11} = H_{22}$ and $H_{12}(= H_{21}) = 0$], we obtain a typical double cone shape (see Figure 5).

Figure 5

Now let us inquire into the physical meaning of the two conditions $H_{11} = H_{22}$ and $H_{12}(= H_{21}) = 0$. If we consider the basis (ϕ_1 and ϕ_2) of the secular equation [2] as the *diabatic* components of the *adiabatic* electronic eigenfunction (a diabatic function describes the energy of a particular spin-coupling or atomic orbital occupancies[14], while the adiabatic function represents the surface of the real state), the crossing condition (real or avoided) is fulfilled when the two diabatic components ϕ_1 and ϕ_2 cross each other,

and this happens when $H_{11} = H_{22}$, i.e., the energy of the two diabatic potentials (H_{11} is the energy for the diabatic function ϕ_1 , and H_{22} is the energy for the diabatic function ϕ_2) is the same.

At the crossing of the diabatic functions ($H_{11} = H_{22}$), the expressions for the energies of the two real states become (from Eq. [3])

$$E_1 = H_{11} - H_{12}$$
$$E_2 = H_{11} + H_{12} \qquad [9]$$

and the energy gap between the two real states is

$$E_2 - E_1 = 2H_{12} \qquad [10]$$

Thus, if the off-diagonal (resonance) term H_{12} is *not zero*, the crossing will be avoided and the potential surfaces of the two real states will "split". The energy separation at an avoided crossing thus depends on the magnitude of H_{12}. H_{12} will be *zero* (and the crossings will be unavoided) when the two electronic states have a different (spatial or spin) symmetry. However, in general, H_{12} is *not generally zero* for states of the same symmetry (which will generate avoided crossings). This is the *noncrossing rule.* Anyway, as we have seen above, this rule is true only for diatomic molecules,[19] and in a polyatomic system one can always have unavoided (i.e., real) crossings for suitable values of a pair of independent co-ordinates ($\mathbf{x_1}$ and $\mathbf{x_2}$), which will simultaneously satisfy Eqs. [5]. In conclusion the most general statement for unavoided crossings[19] is: *for a polyatomic system two states (even with the same symmetry) will intersect along an n-2 dimensional hyperline (i.e., a line in more than 3 dimensions) as the energy is plotted against the n internal nuclear co-ordinates* [the two dimensions referred to above are the two independent variable (i.e., $\mathbf{x_1}$ and $\mathbf{x_2}$) defined previously].

Theoretical investigations of surface crossings have required new theoretical techniques based upon the mathematical description of conical intersections and we now briefly review the central theoretical aspects. For two geometric variables, two surfaces of the same multiplicity intersect as a double cone (Figure 5). If one moves in the plane spanned by the two directions $\mathbf{x_1}$ and $\mathbf{x_2}$ (the so-called "branching space"[46]) the degeneracy is lifted. In n dimensions the degeneracy persists along an n-2 dimensional hyperline (called "intersection space"): if we move from the apex of the cone along any of the remaining n-2 internal co-ordinates defining the intersection space, the degeneracy is not lifted. This n-2 dimensional space is a *hyperline* consisting of an infinite number of conical intersection points (see Figure 5b). It can be demonstrated[47] that these two directions are given as the gradient difference vector

$$\mathbf{x}_1 = \frac{\partial (E_1 - E_2)}{\partial \mathbf{Q}} \qquad [11]$$

and the gradient of the interstate coupling vector

$$\mathbf{x}_2 = \left\langle \mathbf{C}_1^t \left| \frac{\partial H}{\partial \mathbf{Q}} \right| \mathbf{C}_2 \right\rangle \qquad [12]$$

where $\mathbf{C_1}$ and $\mathbf{C_2}$ are the configuration interaction (CI) eigenvectors in a CI problem, H is the CI Hamiltonian, and $\mathbf{Q}$ represents the nuclear configuration vector of the system. The vector $\mathbf{x_2}$ is parallel to the non-adiabatic coupling vector $g(\mathbf{Q})$.

$$g(\mathbf{Q}) = \left\langle \mathbf{C}_1^t \left| \frac{\partial \mathbf{C}_2}{\partial \mathbf{Q}} \right\rangle = \frac{\left\langle \mathbf{C}_1^t \left| \frac{\partial H}{\partial \mathbf{Q}} \right| \mathbf{C}_2 \right\rangle}{E_1 - E_2} \right. \qquad [13]$$

The vector $g(\mathbf{Q})$ is the coupling term that gives the magnitude of the coupling between the Born-Oppenheimer states described by $\mathbf{C_1}$ and $\mathbf{C_2}$ as a function of the nuclear motion along $\mathbf{Q}$.

Conical Intersection Structure

Figure 6

Figure 7

To understand the relationship between the surface crossing and photochemical reactivity, it is useful to draw a parallel between the role of a transition state in thermal reactivity and that of a conical intersection in photochemical reactivity[14]. In a thermal reaction, the transition state (**TS**) forms a bottleneck through which the reaction must pass, on its way from reactants (**R**) to products (**P**) (Figure 6a). The motion through the **TS** is described by a single vector, the transition vector $\mathbf{x_1}$ (i.e., the eigenvector related to the imaginary vibrational frequency). A transition state separates the reactant and product energy wells along the reaction path. An accessible conical intersection (**CI**) (Figure 6b) also forms a bottleneck that separates the excited state branch of the reaction path from the ground state branch. The crucial difference between conical intersections and transition states is that, while the transition state must connect the reactant energy well to a single product well via a single reaction path, an intersection is a "spike" on the ground state energy surface (see Figure 6b), and thus it may connect the excited state reactant to two or more products ($\mathbf{P_1}$ and $\mathbf{P_2}$) on the ground state via a branching of the excited reaction path (in the plane $\mathbf{x_1}$ and $\mathbf{x_2}$) into different ground state relaxation valleys. The branching is possible even in the first order approximation because of the elliptic nature of the double cone; however in the case of an elliptic cone the branching will occur at most along two directions (see $\mathbf{P_1}$ and $\mathbf{P_2}$ in Figure 6b).The nature of the products generated following decay at a surface crossing will depend on the ground state valleys (relaxation paths) that can be accessed from that particular structure.

Different topological situations are possible for unavoided crossings between surfaces. One can have intersections between states of different spin multiplicity (an n-1 dimensional intersection space in this case, since the interstate coupling vector vanishes by symmetry), or between two singlet surfaces or two triplets (and one has an n-2 dimensional conical intersection hyperline in this case). We have encountered situations where both types of intersection occur at the same geometry[32]. These three various topological possibilities are summarised in Figure 7a-c. Notice that for the examples shown in Figure 7a-c, the gradient of both the surfaces at the crossing is not zero. A conical intersection is just a Jahn-Teller[48,49] like degeneracy that occurs without symmetry. One might ask if a Renner-Teller[48] like degeneracy (i.e., the gradients of both surfaces go to zero at the degeneracy) can occur without having its origin in the symmetry of the states. This situation is shown in Figure 7d and is characterised by the fact that the gradients of both states is zero (i.e., they are real minima). Thus this situation is a "touching" rather than a crossing.

The topography of the potential energy surfaces in the vicinity of a conical intersection can also be characterised by the relative orientation of the two potential surfaces, as discussed by Ruedenberg et al.[46]. In this review we will use Ruedenberg's terminology: peaked, sloped and intermediate as shown in Figure 8. Often the chemically relevant conical intersection point is located along a valley on the excited state potential energy surface (i.e., a peaked intersection). Figure 9 illustrates a two-dimensional model example that occurs in the photochemical *trans* → *cis* isomerization of octatetraene[28]. Here two potential energy surfaces are *connected* via a conical intersection. This intersection appears as a single point (**CI**) since the surfaces are plotted along the branching space ($\mathbf{x_1}$, $\mathbf{x_2}$). The intermediate $\mathbf{M^*}$ is reached by relaxation from the Franck-Condon region (**FC**), and it is separated from the intersection point by a transition state (**TS**). In this case (a peaked type of intersection) the molecular structure of the intersection and the reaction pathway leading to it can be studied by computing the MEP connecting **FC** to $\mathbf{M^*}$ and $\mathbf{M^*}$ to **CI** using the standard intrinsic reaction co-ordinate

(IRC) method[50]. However, there are situations (sloped intersections, see Figures 4c and 8b) where there is no transition state connecting **M*** to the intersection point. In such situations, mechanistic information must be obtained by locating the lowest lying intersection point along the n-2 intersection space of the molecule. The practical computation of the molecular structure of a conical intersection energy minimum[47,51] will be illustrated in the next subsection. This technique provides information on the structure and accessibility of the intersection point which controls the locus and efficiency of internal conversion.

Figure 8

Figure 9

Nonadiabatic events (transition from the excited state to the ground state at the conical intersection) pose a serious challenge because the non-adiabatic transition is rigorously quantum mechanical without a well-defined classical analogue. At a simple level of theory[13] (we return to a better treatment subsequently) the probability of a surface hop is given as

$$P = \exp\left[-(\pi / 4)\xi\right] \qquad [14]$$

where the Massey parameter is

$$\xi = \frac{\Delta E(\mathbf{Q})}{\hbar \dot{\mathbf{Q}}\ g(\mathbf{Q})} \qquad [15]$$

Thus this simple theory predicts that radiationless transitions will occur when the energy gap $\Delta E(\mathbf{Q})$ *is small and the scalar product between the velocity vector and*

the non-adiabatic coupling $\dot{\mathbf{Q}}\ g(\mathbf{Q})$ *is large.* Here $\dot{\mathbf{Q}} = \frac{\partial \mathbf{Q}}{\partial t}$ and $g(\mathbf{Q})$ is defined in Eq. [13].

The motion to ground state photoproducts following decay via internal conversion at a conical intersection channel requires a study of the possible ground state relaxation process. A new method (called initial relaxation direction (IRD) method) to locate and characterise all the relaxation directions that originate at the lower vertex of the conical intersection cone, has been recently implemented[52], and will be illustrated in detail in the next section. The MEP starting along these relaxation directions defines the ground state valleys which determine the possible relaxation paths and ultimately the photoproducts which can be generated by decay. Although this information is *structural* (i.e., *non-dynamical*), it provides insight into the mechanism of photoproduct formation from vibrationally cold excited state reactants such as those encountered in many experiments where slow excited state motion or/and thermal equilibration is possible (in cool jets, in cold matrices and in solution).

When such structural or static information is not sufficient (i.e., the excited state may not decay at the minimum of the conical intersection line, or the momentum developed on the excited state branch of the reaction co-ordinate may be sufficient to drive the ground state reactive trajectory along paths that are far from the ground state valleys), a dynamics treatment of the excited state/ground state motion is required[53,54]. These techniques will be also illustrated in the next subsection.

An Example: the S_1/S_0 Conical Intersection of Benzene

Figure 10

We now give an example of the way in which the topological features just discussed occur in practical problems. In S_1 benzene there is a ~3000 cm^{-1} threshold for the disappearance of S_1 fluorescence (see Refs. 25 and 54 and references cited therein). This observation is assigned to the opening of a very efficient, radiationless decay channel (termed "channel 3") leading to the production of fulvene and benzvalene via a prefulvene intermediate (see Figure 10a). Ab initio CAS-SCF[12] (complete active space SCF) calculations show[25] that the general surface topology of the excited state energy surface is consistent with that shown in Figure 5a (and illustrated in three dimensions in Figure 9) and we have shown this in Figure 10b. Thus the observed energy threshold, which is reproduced by multi-reference MP2 (Møller-Plesset 2) computations[55] corresponds to the energy barrier which separates S_1 benzene from an S_1/S_0 conical intersection point.

Figure 11 (From Ref. 25.)

A molecular species has only a transient existence in the region of a conical intersections. Thus, the molecular structure can only be derived from theoretical computations. The optimised conical intersection structure for S_1 benzene is shown in Figure 11. The structure contains a triangular arrangement of three carbon centres corresponding to a $-(CH)_3-$ kink of the carbon skeleton. The electronic structure corresponds to 3 weakly interacting electrons in a triangular arrangement which are loosely coupled to an isolated radical centre (this is delocalised on an allyl fragment). This type of conical intersection structure appears to be a general feature in conjugated systems and has been documented in a series of polyene and polyene radicals[27]. We will illustrate this point in the last subsection. The electronic origin of this feature can be understood by comparison with H_3 where any equilateral triangle configuration corresponds to a point on the D_0/D_1 conical intersection (this is an example of Jahn-Teller degeneracy) in which the three H electrons have identical pairwise interactions.

We now discuss the -(CH)3- kink electronic structure and coupling involved in photoproduct formation after decay back to the ground state. In the conical intersection surface topology, illustrated in Figure 10b, the two geometrical distortions that lift the degeneracy ($\mathbf{x_1}$ and $\mathbf{x_2}$) are given in Figure 12. By examining the molecular structure of the conical intersection, its electronic distribution and the directions indicated by the $\mathbf{x_1}$ and $\mathbf{x_2}$ vectors, we can derive information on the photochemical reaction path and on the possible coupling patterns involving the three unpaired electrons of the kink and leading to the final photoproducts. Three different pairings (1-6, 5-6, and 1-5: see Figure 11 for numbering) of two of the three electrons of the kink are possible (see Figure 10b). The gradient difference vector $\mathbf{x_1}$, which is almost parallel to the S_1 transition vector, predicts a relaxation towards the pre-fulvene diradical in the positive direction (1-5 pairing) and a planar ground state benzene in the negative direction (i.e., reversing the arrows in Figure 12). The other two couplings are described by the non-adiabatic coupling vector $\mathbf{x_2}$ (shown in Figure 12) which is the other geometrical co-ordinate shown in Figure 10b. It describes the simultaneous double bond re-construction which occurs upon relaxation. This direction corresponds to localising the π bonds in either the 1-6 or 5-6 positions (1-6 and 5-6 pairings in the positive and negative direction of $\mathbf{x_2}$ respectively). Thus from Figure 10b, a "circuit" of the conical intersection changes the coupling in the triangular arrangement of the three carbon centres corresponding to the -(CH)3- kink of the carbon skeleton.

This discussion is more general than it appears. As we will show in the next section (see Figure 15), for the conical intersection geometry that has been optimised on the S_1 surface for the problem of cyclohexadiene/hexatriene photochemical interconversion, one again sees the three different pairings of two out of three electrons. The recoupling of the three electrons of the -(CH)3- kink appears to be a general feature in the decay and ground state relaxation valleys departing from conical intersections in polyenes.

Figure 12

PRACTICAL COMPUTATION OF PHOTOCHEMICAL REACTION PATHS

In this section, we describe the computational strategies and techniques which are needed to determine a photochemical reaction path from the Franck-Condon point (**FC**) to the ground state photoproduct (**P**). The methods used comprise: methods for computing the excited state electronic energy, methods to determine the molecular structure of stationary points [intermediates ($\mathbf{M}^*$), transition states (**TS**)], low-lying crossings [either a conical intersection (**CI**) or a singlet-triplet crossing] and to construct excited state reaction paths and ground state relaxation paths in term of MEP (see Figure 9 for a model surface). We will also give some discussion of dynamics and application of semi-classical trajectories.

Quantum Chemical Methods and Software for Excited State Energy and Gradient Computations

The study of photochemical mechanisms presents a considerable challenge for computational chemistry. The objective is a complete description of the reaction path from the Franck-Condon region to the ground state product. Thus the details of the excited state reaction path and the region where a non-adiabatic event takes place at a surface crossing must be treated in an accurate and balanced way. One needs both analytical gradients and second derivatives at all points on the potential energy surface. Dynamic electron correlation (i.e., correction for the incorrect instantaneous repulsion of electrons in doubly occupied orbital) is crucial for accurate energies.

There are two fundamentally different approaches to the computation of excited states which we shall refer to as wavefunction methods and response methods. The oldest approach, which is currently undergoing a revival, are the response theories in

which the excited state is computed as the first order response of the ground state wavefunction. While the derivation of response methods is complex, and beyond the scope of this tutorial, at the simplest level, these response methods reduce to the CI (configuration interaction) singles (CIS)[56] approach. The CIS method can yield a good representation of those excited states which are dominated by single excitations from the ground state and can often provide a good starting point for computations. This method also forms the basis of most semi empirical approaches. However methods such as CIS neglect the effects of dynamic electron correlation. At higher levels, response theories include the various Equation of Motion (EOM) approaches which have seen much recent development in a coupled cluster implementation[57,58]. The most recent developments of response methods are referred to as time-dependent density functional theory (DFT)[59,60]. However, in both EOM and time-dependent DFT, one ends up with an "effective hamiltonian" in the space of a single excitation CI from the ground state (i.e., on the space of CI singles), where the effects of dynamic correlation are included. Response methods are limited to situations where the problem can be described in terms of the "linear response" of the ground state. What this means in practise is that the excited state must have a non-zero projection on the space of single excitations. However, the excited states involved in photochemical processes often involve (after decay from the optical state) essentially doubly excited states and curve crossings with the ground state. While response methods seem to be capable of reproducing the energy difference between ground and excited states (i.e., vertical excitation energies), they are completely untested for the type of problem that we are addressing in this chapter. However this problem is currently a field of intense research activity.

Standard wavefunction methods (i.e., other than DFT), which have been extensively applied both to the computation of vertical (i.e., at ground state equilibrium geometry) excitation energies and excited state reaction paths, are the current preferred method for applications in this field. Wavefunction methods that are used in studying photochemical mechanisms are limited to those that can describe excited states correctly.

Unfortunately, standard methods for the evaluation of the ground state PES such as SCF and DFT cannot describe excited states because they are restricted to the aufbau principle.

The ab initio CAS-SCF method[12] is the main wavefunction method used for geometry optimisation since it permits the gradient and second derivatives to be computed analytically,[61] and this method has been implemented in widely distributed programs such as Gaussian 94 [62], MOLCAS[63], COLUMBUS[64], and GAMESS.[65] (See Ref. 66 for a complete quantum chemical software compendium and a complete list of computer packages that can deal with excited state computations). However, when accurate energetics are required, a treatment of dynamic correlation with the MP2 method has been implemented (CAS-SCF/MP2),[67,68] and this gives reliable results at low cost. Another method, which gives the similar results to CAS-SCF/MP2, is the multireference configuration interaction method (MR-CI)[69]; however this method is at present limited to small systems, due to its high computational cost.

Analytical gradients and hessians are available for CAS-SCF and it is expected that this technology will be extended to the MR-CI and MP2 methods soon. Further, by virtue of the multireference approach, a balanced description of ground and excited states is achieved. Unfortunately, unlike “black box” such as first order response methods (e.g., time dependent DFT), CAS-based methods require some considerable skill and experience to use effectively. In the last subsection of this chapter, we will present some case studies that serve to illustrate the main conceptual issues related to computation of excited state potential surfaces. The reader who is contemplating performing computations is urged to study some of the original cited papers in order to appreciate the practical issues.

There is also a large literature of excited state computations carried out using semiempirical methods with CI such as ZINDO [70] and MNDO[71]; these methods have been applied to photochemical problems by Klessinger and co-workers[72], Momicchioli

and co-workers[73], and Orlandi and co-workers[74]; however, gradient based methods for surface crossings have not yet been implemented in these methods.

In recent years, there has been considerable interest in combining quantum mechanics with force field methods such as molecular mechanics (MM) in order to model large molecular systems. In general, such methods are based upon SCF theory which cannot be applied to excited states. Recently, we developed[75,76] an approach based upon valence bond (VB) theory (which uses a parameterized Heisenberg Hamiltonian[77-79] to represent the quantum mechanical part in a VB space) together with the MM force field. This approach yields a modeling method, called MM-VB (i.e., Molecular Mechanics Valence Bond)[75,76] that reproduces the results of CAS-SCF computations for ground and excited states, yet is fast enough that dynamics simulations are possible. A recent benchmark[80] gives a good indication of the accuracy of such techniques in styrene photophysics.

In conclusion, presently, the ab initio CAS-SCF method (together with CAS-SCF/MP2) is currently the preferred choice for computing the PES of excited states. This method can treat up to 12 active electrons in routine application. When the size or the complexity of the molecular system under investigation does not allow the use of ab initio methods, information on the general structure of the potential energy surface can still be obtained by using hybrid methods such us MM-VB. Since the purpose of this tutorial is not to discuss general methods for excited state energy computation (vertical excitation energies, etc.) we will concentrate, in the following, on the special problems associated with the computation of reaction paths which span one or more potential energy surfaces.

Conical Intersection Optimisation

The process of locating and computing the structure of an energy minimum or saddle point on the potential energy surface is usually referred to as geometry

optimisation. At both minima and saddle points, the gradient must be zero. Usually a geometry optimiser starts its search at a suitable initial molecular structure. It evaluates the energy and gradient (the gradient corresponds to the direction in which the energy decreases most rapidly: the steepest descent direction) and determines the direction and magnitude of the next structure that should be closer to the target. The Hessian is also used to specify the curvature of the surface and provide a quadratic representation of the PES in the vicinity of the point. In this subsection, we shall discuss the special problem of optimising the surface crossing and in finding relaxation paths from it.

As reported in the introduction, we have indicated that there are situations where there is no transition state connecting an excited state intermediate (**M***) to the conical intersection point (sloped conical intersections, see Figure 4c and 8b). In such situations, mechanistic information associated with surface crossings must be obtained by locating the lowest lying intersection point along the n-2 intersection space of the molecule.

The practical computation of the molecular structure of a conical intersection energy minimum can be illustrated by making an analogy with the optimisation of a transition structure (see Figure 6). A transition structure is the highest energy point along the path (MEP[1]) joining reactants to products and the lowest energy point along all the other n-1 directions orthogonal to it. One can optimise such a structure by minimising the energy in n-1 orthogonal directions, and maximising the energy in the remaining direction corresponding to the reaction path (i.e., the transition vector $\mathbf{x_1}$ in Figure 6a). The technique for locating the lowest energy intersection point[47,51] exploits the fact that the branching space directions $\mathbf{x_1}$ and $\mathbf{x_2}$ play a role analogous to the reaction path at the transition state. Accordingly, the lowest energy point on a conical intersection is obtained by minimising the energy in the n-2 dimensional intersection space ($\mathbf{x_3}$, $\mathbf{x_4}$,..., $\mathbf{x_n}$) which preserves the degeneracy (see Figure 5b) and minimising the energy gap in the branching space ($\mathbf{x_1}$ and $\mathbf{x_2}$). In practise, in order to properly locate these low-energy stationary points where two potential energy surfaces have the same energy, one must

carry out constrained geometry optimisations where the geometry is optimised in directions orthogonal to the two directions $\mathbf{x_1}$ and $\mathbf{x_2}$. It is important to appreciate that the gradient on the excited state PES will not be zero at an optimised conical intersection point (see Figure 7a,b), because it looks like the vertex of an inverted cone (see Figure 5 and 6b). Rather, it is the projection of the gradient of the excited state PES onto the orthogonal complement of $\mathbf{x_1}$ and $\mathbf{x_2}$ (i.e., the n-2 dimensional hyperline) that goes to zero when the geometry of the conical intersection is optimised. This situation is distinguished from a "avoided crossing minimum" or Renner-Teller degeneracy of two surfaces (see Figure 7d: indeed this is a "touching" rather than an intersection point) which correspond to real minima where the gradient on the excited state PES would go to zero. Thus, in an optimised conical intersection point, conditions (**i**) and (**ii**) (Eqs. [16]) have to be fulfilled:

$$\textbf{(i)}\quad E_2 - E_1 = 0$$
$$\textbf{(ii)}\quad \frac{\delta E}{\delta \mathbf{x_3}} = \frac{\delta E}{\delta \mathbf{x_4}} = ... = \frac{\delta E}{\delta \mathbf{x_n}} = 0 \qquad [16]$$

The practical algorithm[47,51] which was first implemented in the Gaussian 94 programme package[62] can be described as follows. For the minimisation of E_2 - E_1 in the $\mathbf{x_1}$ and $\mathbf{x_2}$ plane we have:

$$\frac{\partial}{\partial \mathbf{Q}}\left(E_2 - E_1\right)^2 = -2\left(E_2 - E_1\right)\mathbf{x_1} \qquad [17]$$

where $\mathbf{x_1}$ is the gradient difference vector (see Eq. [11]). The length of $\mathbf{x_1}$ has no significance - only its direction ($|\mathbf{x_1}|$ will be large if the potential energy surfaces have opposite slope but very small if they have nearly the same slope). This means that the size of the step should only depend upon E_2 - E_1 , and suggests that we should take the gradient along the step to the minimum of E_2 - E_1 to be

$$\mathbf{f} = -2\left|E_2 - E_1\right|\frac{\mathbf{x_1}}{\sqrt{\mathbf{x_1}\ \mathbf{x_1}}}\,. \qquad [18]$$

Clearly **f** will go to zero when E_2=E_1, independently of the magnitude of $\mathbf{x_1}$. Note, however, the gradient will also go to zero if E_1 is different from E_2 but the two surfaces are parallel (i.e., $\mathbf{x_1}$, the gradient difference vector, has zero length). In this case the method would fail. This situation will occur for a Renner-Teller like degeneracy for example. Of course, in this case, the geometry can be found by normal unconstrained geometry optimization.

If we now define the projection of the gradient of E_2 onto the (n-2) orthogonal complement to the plane $\mathbf{x_1}$, $\mathbf{x_2}$ as

$$\mathbf{g} = \mathbf{P}\frac{\partial E_2}{\partial \mathbf{Q}} \qquad [19]$$

where **P** is the projection operator, then the gradient to be used in the optimisation becomes

$$\bar{\mathbf{g}} = \mathbf{g} + \mathbf{f} \qquad [20]$$

The general behaviour of such optimisation procedure is illustrated in Figure 13 where we report two PES intersecting along the $\mathbf{x_1}$ and "intersection space" co-ordinates ($\mathbf{x_3}$, .., $\mathbf{x_n}$). While this example is not realistic because we have started very far from the optimized structure, notice that, starting from this initial structure (initial point), the method first finds the closest intersection point. After that, it moves downhill along the intersection space.

Figure 13

Locating Decay Paths from a Conical Intersection

Since the minima and saddle point are well defined points on the PES, it is possible to define a unique reaction path. The MEP[1] can be defined as the path traced by a classical particle sliding with infinitesimal velocity from a saddle point down to each of the minima. The MEP [which can be computed by using the intrinsic reaction co-ordinate (IRC)[81] method] is a geometrical or mathematical feature of the PES, like minima, maxima and saddle points. Since molecules have more than infinitesimal kinetic energy, a classical trajectory will not follow the MEP and may in fact deviate quite widely from it such as in the case of a "hot" system (i.e., with an high excess vibrational energy) where a dynamics treatment of the motion on the PES would be required. However, the MEP may be a convenient measure of the progress of a molecule in a reaction since in general a molecule will move, on the *average*, along the MEP in a *well defined* valley, and it is a good approximation of the motion of vibrationally cold systems (e.g., for photochemical reactions where the excited state reactant has a small/controlled amount of vibrational excess energy).

We have shown that an accessible conical intersection forms a bottleneck that separates the excited state branch of a non-adiabatic photochemical reaction path from the ground state branch, thus connecting the excited state reactant to *two or more* products on the ground state via a branching of the excited reaction path into several ground state relaxation channels (see Figure 6b). The nature of the products generated following decay at a surface crossing will depend on the ground state valleys (reaction paths) that can be accessed from that particular structure. We have recently implemented a gradient-driven algorithm to locate and characterise all the relaxation directions departing from a single conical intersection point[52]. The MEP starting along these relaxation directions defines the ground state valleys which determine the possible relaxation processes and the photoproducts. This information is *structural* (and thus excludes *dynamical* effects such as lifetimes and quantum yields) and provides insight into the mechanism of

photoproduct formation from vibrationally cold excited state reactants such as those encountered in many experiments where slow excited state motion or/and thermal equilibration is possible (in cool jets, in cold matrices and in solution). Under these conditions of low vibrational excess energy, semiclassical dynamics yields the same *mechanistic* information as from topological investigation of the PES, because its structure is expected to play the dominant role in determining the *initial* molecular motion in the decay region.

The MEP connecting the reactant to the product of a thermal reaction is uniquely defined by the associated transition structure (**TS**). The direction of the transition vector (i.e., the normal co-ordinate corresponding to the imaginary frequency of the **TS**) is used to start a MEP computation. One takes a small step along this vector $\mathbf{x_1}$ (shown in Figure 6a) to points **R** or **P** and then follows the steepest descent paths connecting this point to the product or reactant well. The small step vector defines the *initial relaxation direction* (IRD) towards the product or reactant. It is obvious from Figure 6b that this procedure cannot be used to find the IRD for a photochemical reaction since, as discussed above, the down hill direction lies in the plane $\mathbf{x_1, x_2}$. The general situation is illustrated in Figure 14a.

In the linear approximation, since the cone is elliptic (see discussion in the previous section) two steep sides (see Figure 14b) exist in the immediate vicinity of the apex of the cone. As one moves away from the apex along these steep directions, real reaction valleys (Figure 14a) develop leading to final photoproduct minima. Thus in reality the first order approximation will break down at larger distances and more complicated cross sections and more than two relaxation channels exist. Also there are symmetric cases (such as H_3) where the tip of the cone will never be possibly described by Eq. [8] because one has three equivalent relaxation channels from the very beginning of the tip of the cone.

Figure 14

In Figure 14b we show the potential energy surface for a "model" elliptic conical intersection[46] plotted in the branching plane ($\mathbf{x_1}$,$\mathbf{x_2}$). Because, as stated previously, the cone is elliptic in the linear approximation (i.e., the base of the cone is an ellipse rather than a circle), there are two "steep" sides of the ground state cone surface and two "ridges". It is thus obvious that there are two preferred directions for downhill motion located on the steep sides of the ground state cone surface. A simple procedure for defining these directions involves the computation of the energy profile along a circular cross-section of the branching plane centred on the vertex of the cone (0,0) as illustrated in Figure 14b/c. This energy profile is given in Figure 14c as a function of the angle α and for a suitable choice of the radius *d*. It can be seen that the profile contains two different energy minima. These minima ($\mathbf{M_1}$ and $\mathbf{M_2}$ in Figure 14b) uniquely define the IRD from the vertex of the cone. The two steepest descent lines starting at $\mathbf{M_1}$ and $\mathbf{M_2}$ define two MEPs describing the relaxation processes in the same way in which the transition vector $\mathbf{x_1}$ (see Figure 6a) defines the MEP connecting reactant to products. Notice that there are also two energy maxima $\mathbf{TS_{21}}$ and $\mathbf{TS_{12}}$ in Figure 14b/c. These can be interpreted as the "transition structures" connecting $\mathbf{M_1}$ and $\mathbf{M_2}$ along the chosen circular cross-section. It can be seen in Figure 14b/c that these transition structures locate the energy ridges which separate the IRD "valleys" located by $\mathbf{M_1}$ and $\mathbf{M_2}$. Thus, while there is no analogue of the transition vector for a conical intersection, the simple case of an elliptic cone shows that the IRD are still uniquely defined in terms of $\mathbf{M_1}$ and $\mathbf{M_2}$. *Notice that while the IRD from a* ***TS*** *connects the reactant to the product, there are two IRD from an elliptic conical intersection leading to two different photoproduct valleys* (and one of these photoproducts may correspond to the original reactant).

For the elliptic (i.e., first-order[46]) cone model, discussed above, there can be at most two minima ($\mathbf{M_1}$ and $\mathbf{M_2}$) defining two distinct IRD (excluding the case where the cone becomes circular in which case there are an infinite number of equivalent directions

of relaxation). These minima are located on the branching plane ($\mathbf{x_1}$,$\mathbf{x_2}$). However, this model of the potential energy sheets at a conical intersection point is not general enough to give a correct description of *all* relaxation paths for a real system. Firstly, there may be more than two possible IRD originating from the same conical intersection. Secondly, some IRD may lie out of the branching plane because the real ($\mathbf{x_1}$,$\mathbf{x_2}$) space is, in general, curved. However, the ideas introduced above can be easily extended to search for IRD in the full n-dimensional space surrounding a conical intersection point by replacing the circular cross-section with a (hyper)spherical cross-section centred at the vertex of the cone. Locating stationary points on the hypersphere involves constrained geometry optimisation, in mass-weighted co-ordinates, with a "frozen" variable *d*. Although all results (IRD vectors and MEP co-ordinates) are generally given in mass-weighted Cartesian co-ordinates, the actual computations are carried out using mass-weighted internal co-ordinates[81]. We have presented the full mathematical details elsewhere[52].

We must emphasise that the procedure outlined above is designed to locate the points where the relaxation paths begin (i.e., they define the IRD). Once these points have been found for some small value of *d*, then one must compute the associated MEP which defines the relaxation paths leading to a ground state energy minimum (as stated before). Thus the approach outlined above provides a systematic way to find the MEP connecting the vertex of the cone to the various ground state photoproduct wells. Since more than one MEP originates from the same conical intersection point, this procedure also describes the branching of the excited state reaction path occurring at the intersection point.

A simple example serves to illustrate the above approach. In Figure 15 we show the conical intersection geometry that has been optimised on the S_1 surface for the problem of cyclohexadiene (**CHD**) / *cZc*-hexatriene (***cZc*-HT**) photochemical interconversion[82]. This structure has a characteristic -$(CH)_3$- kink (this geometric triangular arrangement is typical of polyene conical intersections[27], as we will see in the

next section), and three different ground state recoupling paths are possible, as shown in Figure 16a. Thus one expects to find three ground state reaction pathways (leading to **R**, $\mathbf{P_1}$ and $\mathbf{P_2}$ as illustrated schematically in Figure 16b) corresponding to the three different recoupling patterns involving the triangular kink (see the analogy with the three recoupling patters in benzene discussed in the previous section and shown in Figure 10). The real (computed) surface topology is illustrated in Figure 17. Close to the apex of the cone there are only the two reaction valleys directed toward **R** and $\mathbf{P_1}$, whereas the direction leading to $\mathbf{P_2}$ (the more unstable diradical intermediate) is a ridge. The valley to $\mathbf{P_2}$ develops only at a larger distance from the apex of the cone (see Figure 17).

Figure 15

Figure 16

Figure 17

Thus calculations show[36,82] and experiments confirm[4,5,83-87] that there are two almost equivalent relaxation paths, which will be populated after decay from the conical intersection: one leading to cyclohexadiene (**R**) and the other to hexatriene ($\mathbf{P_1}$), with very similar quantum yields (i.e., product ratio). (We shall return to discuss this problem in a little more detail in the next section).

Semi-classical Trajectories

The techniques outlined above provide information on the structure and accessibility of the photochemical reaction paths. As mentioned, this information is *structural* (i.e., *non-dynamical*) and provides insight into the mechanism of photoproduct formation from vibrationally "cold" excited state reactants such as those encountered in many experiments where slow excited state motion or/and thermal equilibration is possible (in cool jets, in cold matrices and in solution).

In many cases, such structural or static information is not sufficient. The excited state may not decay at the point where the excited state path (MEP) intersects the n-2 hyperline. Alternatively, the momentum developed on the excited state branch of the reaction co-ordinate may be sufficient to drive the ground state reactive trajectory along paths that are far from the ground state valleys. In such cases, a dynamics treatment of the excited state/ground state motion is required for mechanistic investigations. Furthermore a dynamic treatment is required to gain information of the timescales and quantum yields of the reaction.

In principle, the current implementation of Car-Parrinello[88], which is based on a local DFT method, provides a method for ab initio molecular dynamics. This method propagates the nuclei classically in concert with wavefunction propagation using semi-classical equations of motion. But since this method is based upon DFT, it cannot describe an excited state PES. Further, the wavefunction is propagated using classical dynamics, and is thus inapplicable to curve crossing problems. For small systems, a parameterized potential can be developed and full quantum dynamical treatment is possible[53]. In our own work[54], we have used classical dynamics with a hybrid quantum-mechanical/force-field (MM-VB)[75,76]. This method employs a "direct" procedure for solving the equations of motion (i.e., the gradient that drives the dynamics is evaluated "on the fly"), and thus one avoids the tedious, and often unfeasible, parameterisation of an analytical expression of a multidimensional energy surface[53]. The trajectory-surface-hopping algorithm of Tully and Preston[89-91] is used to propagate excited state trajectories onto the ground state in the region of a conical intersection.

We now briefly describe the way in which the non-adiabatic event (surface hop) can be described in "on the fly" dynamics methods. We can represent the time dependent wavefunction in the CI space as a vector:

$$a(t) = \begin{pmatrix} C_1(t) \\ \bullet \\ \bullet \\ C_K(t) \\ \bullet \end{pmatrix} \qquad [21]$$

where C_K is a complex coefficient giving the contribution of state K. If the time step is sufficiently small, the solution of the time dependent Schrödinger equation can be propagated in concert with the nuclei in the dynamics simulation as

$$a(t) = \exp[iH(t)t]a(0) \qquad [22]$$

where H is the matrix representation of the Hamiltonian in the CI basis. The projection ($\langle a(t)|\Psi^k\rangle$) of the $a(t)$ on the adiabatic basis states (i.e., Ψ^k, eigenvectors of H) gives the "occupancy" of these states as illustrated in Figure 18. In the surface hop method, the gradient is always computed from an adiabatic basis state (i.e., an eigenvector of H) and the projection of the $a(t)$ on the adiabatic basis states is used to decide which adiabatic basis state is used for the gradient. The reader is referred to Refs. 26 and 92 for examples of the application of the surface hop method using quantum chemistry methods.

Figure 18

Surface hop approaches are not very well defined for the case where the trajectory re-crosses the region of strong coupling many times[93,94]. This problem occurs in the case of a sloped intersection (see Figure 4c or Figure 8b). One possible solution is the "multiple spawning" method of Levine and Martinez[95,96] where trajectories are spawned each time the trajectory passes through the region of strong interaction and a frozen gaussian (representing a wavepacket) is associated with each spawned trajectory so that the population transfer can be computed quantum mechanically. We have recently implemented[97] a third approach that uses mixed state dynamics (first used with a

diatomics-in-molecules model by Gadea and co-workers[98]). Here the nuclear dynamics are controlled by the *Ehrenfest* force (i.e., the gradient is computed directly from the $a(t)$ of Eq. [22]). Thus the trajectory "feels" both potential surfaces and the non-adiabatic couplings all the time. The most important aspect of mixed state approaches is the integration of the time-dependent Schrödinger equation for the electronic wavefunction in concert with nuclear propagation so that the method is closer to exact quantum methods than the surface hop approach. This method has been used successfully for investigation of the excited state lifetimes and decay process[97]; however, the accurate determination of quantum yields remains an outstanding problem.

The problem of combining dynamics with quantum chemistry is at the forefront of current research. The best method to be used will emerge as a compromise between quantum mechanical rigor and computational feasibility[99].

MECHANISTIC ORGANIC PHOTOCHEMISTRY: SOME CASE STUDIES

As reported in the introductory section, real crossings (such as conical intersections and singlet-triplet crossings) have been demonstrated to occur with a previously unsuspected frequency in organic systems[13,14]. Thus decay at a real crossings provides a common mechanism for excited state radiationless transitions and for the generation of photoproducts. Although there are, in principle, at least three different ways of generating a photoproduct, via an adiabatic reaction, via decay at an avoided crossing and via decay at a real crossing (see Figure 1), here we will deal exclusively with the latter type of process.

Thus, the investigation of the mechanism of a photochemical reaction requires, as a primary step, the investigation of the structure and energetics of the low-lying real crossings for the system under investigation and the study of the ground state reaction paths which originates at this decay funnel with the methodology described in the section on computation methods. The purpose of this section is to provide some background (by way of examples) to others who may wish to initiate theoretical work on photochemical methods. Thus, within the theoretical framework described in the previous sections, we hope that the case studies which we now discuss will give the reader some insight into the type of problems that may be encountered in some very different photochemical systems. Recent computational results do indicate some general features of surface crossings and of the related photochemical reaction paths. Here, we make an attempt to classify these features from a conceptual and chemical point of view. These case studies will also serve to indicate that present theoretical methods and computational technology can go a long way towards a complete understanding of a photochemical reaction mechanisms.

Through the analysis of some selected case studies, we hope to establish the following ideas which appear to be general:

(a) the photochemistry of conjugated hydrocarbons can be rationalised by the *common electronic and molecular structure of the surface crossing* between a covalent excited state and the ground state;

(b) the photochemistry of azo-alkanes, and enones is dominated by *intersections of n-*π^* *and* π–π^* *states* with the ground state as well as by the intervention of the triplet manifold;

(c) the photochemistry of protonated Schiff bases is also based on conical intersections; however, the excited state is ionic and corresponds to an intramolecular charge transfer state, thus the theoretical aspects of the problem are distinct from polyenes;

(d) the quantum yield in the radiationless decay and competitive photoproduct formation process in cyclohexadiene/*cZc*-hexatriene (**1**) system is controlled by *competitive ground state relaxation paths* which originate from a single conical intersection channel;

(e) *all-trans* hepta-2,4,6-trieniminium cation (**2**), a retinal protonated Schiff base model, may undergo *trans* → *cis* isomerization at either of the double-bonds in position 2 and 4. Thus, the photochemistry is dominated by the structure of the *competitive excited state reaction paths* leading to distinct conical intersection structures.

Structures 1 and 2

Three-electron Conical Intersections of Conjugated Hydrocarbons

The application of different spectroscopic techniques to low temperature samples of "isolated" conjugated molecules[100-102] has begun to provide very detailed information on the excited state dynamics of these organic systems and indicates that there is a small threshold energy to ultrafast radiationless decay. Use of the ab initio methods described in previous subsections suggest that the general mechanism which "triggers" the decay is a displacement of the electronically excited equilibrium structure towards a "critical" configuration where the excited and ground states cross at a conical intersection[27].

Figure 19

The molecular geometry at the point of decay shows, in many examples, a "kink" located at a -$(CH)_3$- segment . In Figure 19 we compare the structure of this -$(CH)_3$- segment for *all-trans* octatetraene (*all-trans*-OT), S_1 benzene and S_1 cyclohexadiene intersections. Comparison of these structures reveals common structural and electronic features. Each structure contains a triangular arrangement of three carbon centres corresponding to a -$(CH)_3$- kink of the carbon skeleton in *all-trans* OT[27,28] and benzene[25] and to a triangular arrangement of the -CH_2 and -CH-CH_2 terminal fragments in cyclohexadiene[36]. The electronic structure in each case corresponds to 3 weakly interacting electrons in a triangular arrangement (like H_3)[103] which are loosely coupled to an isolated radical centre (this is delocalised on an allyl fragment in *all-trans* OT, benzene and cyclohexadiene).

This type of conical intersection appears to be a general feature of linear polyenes and polyene radicals. These intersections are located at the end of the excited state reaction path, i.e., the MEP on the S_1 potential energy surface which has the general structure illustrated in Figure 4a (for short polyenes, such as butadiene, it has the general structure illustrated in Figure 4b). The structure and energetics of the excited state decay path for six (n=3,...,8) *all-trans* conjugated hydrocarbons, three polyenes (butadiene, hexatriene and octatetraene) and three polyene radicals (allyl, pentadienyl and heptatrienyl), have been documented using the ab initio CAS-SCF method with the DZ+d basis set and an active space including all π and π^* orbitals and electrons[27].

Conical Intersections of n-π Excited States*

In other classes of organic molecules, the electronic structure of the lowest lying intersection changes. We have published detailed results on the olefin-carbonyl Paterno-Buchi system[30], α,β-enones[31], β,γ-enones[32], azo-compounds (diazomethane[33] and

cyclic diazoalkenes[104]) and acylcyclopropenes[34] photorearrangements. Whereas hydrocarbon photochemistry typically involves a low energy π-π^* doubly-excited covalent state, the singlet photochemistry of carbonyl and azo-compounds is dominated by n to π^* excitations.

Structure 3

As an example of this class of system, we discuss some results on the photochemistry of diazabicyclo[2.1.1]hept-2-ene (DBH) (**3**). The photochemistry of this system is remarkably complex because it involves a study of the ground state S_0 surface as well as ^{1}(n-π^*), ^{3}(n-π^*), and ^{3}(π-π^*) surfaces and their crossings. All the topological features suggested in Figure 6 actually occur in practise, and a complete understanding of the photochemistry of this species involves a study of the evolution of singlet and triplet photoexcited DBH along a network of eighteen ground and excited state intermediates, seventeen transition structures and ten "funnels", where internal conversion (IC) or intersystem crossing (ISC) occurs[104]. While the mechanistic photochemist specifies a mechanism in terms of a sequence of molecular structures that occur along various reaction paths, one can use theoretical computations as a complementary and powerful tool to investigate reaction mechanism. One can use theoretical computation to actually *find* a viable mechanism, *determine* the nature of the structures involved (intermediates, transition states, surface crossings etc), and *discover* whether they lie on the excited or ground state branch of the reaction path and whether they are on the triplet manifold (accessible via triplet sensitisation or intersystem crossing) or if they lie on the singlet manifold (via direct irradiation). This information is essential to generate some understanding, also allowing us to generalise the results in a qualitative way. Thus, our purpose in discussing DBH is to illustrate how these goals can be achieved in practise.

Figure 20 (Adapted from Ref. 104.)

The reaction pathways for the photochemistry of 2,3-diazabicyclo [2.2.1] hept-2-ene (DBH) species (**3**) are illustrated schematically in Figure 20 as a sequence of structures along a network of reaction paths. The DBH species (**3**) and its derivatives denitrogenate photochemically (and thermally) through a α C-N cleavage to yield cyclopentanediyl 1,3 biradicals (**7** and **8**) . These biradicals usually cyclize to housanes or they may undergo rearrangement to form cyclopentenes via 1,2 hydrogen-shift. Photochemical transformations of DBH derivatives other than denitrogenation have been observed in a few cases. When certain prerequisites (e.g., increased ring stiffness and strain effects) are met, β C-C cleavage occurs. Increased ring stiffness due to the additional etheno bridge and simultaneous allylic stabilization of the resulting biradical results in the concurrent formation of azirane (**9**) and the usual housane products in DBH.

Figure 21 (Adapted from Ref. 104.)

The companion schematic representation of the diazenyl region of the computed potential surface is shown in Figure 21 where the intermediates are labelled in the same way as Figure 20. The accuracy of the methodology used in this study has been tested against other azoalkane spectroscopic data[105]. For instance, the computed 0–0 singlet excitation energies are 84.0 kcal/mol [82.7 including zero point energy (ZPE) correction] for pyrazoline (experimental value 82 kcal/mol) and 73.7 kcal/mol for 2,3-diazabicyclo[2.2.2]oct-2-ene (DBO) (**12**) (experimental value 76 kcal/mol). Second, the energy barriers for α C-N bond cleavage of singlet-excited pyrazoline and DBO are 7.6 (6.4 including ZPE correction) and 11.4 kcal/mol, which compares with experimental values of 6-9 for a pyrazoline derivative and 8.6–10.2 kcal/mol for DBO derivatives.

Structure 12

Three cyclic excited state species are reached following evolution from the Franck-Condon region: two metastable singlet (n-π*) and triplet (n-π*) species (**4** and **6**) and a

stable excited state $^3(n\text{-}\pi^*)$-$^3(\pi\text{-}\pi^*)$ intermediate (**5**). **4** can decay directly to S_0 (via the conical intersection labelled **10**,**11**) or undergo ISC to generate **5** or/and **6**. **6** can directly decay to the T_1 diazenyl biradical or undergo IC to generate the mixed $^3(n\text{-}\pi^*)$-$^3(\pi\text{-}\pi^*)$ intermediate **5**. Finally, the much more stable **5** cannot be converted to the other excited state intermediates but can only react via either α C–N and β C–C cleavage (to generate **11** and **9**, respectively).

It is clear that the photochemistry of azo compounds is complex because of the delicate intertwining of the $^3(n\text{-}\pi^*)$, $^3(\pi\text{-}\pi^*)$, and $^1(n\text{-}\pi^*)$ states. The surface crossing region of the diazenyl biradicals is quite novel in that a four fold crossing occurs, i.e., the $^1(n\text{-}\pi^*)/S_0$ crossing occurs at the same geometry as the $^3(n\text{-}\pi^*)$ /$^3(\pi\text{-}\pi^*)$ crossing (see structure **10**,**11** in Figure 21). The diazenyl biradical exists in C-N-N bent forms or in a C-N-N linear form. The bent forms correspond to real biradical intermediates with three possible conformations (exo, endo **11**, or exo-endo **10**, see Figure 20) and are generated by decay at the conical intersection corresponding to the linear form (see Figure 21). Indeed the linear form corresponding to structure **10**,**11** corresponds to an *highly unstable* configuration where the S_0, $^3(\pi\text{–}\pi^*)$, $^3(n\text{–}\pi^*)$ and $^1(n\text{–}\pi^*)$ states are degenerate and forms a multiple funnel. This is entered via alpha-cleavage by overcoming the S_1 or T_2 $^{1/3}(n\text{–}\pi^*)$ transition structures shown in Figure 21.

Figure 22

In Figure 22 we show the molecular and electronic structure of DBH at the conical intersection **10**,**11**. The origin of the four-fold crossing can easily be rationalised from the character of the two unpaired electrons in these structures (see dotted line in Figure 22). These two electrons can be considered almost uncoupled from each other, and since the coupling between the two radical centres is so small, the triplet and singlet states must be degenerate. Furthermore, one nitrogen atom is left with a singly occupied *p*-orbital and

a lone-pair located along orthogonal axes in space. The $^1(n–\pi^*)$ and $^3(n–\pi^*)$ states can be derived from the S_0 and $^3(\pi–\pi^*)$ states by swapping the relative occupancies of the singly occupied *p*-orbital and lone-pair. However this difference will not affect the energy and therefore all four states [$^1(n–\pi^*)$, S_0, $^3(n–\pi^*)$ and $^3(\pi–\pi^*)$] will be degenerate. This behaviour is consistent with the directions defined by the gradient difference and derivative coupling vectors at the multiple funnel (corresponding to "superimposed" S_0/S_1 and T_1/T_2 conical intersections) which indicate the type of molecular distortion required to lift the degeneracy. These vectors correspond to two "orthogonal" bendings of the N-N-C angle, which would split the degeneracy by increasing the coupling between the two radical centres.

The decay channel for the triplet-sensitised photolysis also has an unusual surface topology which is indicated in Figure 21. In the Franck-Condon region, T_2 has $(\pi–\pi^*)$ character and lies ~34 kcal mol^{-1} above T_1 which has $(n–\pi^*)$ character. As the structure of the molecule gets distorted from the Franck-Condon geometry, the $^3(\pi–\pi^*)$ and $^3(n–\pi^*)$ states become strongly mixed so that it becomes difficult to distinguish between the two triplet states, especially at structures where the C–N=N–C bridge is twisted. In other words, the electronic structures of the T_1 and T_2 states become a combination of $(\pi–\pi^*)$ and $(n–\pi^*)$ configurations. Near the triplet $(n–\pi^*)$ energy minimum (**6**) there is a conical intersection between the $(\pi–\pi^*)$ and $(n–\pi^*)$ triplet states. The electronic structure of the T_1 and T_2 states in the vicinity of the intersection can be understood on the basis of the derivative coupling and gradient difference vectors. The derivative coupling vector involves an N-N-C bending, and the gradient difference vector involves twisting of the C–N=N–C bridge (see Figure 21). The N-N-C bending distortion causes the "pure" $(n–\pi^*)$ and $(\pi–\pi^*)$ states to cross. Thus on one side of the upper (T_2) cone is the $(n–\pi^*)$ state and on the other side is the $(\pi–\pi^*)$ structure (this structure corresponds to a steep T_2/T_1 intersection point). No stable $(\pi–\pi^*)$ minimum has been located on T_2. The orthogonal C–N=N–C distortion has the effect of producing "mixed" $(n–\pi^*)$ and $(\pi–\pi^*)$ states, i.e., states which can be represented by a mixture of $(n–\pi^*)$ and $(\pi–\pi^*)$ character.

Thus decaying from the tip of the conical intersection in the direction of the gradient difference vector generates the mixed (n–π^*)-(π–π^*) minimum (**5**) on the T_1 state (in this structure, the n and π orbitals are strongly mixed so that the location of the two radical centres is not unambiguous). These effects are typical of the presence of a conical intersection: as one moves in a circle centred on the conical intersection point, the wavefunction changes in a continuous fashion from (n–π^*) to (n–π^*)+(π–π^*) to (π–π^*) to (π–π^*)-(n–π^*) to -(n–π^*).

From the preceding discussion, a few of the complexities of the photochemistry that is typical of carbonyl and azo-compounds are apparent. Results on the olefin-carbonyl Paterno-Buchi system[30], α,β-enones[31], β,γ-enones[32], azo-compounds (diazomethane[33] and cyclic diazoalkenes[104]) and acylcyclopropenes[34] photorearrangements show similar features. Here one encounters four-fold intersections as well as conical intersections and singlet triplet crossings. Thus the potential surfaces are more complex than in hydrocarbon photochemistry.

The S1/S0 Conical Intersection of Protonated Schiff Bases

The photoisomerization of protonated Schiff bases (protonated imines) occurs along a fully barrierless reaction path[37,38,39,40] (see model surface in Figure 4b). However, due to the different electronic nature of the S_1 state, the molecular structure and electronic distribution of the lowest-lying conical intersection is completely different from that of polyene hydrocarbons. The S_1 state of *cis* $C_5H_6NH_2^+$, a short protonated Schiff base analogue of *tZt* hexa-1,3,5-triene (**13**), is ionic $1B_u$-like[37] , whereas the S_1 energy surface of the corresponding polyene[106] is the covalent $2A_g$ state. In what follows, we will see that relaxation in this ionic state leads to an intramolecular charge transfer state.

Structure 13

The evolution of the *cis* $C_5H_6NH_2^+$ isomer along the *interstate* MEP connecting the **FC** structure of the *cis* isomer to the S_0 *trans* and *cis* product wells is illustrated in Figure 23.

Figure 23 (From Ref. 37.)

Along this path, the energy difference between the S_1 and S_2 (covalent $2A_g$-like) states is large (>25 kcal mol^{-1}), and thus it appears that covalent S_2 is not involved in the reaction. The S_1 relaxation path ends at a point where the S_1 ($1B_u$-like) and S_0 potential energy surfaces cross at a conical intersection. The intersection point has a central double bond twisted by ~80°, which provides a route for fully efficient non-adiabatic *cis-trans* isomerization. Starting from this point, we have located, via computation, two S_0 relaxation paths. The first path is a continuation of the excited state path and ends at the *all-trans* $C_5H_6NH_2^+$ well. The second path describes the back-formation of the reactant.

Whereas both the doubly excited π-π* state of polyenes and singly excited n-π* state of azoalkanes and carbonyl compounds are diradical in nature and do not involve charge transfer from a region of the molecule to another, the singly excited $\pi-\pi^*$ state of protonated Schiff bases does. Figure 24 shows the evolution of the Mulliken charges (with hydrogens summed into neighbouring heavy atoms) along the reaction co-ordinate. The *cis* $S_0 \rightarrow S_1$ **FC** excitation results in a partial single electron transfer towards the NH_2 end of the molecule which is consistent with the charge transfer associated with the HOMO-LUMO singly excited $1B_u$-like nature of S_1[107,108]. Accordingly, the positive charge migrates towards the -CH_2 molecular end. The most striking feature is the large, but regular, increase (from ~0.0 to +0.39) of the charge at the γ carbon centre along the S_1 path. This centre is adjacent to the rotating bond, and a stabilization of its positive charge must have an important effect on the stability of the twisted configuration. Along the isomerization co-ordinate the excited state charge distribution is smoothly changed and

this change continues into the ground state branch of the reaction (i.e., after decay) where the positive charge is shifted back toward the -NH_2 molecular end. As shown in Figure 24, in the vicinity of the conical intersection point about 70% of the positive charge is localised on the allyl fragment due to depopulation of its singly occupied molecular orbital (SOMO). Note that in the *cis* $C_5H_6NH_2^+$ isomer, the increase in polarization along the computed MEP is gradual and a polarization corresponding to the migration of ~0.5 electrons towards the -CH-CH=NH_2 is already present in the untwisted **FC** region. This situation is described by the four resonance formulae reported in Figure 25.

Figure 24 (Adapted from Ref. 37.)

Figure 25 (From Ref. 37.)

The existence of a conical intersection point and the motion of charge observed along the computed isomerization co-ordinate can be rationalised using the "two-electron two-orbital model" of Michl, Bonacic-Koutecky, et al.[10,109] According to this theory, the twisted conical intersection structure corresponds to a "critically heterosymmetric biradicaloid". A *heterosymmetric biradicaloid* is a structure where two localised orbitals have different energies but do not interact. This is the situation found in the conical intersection structure presented above where one has that the SOMO π-orbital of the allyl fragment and the SOMO π-orbital of the -$CHCH_2NH_2^+$ fragment are not overlapping. In this condition, the energy separation of the ionic S_1 and covalent S_0 states depends on the difference between the ionization potential of the allyl SOMO and the electron affinity of the -$CHCH_2NH_2^+$ SOMO. These quantities can be changed as a function of the fragment structure. Thus along the last part of the S_1 reaction co-ordinate the geometry of the two fragments is such that these energies become equal. Consequently, the S_1 energy is lowered, and ultimately the S_1 surface crosses with the S_0 surface. This interpretation is strongly supported by the π electron densities for the degenerate S_0 and S_1 states reported

in Figure 26. In the $S_0 \rightarrow S_1$ transition, the two SOMO π-orbitals electron occupation is shown to differ by one electron shift from the allyl fragment to the $-CHCH_2NH_2^+$ fragment, according to the previous model.

Figure 26 (From Ref. 37.)

Competitive Ground State Relaxation Paths from Conical Intersection

We now return to the problem of branching at a conical intersection that was discussed briefly in the previous section. For a photochemical reaction involving decay at a conical intersection, the reaction co-ordinate will have two branches. The first (excited state) branch describes the evolution of the molecular structure of the excited state intermediate until a decay point is reached. At this point, the second (ground state) branch of the reaction co-ordinate begins, which describes the relaxation process ultimately leading to product formation. As we have discussed previously, the ground state relaxation paths departing from a single conical intersection point can be unambiguously defined and computed with a gradient-driven method[52]. We will now illustrate an application of such methods to the description of the radiationless decay and competitive photoproduct formation process in cyclohexadiene (**CHD**)/*cZc*-hexatriene (***cZc*-HT**) (**1**) system[36,82,110] in more detail.

Irradiation at 254 nm transforms 2,5-di-*tert*-butylhexa-1,3,5-triene (**14**) (a hexatriene with a dominant *cZc* equilibrium conformation) into the corresponding cyclohexadiene (**15**) with a 0.54 quantum yield. The reverse reaction transforms 1,4-di-*tert*-butylcyclohexa-1,3-diene (**15**) into the corresponding hexatriene (**14**) with a 0.46 quantum yield[83-85]. Consistently, the computed structure of the low-lying part of the S_1 ($2A_1$) potential energy surface of these molecules shows that both the direct

(**CHD** → ***cZc*-HT**) and reverse (***cZc*-HT** → **CHD**) photochemical reactions involve the formation and decay of a common excited state intermediate[110] (see Figure 27).

Structures 14 and 15

Figure 27 (From Ref. 82.)

This intermediate corresponds to excited state ***cZc*-HT** (***cZc*-HT***), and it is predicted to decay to the ground ($1A_1$) state via a conical intersection (**CI$_{CHD}$**) which has been located ~1 kcal mol^{-1} above ***cZc*-HT*** (see Figure 27a). The detailed structure of **CI$_{CHD}$** is given in Figure 15. This is a polyene type conical intersection showing an *interchain* -$(CH)_3$- kink.

Decay through a conical intersection and the subsequent evolution on the ground state surface can be studied using quantum or semi-classical dynamics[53,99,111]. For a "cold" or thermalized excited state of a sizeable organic molecule, the structure of the potential energy surface is expected to play the dominant role in determining the *initial* molecular motion in the decay region. Thus, one expects that excited state stationary points and MEP will provide the important mechanistic information. Given the tetraradical electronic nature of this structure, relaxation from **CI$_{CHD}$** may occur along three different routes, as illustrated in Figure 16 and Figure 27b. Each route is associated with a different bond formation mode which is, in turn, driven by the re-coupling of four weakly interacting electrons. Accordingly, the route labeled **P$_1$** leads to relaxation towards ***cZc*-HT**, the route labeled **R** leads to **CHD,** and the route labeled **P$_2$** leads to a methylenecyclopentene diradical (**MCPD**). The mechanism of product formation in **CHD** photochemistry, in the limit of a "cold" excited state, has been investigated via a systematic search for the ground state relaxation paths departing in the region of **CI$_{CHD}$** and defining the accessible product valleys. We assume that: (i) the photoproducts originate from an excited state intermediate which is sufficiently "cold" that the ground

state trajectories lie very close to the computed MEP, and (ii) the surface hop occurs in the vicinity of the optimised conical intersection point. The results of these computations yield a description of the ground state relaxation paths departing in the vicinity of the $\mathbf{CI_{CHD}}$ structure. The results are illustrated schematically in Figure 17 (see also the corresponding discussion presented in the previous section).

The excited state reaction path connecting the intermediate ***cZc*-HT*** to $\mathbf{CI_{CHD}}$ leads to an intermediate or slightly sloped conical intersection (see Figures 8c and 8b). The excited state path controls the motion leading to decay at $\mathbf{CI_{CHD}}$, and the ground state relaxation paths control the evolution following the decay and the photoproduct formation process. With the hypothesis that significant picosecond vibrational relaxation takes place in solution at room-temperature, the IRD computed in the region of the conical intersection provide insight into the mechanism of the **CHD**/***cZc*-HT** photochemical interconversion. The ***cZc*-HT*** intermediate which is produced by either **CHD** or ***cZc*-HT** irradiation[110], decays via a facile vibrational displacement leading towards the $\mathbf{CI_{CHD}}$ decay point. After decay, the reaction path bifurcates along two ground state relaxation valleys leading to **CHD** and ***cZc*-HT**. A third relaxation valley leading to **MCPD** is not directly connected to the conical intersection point $\mathbf{CI_{CHD}}$ and originates after the energy ridge $\mathbf{RDG_{MCPD}}$ splits into two new ridges (comprising the **MCPD** "valley") around 1.0 amu$^{1/2}$bohr distance from the decay point (see Figure 17). Distances are measured in mass-weighted cartesian coordinates as defined in Ref. 81.

Figure 28

The distances of the initial part of the **CHD**, ***cZc*-HT**, **MCPD** valleys from the decay point and steepness of the slope provides qualitative information on the extent of the "catchment region" associated with a specific photoproduct (see Figure 28). A path (i.e., a MEP determined via IRD computations) which develops close to the conical intersection point and which is lower in energy will be associated with a larger "catchment

region" and therefore there will be a higher probability of populating the associated valley upon decay from the conical intersection. Figure 28 (see also the model surface in Figure 17) suggests that the size of the **CHD** and ***cZc*-HT** "catchment regions" must be similar. Thus we expect that the decay of ***cZc*-HT*** will generate the products **CHD** and ***cZc*-HT** with similar yields. Hence, the photolysis of **CHD** is predicted to generate ***cZc*-HT** with a quantum yield $\Phi_{cZc\text{-HT}} < 1$ because of the competitive **CHD** back formation. On the other hand, the computational results suggest that **MCPD** can only give low quantum yield in the photolysis of **CHD** since the **MCPD** product formation path has a higher valley with respect to the other paths. Furthermore, the **MCPD** product formation path is topologically inhibited because, in the immediate vicinity of the conical intersection, it corresponds to a ridge (i.e., $\mathbf{RDG_{MCPD}}$) and ridge-like paths will only be populated at a high kinetic energy. Because the ridge pathway is not populated, the photolysis of either **CHD** or ***cZc*-HT** must have a similar outcome. In fact, since both these reactants yield the same ***cZc*-HT*** $2A_1$ intermediate[110] ***cZc*-HT** is predicted to yield **CHD** with a quantum yield $\Phi_{cZc\text{-HT}\rightarrow\text{CHD}}$ which is related to the quantum yield of ***cZc*-HT** produced via **CHD** photolysis ($\Phi_{\text{CHD}\rightarrow cZc\text{-HT}}$) by the relation $\Phi_{cZc\text{-HT}\rightarrow\text{CHD}} \approx (1\text{-}\Phi_{\text{CHD}\rightarrow cZc\text{-HT}})$.

The interpretation of the **CHD**/***cZc*-HT** photolysis just presented is compatible with the available experimental data. The ca. 1 kcal mol^{-1} excited state energy barrier computed via multireference MP2 theory[36] is consistent with the observed picosecond lifetime of the $2A_1$ state following **CHD** direct irradiation[4,5]. Although there are no measurements of $\Phi_{\text{CHD}\rightarrow\text{CHD}}$ (i.e., **CHD** back-formation during photolysis of **CHD**) or $\Phi_{cZc\text{-HT}\rightarrow\text{CHD}}$ (i.e., **CHD** formation during photolysis of ***cZc*-HT**), $\Phi_{\text{CHD}\rightarrow cZc\text{-HT}}$ is 0.41,[4,5] i.e., suggesting efficient **CHD** back-formation. On the other hand, irradiation of 2,5-di-*tert*-butylhexa-1,3,5-triene (**14**) produces 1,4-di-*tert*-butylcyclohexa-1,3-diene (**15**) with a 0.54 quantum yield. The reverse reaction occurs with a 0.46 quantum yield[83-85] in agreement with the predicted relationship $\Phi_{\text{CHD}\rightarrow cZc\text{-HT}} \sim (1\text{-}\Phi_{cZc\text{-HT}\rightarrow\text{CHD}})$. In other substituted and polycyclic molecules[86,87] steric and strain effects may

greatly differentiate the slopes of the **CHD** and ***cZc*-HT** valleys leading to values of Φ_{CHD}, $\Phi_{cZc\text{-}HT}$ far from 0.5.

Competitive Excited State Photoisomerization Paths

The *all-trans* hepta-2,4,6-trieniminium cation (a "longer" protonated Schiff base with four conjugated double-bonds) has the S_1 MEP which is similar to the MEP of Figure 23. However, in contrast to the short protonated Schiff base discussed above, this molecule may undergo *trans* → *cis* isomerization at either of the double-bonds in position 2 and 4 as illustrated in Scheme 1.

Scheme 1 (From Ref. 112.)

The presence of competing channels on the excited state that are barrierless or nearly barrierless (see model surface in Figure 4b) is an interesting feature of longer protonated Schiff bases[39,112]. Here we characterise the S_1 MEPs of both these isomerization processes.

Figure 29 (From Ref. 112.)

In Figure 29 we report the two MEPs. Again the structure of such paths is similar to the one of Figure 23 but with a longer energy plateau (from 1 to 3 a.u. and from 1 to 5 a.u. for the C_2-C_3 and C_4-C_5 isomerization, respectively). The two paths are nearly barrierless with only a <1 kcal mol^{-1} energy difference along the long plateau region (in favour of the isomerization at position C_2-C_3). However, the initial part of the MEPs, which is dominated by double-bond expansion, is similar. Thus, in contrast with 2-*cis*-$C_5H_6NH_2^+$, the MEP co-ordinate of this longer protonated Schiff base shows that evolution along the torsional co-ordinate (and therefore either of the two competing paths) begins only after relaxation in the vicinity of the planar stationary point **SP**. Initial

relaxation along a totally symmetric mode followed by motion along non totally symmetric (twisting) modes seems to be a general feature of the excited state behaviour of these and closely related compounds (see Ref. 112).

The results of analytical frequency computations[112] confirm that, in a similar fashion to the short protonated Schiff base, the **FC** structure evolves along a co-ordinate dominated by totally symmetric stretching modes, and the structure of region I is that of a valley (see Figure 30).

Figure 30 (From Ref. 112.)

This is also confirmed by the direction of the gradient at the **FC** point and by the fact that at 0.73 a.u. distance there are real (although extremely small) frequencies (8 and 59 cm^{-1}) along the two relevant torsional modes. As seen in the case of the shorter molecule 2-*cis*-$C_5H_6NH_2^+$, there is one imaginary frequency at the S_1 stationary point. However, the magnitude of this imaginary frequency and of the frequency corresponding to the alternative isomerization mode are only 45 i (C_2-C_3 torsional mode) and 62 cm^{-1} (C_4-C_5 torsional mode), thus reflecting the existence of the energy plateau and the general flatness of region II, as well as competition between the two isomerization processes.

CONCLUSIONS

We hope the reader has been convinced that it is technically feasible to describe a photochemical reaction co-ordinate, *from energy absorption to photoproduct formation*, using methods that are available in standard quantum chemistry packages such as Gaussian 94 (eg. OPT=Conical). The conceptual problems that need to be understood in order to apply quantum chemistry to photochemistry problems relate mainly to the characterisation of the conical intersection funnel. We hope that the theoretical discussion of these problems and the examples given in the last section can provide the information necessary for the reader to carry out computations.

Any mechanistic study undertaken using quantum chemistry methods requires considerable physical and chemical insight. Thus for a thermal reaction, there is no method that will generate automatically all the possible mechanistic pathways that might be relevant. Rather, one still needs to apply skills of chemical intuition and make sensible hypotheses that can then be explored computationally. In excited state chemistry, these problems are even more difficult, and we hope the examples given in the last section are a step in providing this required insight. However, the DBH example shows just how complex these problems can become when many electronic excited states are involved.

In addition to the conceptual and physical problems associated with mechanistic studies in photochemistry, the actual computations are technically difficult to carry out. Wheras with single reference quantum chemistry methods such as SCF, DFT, CIS etc. require no physical insight to use, multi-reference methods such as CAS-SCF require physical insight and technical skill to use effectively. One needs to select a reference space from the outset. Thus, one needs a chemical model or picture of the nature of the excited states involved, and then one must choose a reference space that is compatible with this initial insight. Obviously, one's initial choice must be refined as a computational study progresses but an initial insight is a fundamental prerequisite. It may be that time-

dependent DFT or EOM[57-60] methods will prove to be useful in excited state mechanistic problems. These methods can be used as a black-box. But whether they can be applied to the type of problems which we have discussed remains an open question.

For the future, it is clear that dynamics methods are almost essential if one is going to target the interesting results that are coming from femtosecond spectroscopy and to study quantum yields. These methods are just beginning to be exploited, and this is an exciting new direction for quantum chemistry. Further, in this tutorial we have not commented on the role of the solvent or the role of the environment provided by a biochemical system. There are no special problems related to excited state chemistry for the former, and one can look forward to applications in this field to appear in the near future in biochemical systems .

Acknowledgements

This article is based (in part) on lecture courses given by M. Olivucci at the EPA Summer School in Noorwick, Holland, June 16-20, 1998, and by M. A. Robb at the Jyvaskyla Summer School, Jyvaskyla, Finland, August 3-21, 1998. We are grateful to the organisers of these schools for the opportunity to present this material and especially to the participants for their searching questions.

We are also pleased to acknowledge co-workers (Michael Bearpark, Paolo Celani, Stephane Klein, Naoko Yamamoto, Barry Smith, Thom Vreven) whose work we have used in this tutorial and who have commented on various parts of the manuscript.

This research has been supported (in part) by an EU TMR network grant (ERB 4061 PL95 1290, Quantum Chemistry for the Excited State). We are also grateful to NATO for a travel grant (CRG 950748). The continuous support of the EPSRC (UK) under grants H58070 H94177 J/25123 and K 04811 is also gratefully acknowledged.

References

1. D. G. Truhlar and M. S. Gordon, *Science*, **249**, 491 (1990). From Force-Fields to Dynamics - Classical and Quantal Paths.
2. A. H. Zewail, *J. Phys. Chem.*, **100**, 12701 (1996). Femtochemistry: Recent Progress in Studies of Dynamics and Control of Reactions and Their Transition States.
3. M. O. Trulson and R. A. Mathies, *J. Phys. Chem.*, **94**, 5741 (1990). Excited-State Structure and Dynamics of Isoprene from Absolute Resonance Raman Intensities.
4. P. J. Reid, S. J. Doig, S. D. Wickham, and R. A. Mathies, *J. Am. Chem. Soc.*, **115**, 4754 (1993); and references cited therein. Photochemical Ring-Opening Reactions are Complete In Picoseconds - A Time-Resolved UV Resonance Raman-Study of 1,3-Cyclohexadiene.
5. S. Pullen, L. A. Walker II, B. Donovan, and R. J. Sension, *Chem. Phys. Lett.*, **242**, 415 (1995). Femtosecond Transient Absorption Study of the Ring-Opening Reaction of 1,3-Cyclohexadiene.
6. D. R. Cyr and C. C. Hayden, *J. Chem. Phys.*, **104**, 771 (1996). Femtosecond Time-Resolved Photoionization and Photoelectron-Spectroscopy Studies of Ultrafast Internal-Conversion in 1,3,5-Hexatriene.
7. H. Kandori, Y. Katsuta, M. Ito, and H. Sasabe, *J. Am. Chem. Soc.*, **115**, 2669 (1995). Femtosecond Fluorescence Study of the Rhodopsin Chromophore in Solution.
8. Q. Wang, R. W. Schoenlein, L. A. Peteanu, R. A. Mathies, and C. V. Shank, *Science*, **266**, 422 (1994). Vibrationally Coherent Photochemistry in the Femtosecond Primary Event of Vision.
9. A. Gilbert and J. Baggott, *Essentials of Molecular Photochemistry*, Blackwell Scientific Publications, Oxford, 1991.
10. J. Michl and V. Bonacic-Koutecky, *Electronic Aspects of Organic Photochemistry*, Wiley, New York, 1990.

11. M. Klessinger and J. Michl, *Excited States and Photochemistry of Organic Molecules*, VCH Publishers, New York, 1994.

12. B. O. Roos, in *Adv. Chem. Phys. (Ab Initio Methods in Quantum Chemistry -II)*, K. P. Lawley, Ed., Wiley, New York, 1987, Vol. 69, pp. 399-446. The Complete Active Space Self Consistent Field Method and its Applications in Electronic Structure Calculations.

13. M. Desouter-Lecomte and J. C. Lorquet, *J. Chem. Phys.*, **71**, 4391 (1979). Nonadiabatic Interactions in Unimolecular Decay. IV. Transition Probability as a Function of the Massey Parameter.

14. F. Bernardi, M. Olivucci, and M. A. Robb, *Chem. Soc. Rev.*, **25**, 321 (1996). Potential Energy Surface Crossings in Organic Photochemistry.

15. F. Bernardi, M. Olivucci, J. Michl, and M.A. Robb, *The Spectrum*, **9**, 1 (1997). Conical Intersections in the Theory of Organic Singlet Photochemistry.

16. D. R. Yarkony, *Acc. Chem. Res.*, **31**, 511 (1998). Conical Intersections: Diabolical and Often Misunderstood.

17. D. R. Yarkony, *J. Phys. Chem.*, **100**, 18612 (1996). Current Issues in Nonadiabatic Chemistry.

18. W. T. A. M. Van der Lugt, and L. J. Oosteroff, *J. Am. Chem. Soc.*, **91**, 6042 (1969). Symmetry Control and Photoinduced Reactions.

19. E. Teller, *Isr. J. Chem.*, **7**, 227 (1969). Internal Conversion in Polyatomic Molecules.

20. H. E. Zimmerman, *J. Am. Chem. Soc.*, **88**, 1566 (1966). Molecular Orbital Correlation Diagrams, Mobius Systems, and Factors Controlling Ground- and Excited - State Reactions. II.

21. J. Michl, *Mol. Photochem.*, **4**, 243 (1972). Photochemical Reactions of Large Molecules. I. A Simple Physical Model of Photochemical Reactivity.

22. W. Fuss, K. L. Kompa, S. Lochbrunner, and A. M. Muller, *Chem. Phys.*, **232**, 174 (1998). Pathway Approach to Ultrafast Photochemistry: Potential Surfaces, Conical Intersections and Isomerizations of Small Polyenes.

23. B. E. Kohler, *Chem. Rev.*, **93**, 41 (1993). Octatetraene Photoisomerization.

24. H. Petek, A. J. Bell, Y. S. Choi, K. Yoshihara, B. A. Tounge, and R. L. Christensen, *J. Chem. Phys.*, **98**, 3777 (1993). The 2^1A_g State of t*rans,trans*-1,3,5,7-Octatetraene in Free Jet Expansions.

25. I. J. Palmer, I. N. Ragazos, F. Bernardi, M. Olivucci, and M. A. Robb, *J. Am. Chem. Soc.*, **115**, 673 (1993). An MC-SCF Study of the S_1 and S_2 Photochemical Reactions of Benzene.

26. M. J. Bearpark, F. Bernardi, S. Clifford, M. Olivucci, M.A. Robb, and B. R. Smith, *J. Am. Chem. Soc.*, **118**, 169 (1996). The Azulene S_1 State Decays via a Conical Intersection: A CASSCF Study with MMVB Dynamics.

27. P. Celani, M. Garavelli, S. Ottani, F. Bernardi, M. A. Robb, and M. Olivucci, *J. Am. Chem. Soc.*, **117**, 11584 (1995). Molecular Trigger for the Radiationless Deactivation of Photoexcited Conjugated Hydrocarbons.

28. M. Garavelli, P. Celani, N. Yamamoto, F. Bernardi, M. A. Robb, and M. Olivucci, *J. Am. Chem. Soc.*, **118**, 11656 (1996). The Structure of the Non-adiabatic Photochemical trans → cis Isomerization Channel in all-trans Octatetraene.

29. M.Garavelli, P. Celani, F. Bernardi, M. A. Robb, and M. Olivucci, *J. Am. Chem. Soc.*, **119**, 11487 (1997). Force fields for "Ultrafast" Photochemistry: The S_2 $(1B_u) \rightarrow S_1(2A_g) \rightarrow S_0$ $(1A_g)$ Reaction Path for *all-trans*-Hexa-1,3,5-triene.

30. I. J. Palmer, I. N. Ragazos, F. Bernardi, M. Olivucci, and M. A. Robb, *J. Am. Chem. Soc.*, **116**, 2121 (1994). An MC-SCfF Study of the (Photochemical) Paterno-Buchi reaction.

31. M. Reguero, M. Olivucci, F. Bernardi, and M. A. Robb, *J. Am. Chem. Soc.*, **116**, 2103 (1994); and references cited therein. Excited state Potential Surface Crossings in Acrolein: A Model for Understanding the Photophysics and Photochemistry of $\alpha\ \beta$ enones.

32. S. Wilsey, M. J. Bearpark, F. Bernardi, M. Olivucci, and M. A. Robb, *J. Am. Chem. Soc.*, **118**, 176 (1996). The Mechanism of the Oxa-di-π-methane and [1,3]-Acyl Sigmatropic Rearrangements of β,γ-enones: A Theoretical Study.

33. N. Yamamoto, F. Bernardi, A. Bottoni, M. Olivucci, M. A. Robb, and S. Wilsey, *J. Am. Chem. Soc.*, **116**, 2064 (1994) and references cited therein. Mechanism of Carbene Formation from the Excited States of Diazirine and Diazomethane: An MC-SCF Study.

34. S. Wilsey, M. J. Bearpark, F. Bernardi M. Olivucci, and M. A. Robb, *J. Am. Chem. Soc.*, **118**, 4469 (1996). The Role of Degenerate Biradicals in the Photorearrangement of Acylcyclopropenes to Furans.

35. P. Celani, F. Bernardi, M. Olivucci, and M. A. Robb, *J. Chem. Phys.*, **102**, 5733 (1995). Excited-State Reaction Pathways for *s-cis* Buta-1,3-diene.

36. P. Celani, S. Ottani, M. Olivucci, F. Bernardi, and M. A. Robb,*J. Am. Chem. Soc.*, **116**, 10141 (1994). What Happens during the Picoseconds Lifetime of $2A_1$ Cyclohexa-1,3-diene? A CAS-SCF Study of the Cyclohexadiene / Hexatriene Photochemical Interconversion.

37. M. Garavelli, P. Celani, F. Bernardi, M. A. Robb, and M. Olivucci, *J. Am. Chem. Soc.*, **119**, 6891 (1997). The $C_5H_6NH_2(+)$ Protonated Schiff Base: an Ab-initio "Minimal" Model for Retinal Photoisomerization.

38. T. Vreven, F. Bernardi, M. Garavelli, M. Olivucci, M. A. Robb, and H. B. Schlegel, *J. Am. Chem. Soc.*, **119**, 12687 (1997). Ab initio Photoisomerization Dynamics of a Simple Retinal Chromophore Model.

39. M. Garavelli, T. Vreven, P. Celani, F. Bernardi, M. A. Robb, and M. Olivucci, *J. Am. Chem. Soc.*, **120**, 1285 (1998). Photoisomerization Path for a Realistic Retinal Chromophore Model: the Nonatetraenimminium Cation.

40. M. Garavelli, F. Bernardi, P. Celani, M. A. Robb, M. Olivucci, *J. Photochem. Photobiol .A: Chem*, **114**, 109 (1998). Minimum Energy Paths in the Excited and Ground States of Short Protonated Schiff Bases and of the Analogous Polyenes.

41. W. J. Leigh and J. A. Postigo, *J. Chem. Comm.*, **24**, 1836 (1993). The Role of Central Bond Torsional Motions in the Direct cis ⇄ trans-Photoisomerization of Conjugated Dienes.

42. H. B. Schlegel, in *Adv. Chem. Phys. (Ab Initio Methods in Quantum Chemistry* -I), K. P. Lawley, Ed., Wiley, New York, 1987, Vol. 67, pp. 249-286; and references cited therein. Optimization of Equilibrium Geometries and Transition Structures.

43. J. B. Foresman and A. Frisch, in *Exploring Chemistry with Electronic Structure Methods*; Gaussian, Inc., Pittsburgh, 1996, pp. 39-60; and references cited therein. Geometry Optimizations.

44. E. Teller, *J. Phys. Chem.*, **41**, 109 (1937). The Crossing of Potential Surfaces.

45. G. Herzberg and H. C. Longuet-Higgins, *Discuss. Faraday Soc.*, **35**, 77 (1963). Intersection of Potential Energy Surfaces in Polyatomic Molecules.

46. G. J. Atchity, S. S. Xantheas, and K. Ruedenberg, *J. Chem. Phys.*, **95**, 1862 (1991). Potential Energy Surfaces Near Intersections.

47. I. N. Ragazos, M. A. Robb, F. Bernardi, and M. Olivucci, *Chem. Phys. Lett.*, **197**, 217 (1992). Optimisation and Characterisation of the Lowest Energy Point on a Conical Intersection using an MC-SCF Lagrangian.

48. G. Herzberg, in *Molecular Spectra and Molecular Structure (III. Electronic Spectra and Electronic Structure of Polyatomic Moleculaes)*, Van Nostrand Reinhold Company, New York, 1966.

49. R. F. Frey and E. R. Davidson, in *Advances in Molecular Electronic Structure Theory (Calculation and Characterization of Molecular Potential Energy Surfaces)*, T. H. Dunning, Ed., JAI Press, Inc., London, 1990, Vol. 1, pp. 213-262. The Von Neumann-Wigner and Jahn-Teller Theorems and their Consequences.

50. M. L. McKee and M. Page, in *Reviews in Computational Chemistry*, K. B. Lipkowitz and D. B. Boyd, Eds., VCH Publishers, New York, 1993, Vol. 4, pp. 35-65. Computing Reaction Pathways on Molecular Potential Energy Surfaces.

51. M. J. Bearpark, M. A. Robb, and H. B. Schlegel, *Chem. Phys. Lett.*, **223** , 269 (1994). A Direct Method for the Location of the Lowest Energy Point on a Potential Surface Crossing.

52. P. Celani, M. A. Robb, M. Garavelli, F. Bernardi, and M. Olivucci, *Chem. Phys. Lett.*, **243**, 1 (1995). Geometry Optimisation on a Hypersphere: Application to Finding Reaction Paths from a Conical Intersection.

53. H. Köppel, W. Domcke, and L. S. Cederbaum, in *Adv. Chem. Phys.*, I. Prigogine and S. A. Rice, Eds.,Wiley, New York, 1984, Vol. 57, pp. 59-246. Multimode Molecular Dynamics beyond the Born-Oppenheimer Approximation.

54. B. R. Smith, M. J. Bearpark, M. A. Robb, F. Bernardi, and M. Olivucci, *Chem. Phys. Lett.*, **242**, 27 (1995). Classical Wavepacket Dynamics through a Conical Intersection: Application to the S_1/S_0 Conical Intersection in Benzene.

55. M. A. Robb, F. Bernardi, and M. Olivucci, unpublished results (1997).

56. J. B. Foresman, M. Head-Gordon, J. A. Pople, and M. J. Frisch, *J. Phys. Chem.*, **96**, 135 (1992). Toward a Systematic Molecular Orbital Theory for Excited States.

57. M. Nooijen and R. J. Bartlett, *J. Chem. Phys.*, **107**, 6812 (1997). Similarity transformed equation-of-motion coupled-cluster theory: Details, examples, and comparisons.

58. R. J. Bartlett and J. F. Stanton, in *Reviews in Computational Chemistry*, K. B. Lipkowitz and D. B. Boyd, Eds., VCH Publishers, New York, 1994, Vol. 5, pp. 65-169. Applications of Post-Hartree-Fock Methods: A Tutorial.

59. M. E. Casida, C. Jamorski, K. C. Casida, and D. R. Salahub, *J. Chem. Phys.*, **108**, 4439 (1998). Molecular Excitation Energies to High-Lying Bound States from Time-Dependent Density-Functional Response Theory: Characterization and Correction of the Time-Dependent Local Density Approximation Ionization Threshold.

60. R. Bauernschmitt and R. Ahlrichs, *Chem. Phys. Lett.*, **256** , 454 (1996). Treatment of Electronic Excitations within the Adiabatic Approximation of Time-Dependent Density-Functional Theory.

61. N. Yamamoto, T. Vreven , M. A. Robb, M. J. Frisch, and H. B. Schlegel, *Chem. Phys. Lett.*, **250**, 373 (1996). A Direct Derivative MC-SCF Procedure.

62. Gaussian 94, M. J. Frisch, G. W. Trucks, H. B. Schlegel, P. M. W. Gill, B. G. Johnson, M. A. Robb, J. R. Cheeseman, T. Keith, G. A. Petersson, J. A. Montgomery, K. Raghavachari, M. A. Al-Laham, V. G. Zakrzewski, J. V. Ortiz, J. B. Foresman, J. Cioslowski, B. B. Stefanov, A. Nanayakkara, M. Challacombe, C. Y. Peng, P. Y. Ayala, W. Chen, M. W. Wong, J. L. Andres, E. S. Replogle, R. Gomperts, R. L. Martin, D. J. Fox, J. S. Binkley, D. J. De Frees, J. Baker, J. P. Stewart, M. Head-Gordon, C. Gonzalez, and J. A. Pople, Gaussian, Inc., Pittsburgh PA, 1995.

63. MOLCAS, Version 4. K. Andersson, M. R .A. Blomberg, M. P. Fülscher, G. Karlström, R. Lindh, P.-Å. Malmqvist, P. Neogrády, J. Olsen, B. O. Roos, A. J. Sadlej, M. Schütz, L. Seijo, L. Serrano-Andrés, P. E. M. Siegbahn, and P.-O. Widmark, Lund University, Sweden, 1997.

64. H. Dachsel, R. Shepard, J. Nieplocha, and R. J. Harrison, *J. Comput. Chem.* **18**, 430 (1997). A Massively Parallel Multireference Configuration Interaction Program: The Parallel COLUMBUS Program.

65. M. W. Schmidt, K. K. Baldridge, J. A. Boatz, S. T. Elbert, M. S. Gordon, J. J. Jensen, S. Koseki, N. Matsunaga, K. A. Nguyen, S. Su, T. L. Windus, M. Dupuis, J. A. Montgomery *J. Comput. Chem.* **14**, 1347 (1993). General Atomic and Molecular Electronic-Structure System.

66. D. B. Boyd, in *Reviews in Computational Chemistry*, K. B. Lipkowitz and D. B. Boyd, Eds., Wiley-VCH, New York, 1997, Vol. 11, pp. 373-399. Appendix: Compendium of Software and Internet Tools for Computational Chemistry.

67. J. J. McDouall, K. Peasley, and M. A. Robb, *Chem. Phys. Lett.*, **148**, 183 (1988). A Simple MC-SCF Perturbation Theory: Orthogonal Valence Bond Moller-Plesset 2 (OVB-MP2).

68. K. Andersson, P. A. Malmqvist, and B. O. Roos, *J. Chem. Phys.*, **96**, 1218 (1992). 2nd-Order Perturbation-Theory with a Complete Active Space Self-Consistent Field Reference Function.

69. P. M. Kozlowski, M. Dupuis, and E. R. Davidson, *J. Am. Chem. Soc.*, **117**, 774 (1995). The Cope Rearrangement Revisited with Multireference Perturbation-Theory.

70. J. E. Ridley and M. C. Zerner, *Theor. Chim. Acta* , **32**, 111 (1973). An Intermediate Neglect of Differential Overlap Technique for Spectroscopy: Pyrrole and the Azines.

71. J. J. P. Stewart, *J. Computer-Aided Mol. Design*, **4,** 1 (1990). Special Issue - MOPAC - A Semiempirical Molecular-Orbital Program.

72. J. Bentzian and M. Klessinger, *J. Org. Chem.*, **59**, 4887 (1994). Theoretical Investigations on the Regiochemistry and Stereochemistry of the Photochemical [2+2]-Cycloaddition of Propene.

73. M. Caselli, F. Momicchioli, and G. Ponterini, *Chem. Phys. Lett.*, **216**, 41 (1993). Modeling of the Cis-Trans Partitioning in the Photoisomerizations of Cyanines and Stilbene Derivatives.

74. F. W. Langkilde, R. Wilbrandt, A. M. Brouwer, F. Negri, F. Zerbetto, and G. Orlandi, *J. Phys. Chem. A*, **98**, 2254 (1994). Molecular-Structure of Stilbene in the T_1 State - Transient Resonance Raman-Spectra of Stilbene Isotopomers and Quantum-Chemical Calculations.

75. F. Bernardi, M. Olivucci, and M. A. Robb, *J. Am. Chem. Soc.*, **114**, 1606 (1992). Simulation of MC-SCF Results on Covalent Organic Multi-bond Reactions: Molecular Mechanics with Valence-Bond (MM-VB).

76. M. J. Bearpark, F. Bernardi, M. Olivucci, and M. A. Robb, *Chem. Phys. Lett.*, **217**, 513 (1994). Molecular Mechanics - Valence Bond Methods for Large Active Spaces: Application to Conjugated Polycyclic Hydrocarbons.

77. M. Said, D. Maynau, J. P. Malrieu, and M. A. G. Bach, *J. Am. Chem.Soc.*, **106**, 571 (1984). A Nonempirical Heisenberg Hamiltonian for the Study of Conjugated Hydrocarbons - Ground-State Conformational Studies.

78. D. Maynau, P. Durand, J. P. Duadey, and J. P. Malrieu, *Phys. Rev. A*, **28**, 3193 (1983). Direct Determination of Effective-Hamiltonians by Wave-Operator Methods. 2. Application to Effective-Spin Interactions in π-Electron Systems.

79. P. Durand and J. P. Malrieu, in *Adv. Chem. Phys. (Ab Initio Methods in Quantum Chemistry* -I), K. P. Lawley, Ed., Wiley, New York, 1987, Vol. 67, pp. 321-412. Effective Hamiltonians and Pseudo-Operators as Tools for Rigorous Modelling.

80. M. J. Bearpark, F. Bernardi, M. Olivucci, and M. A. Robb, *J. Phys. Chem. A*, **101**, 8395 (1997). Benchmarking MMVB: The Photophysics of Styrene and Indene.

81. C. Gonzalez and H. B. Schlegel, *J. Phys. Chem.*, **94**, 5523 (1990). Reaction-Path Following in Mass-Weighted Internal Coordinates.

82. M. Garavelli, P. Celani, M. Fato, M. Olivucci, and M.A. Robb, *J. Phys. Chem.* A, **101**, 2023 (1997). Relaxation Paths from a Conical Intersection: The Mechanism of Product-Formation in Cyclohexadiene/Hexatriene Photochemical Interconversion.

83. H. J. C. Jacobs, *Pure Appl. Chem.*, **67**, 63 (1995). Photochemistry of Conjugated Trienes - Vitamin-D Revisited.

84. A. M. Brouwer, J. Cornelisse, and H. J. C. Jacobs, *J. Photochem. Photobiol A: Chem.*, **42**, 117 (1988). Deuterium-Isotope Effects in the Photochemistry of 2,5-Dimethylhexatrienes and 2,5-di-*tert*-butyl-1,3,5-Hexatrienes.

85. A. M. Brouwer, J. Cornelisse, and H. J. C. Jacobs, *J. Photochem. Photobiol A: Chem.*, **42**, 313 (1988). Photochemistry of 2,5-dimethyl and 2,5-di-*tert*-butyl-1,3,5-Hexatrienes - Conformation and Reactivity - A Quantitative Study.

86. B. Matuszewski, A. W. Burgstahler, and R. S. Givens, *J. Am. Chem. Soc.*, **104**, 6875 (1982). Preservation of Chirality in the Photochemical Interconversion of *trans*-Δ-1,3-Hexalin and *trans,cis,trans*-Cyclodeca-1,3,5-triene.

87. W. G. Dauben, J. Rabinowitz, N. D. Vietmeyer, and P. H. Wendschuh, *J. Am. Chem.Soc.*, **94**, 4285 (1972). Photoequilibria between 1,3-Cyclohexadienes and 1,3,5-Hexatrienes. Photochemistry of 3-Alkyl-6,6,9,9-tetramethyl-$\Delta^{3,5(10)}$-hexalins.

88. R. Car and M. Parrinello, *Phys. Rev. Lett.*, **55**, 2471 (1985). Unified Approach for Molecular-Dynamics and Density-Functional Theory.

89. R. K. Preston and J. C. Tully, *J. Chem. Phys.*, **54**, 4297 (1971). Effects of Surface Crossing in Chemical Reactions: The H_3^+ System.

90. J. C. Tully and R. K. Preston, *J. Chem. Phys.*, **55**, 562 (1971). Trajectory Surface Hopping Approach to Nonadiabatic Molecular Collisions: The Reaction of H^+ with D_2.

91. N. C. Blais and D. G. Truhlar, *J. Chem. Phys.*, **79**, 1334 (1983). Trajectory-Surface-Hopping Study of Na ($3p\ ^2P$) + H_2 → Na ($3s\ ^2S$) + H_2 (v', j', θ).

92. M. J. Bearpark, F. Bernardi, M. Olivucci, M. A. Robb, and B. R. Smith, *J. Am. Chem. Soc.*, **118**, 5254 (1996). Can Fulvene S_1 Decay be Controlled? A CASSCF Study with MMVB Dynamics.

93. T. S. Rose, M. J. Rosker, and A. H. Zewail, *J. Chem. Phys.*, **91**, 7415 (1989). Femtosecond Real-Time Probing of Reactions. 4. The Reactions of Alkali-Halides.

94. M. J. Rosker, M. Dantus, and A. H. Zewail, *J. Chem. Phys.*, **91**, 6113 (1989). Femtosecond Real-Time Probing of Reactions. 1. The Technique.

95. T. J. Martinez, M. Ben-Nun, and G. Askenazi, *J. Chem. Phys.*, **104**, 2847 (1996). Classical Quantal Method for Multistate Dynamics - A Computational Study.

96. T. J. Martinez, M. Ben-Nun, and R. D. Levine, *J. Phys. Chem.*, **100**, 7884 (1996). Multi-Electronic-State Molecular-Dynamics - A Wave-Function Approach with Applications.

97. S. Klein, M. J. Bearpark, B. R. Smith, M. A. Robb, M. Olivucci, and F. Bernardi, *Chem. Phys. Lett*, **293,** 259 (1998). Mixed State "on the fly" Non-adiabatic Dynamics: the Role of the Conical Intersection Topology.

98. M. Amarouche, F. X. Gadea, and J. Durup, *Chemical Physics*, **130**, 145 (1989). A Proposal for the Theoretical Treatment of Multi-Electronic-State Molecular-Dynamics - Hemiquantal Dynamics with the Whole DIM Basis (HWD) - A Test on the Evolution of Excited Ar^{3+} Cluster Ions.

99. U. Manthe and H. Koppel, *J. Chem.Phys,* **93**, 1658 (1990). Dynamics on Potential-Energy Surfaces with a Conical Intersection - Adiabatic, Intermediate, and Diabatic Behavior.

100. M. N. R. Ashfold, S. G. Clement, J. D. Howe, and C. M. Western, *J. Chem. Soc. Faraday Trans.* , **89**, 1153 (1993). Multiphoton Ionization Spectroscopy of Free-Radical Species.

101. V. Vaida, *Acc. Chem. Res.*, **19**, 114 (1986). Electronic Absorption-Spectroscopy of Jet-Cooled Molecules.

102. H. Petek, A. J. Bell, R. L. Christensen, and K. Yoshihara, *SPIE*, **1638**, 345 (1992). Vibrational Spectroscopy and Picosecond Dynamics of Gaseous Trienes and Octatetraenes in S_1 and S_2 Electronic States.

103. C. A. Mead and D. G. Truhlar, *J. Chem. Phys.*, **70**, 2284 (1979). On the Determination of Born-Oppenheimer Nuclear Motion Wave Functions Including Complications due to Conical Intersection and Identical Nuclei.

104. N. Yamamoto, M. Olivucci, P. Celani, F. Bernardi, and M. A. Robb, *J. Am. Chem. Soc.*, **120**, 2391 (1998). An MC-SCF / MP2 Study of Photochemistry of 2,3-Diazabicyclo[2.2.1]hept-2 ene.

105. W. M. Nau, G. Greiner, J. Wall, H. Rau, M. Olivucci, and M. A. Robb, *Angew. Chem. International Ed.,* **37**, 98 (1998). The Mechanism for Hydrogen Abstraction by n,π* Excited Singlet States: Evidence for Thermal Activation and Deactivation through a Conical Intersection.

106. M. Olivucci, F. Bernardi, Ioannis Ragazos, and M. A. Robb, *J. Am. Chem. Soc.*, **116**, 1077 (1994). Excited state cis-trans Isomerisation of cis-Hexatriene. A CAS-SCF Study.

107. K. A. Freedman and R. S. Becker, *J. Am. Chem. Soc.*, **108**, 1245 (1986). Comparative Investigation of the Photoisomerization of the Protonated and Unprotonated Normal-Butylamine Schiff-Bases of 9-cis-Retinals, 11-cis-Retinals, 13-cis-Retinals, and all-trans-Retinals.

108. P. Du and E. R. Davidson, *J. Phys. Chem.*, **94**, 7013 (1990). Ab-initio Study on the Excitation-Energies of the Protonated Schiff-Base of 11-cis-Retinal.

109. V. Bonacic-Koutecky, K. Schöffel, and J. Michl, *Theor. Chim. Acta*, **72**, 459 (1987). Critically Heterosymmetric Biradicaloid Geometries of Protonated Schiff-Bases - Possible Consequences for Photochemistry and Photobiology.

110. P Celani, F. Bernardi, M. A. Robb, and M. Olivucci, *J. Phys. Chem.*, **100**, 19364 (1996). Do Photochemical Ring-Openings Occur on the Spectroscopic State? $1B_2$ Pathways for the Cyclohexadiene/Hexatriene Photochemical Interconversion.

111. W. Domcke and G. Stock, in *Adv. Chem. Phys.*, I. Prigogine and S. A. Rice, Eds., Wiley, New York, 1997, Vol. 100, pp. 1-169. Theory of Ultrafast Nonadiabatic Excited-State Processes and their Spectroscopic Detection in Real Time.

112. M. Garavelli, F. Bernardi, M. Olivucci, T. Vreven, S. Klein, P. Celani, and M. A. Robb, *Faraday Discuss.*, **110**, 51 (1998). Potential-energy Surfaces for Ultrafast Photochemistry: Static and Dynamic Aspects.

Figure Captions

Figure 1. Schematic view of a course of a photochemical reaction.

Figure 2. Topological relation between an avoided crossing and a conical intersection. The avoided crossing is a the cross-section through the cone along R-P. The minimum energy path is **R-CI-P** and passes through the apex of the cone.

Figure 3. "Opening" of a fast radiationless decay channel in *all-trans* octatetraene in (a) matrix isolated conditions and in (b) expanding cool-jet. (From Ref. 14).

Figure 4. "Opening" of a radiationless decay channel via conical intersection for a (a) barrier controlled reaction, (b) barrierless path, and (c) uphill path without transition state (sloped conical intersection).

Figure 5. Typical double cone topology for a conical intersection (a), and relation between the "branching space" ($\mathbf{x_1}$, $\mathbf{x_2}$) and the "intersection space" (spanning the remainder of the n-2 dimensional space of internal geometric variables (b).

Figure 6. Comparison of the role of a transition state (**TS**) in thermal reactivity (a), and the role of a conical intersection (**CI**) in photochemical reactivity (b).

Figure 7. Topological possibilities for the crossing of two states: (a) typical n-2 dimensional conical intersection between two states of the same spin multiplicity (i.e. two singlets or two triplets); (b) n-1 dimensional intersection between two states of different spin multiplicity (i.e. singlet and triplet); (c) singlet and triplet conical intersection occurring at the same geometry[32]; (d) Rennet-Teller like degeneracy[48] (a "touching" rather than a crossing). While for examples a-c the gradient of both surfaces at the crossing is different from zero, in example d it is zero.

Figure 8. Topological possibilities for conical intersections characterised according to Ref. 46: (a) peaked, (b) sloped, and (c) intermediate conical intersection.

Figure 9. Two-dimensional model surface for the photochemical *cis* → *trans* isomerization of octatetraene.

Figure 10. (a) Photochemical transformation of benzene to fulvene and benzalvene. (b) The change in spin coupling for a circuit around the apex of the **CI** in the plane $\mathbf{x_1}$, $\mathbf{x_2}$. Bold lines between atoms represent bonding interaction, whereas "up" and "down" arrows are used to designate +1/2 and -1/2 electron spin, respectively.

Figure 11. Computed S_1/S_0 conical intersection structure for benzene. The relevant geometrical parameters are in Å. The -$(CH)_3$- kink is framed. (From Ref. 25.)

Figure 12. Computed branching space vectors (gradient difference vector $\mathbf{x_1}$ and non-adiabatic coupling vector $\mathbf{x_2}$) for S_1/S_0 conical intersection of benzene.

Figure 13. General behaviour of a conical intersection optimization procedure. This is a contrived example which was started from an almost planar geometry (much further from the optimum geometry than normal practise). The curve shows the rapid approach to the degenerate situation followed by minimization (retaining the degeneracy).

Figure 14. This picture illustrates the general procedure used to locate the initial relaxation direction (IRD) toward the possible decay products. (a) General photochemical relaxation path leading (via conical intersection decay) to three different final structures, (b) potential energy surface for a "model" elliptic conical intersection plotted in the branching plane, and (c) corresponding energy profile (as a function of the angle α) along a circular cross section centred on the conical intersection point and with radius *d*.

Figure 15. Computed S_1/S_0 conical intersection structure for the problem of cyclohexadiene/hexatriene photochemical interconversion. The relevant geometrical parameters are in Å.

Figure 16. (a) The three different electron recoupling patterns from the conical intersection shown in Figure 15 and (b) the branching of the photochemical reaction path through a conical intersection.

Figure 17. Computed relaxation paths from the conical intersection of Figure 15. While only two similar valleys develop close to the crossing point, the third one (initially a ridge) starts far and is energetically unfavoured.

Figure 18. "Occupancy" of the states (i.e. projection on the adiabatic basis states of *a(t)* given in Eq. [22]) for a molecular system wavefunction on the S_1 excited (Ψ_1) or S_0 ground (Ψ_0) states.

Figure 19. Structures of S_1/S_0 conical intersections in conjugated hydrocarbons showing the -$(CH)_3$- kink structure in *all-trans* octatetraene, benzene, and cyclohexadiene. Also the typical triangular D_1/D_0 conical intersection for H_3 is illustrated.

Figure 20. Sequence of structures along the reaction paths network computed in the photochemistry of 2,3-diazabicyclo [2.2.1] hept-2-ene (DBH) species (**3**). (Adapted from Ref. 104.)

Figure 21. Companion schematic representation for the computed diazenyl region potential surface (the intermediates are labelled in the same way as Figure 20). (Adapted from Ref. 104.)

Figure 22. DBH ground state equilibrium structure **3** and molecular and electronic structure for the computed low-lying real crossing **10,11**. In this system the $S_1(n\text{-}\pi^*)/S_0$, $T_2(n\text{-}\pi^*)/T_1(\pi\text{-}\pi^*)$ conical intersections and the $T_1(\pi\text{-}\pi^*)/S_0$ and $T_2(n\text{-}\pi^*)/S_0$ triplet/singlet crossings occur at the same molecular structure. The relevant geometrical parameters are in Å.

Figure 23. Energy profiles along the three MEPs describing the relaxation from the Franck-Condon (**FC**) and conical intersection (**CI**) points. Open squares and full squares curves define the excited ($1B_u$-like) and ground state branches of the *cis* → *trans* photoisomerization path. Full triangles define the ground state *cis* back-formation path. Open circles show the dark ($2A_g$-like) state energy along the excited state branch of the photoisomerization path. The structures (geometrical parameters in Å and degrees) document the geometrical progression along the photoisomerization path. (From Ref. 37.)

Figure 24. Evolution of the charge distribution along the excited ($1B_u$-like) and ground state branches of the *cis* → *trans* photoisomerization MEP (see Figure 23) connecting *cis* $C_5H_6NH_2^+$ (**FC**) to *trans* $C_5H_6NH_2^+$ (**trans**). The charges are given in a.u. and the value of the central torsional angle is given in degrees. (Adapted from Ref. 37.)

Figure 25. Resonance formulae describing the gradual increase in polarization along the photoisomerization MEP of the *cis* $C_5H_6NH_2^+$ isomer. (From Ref. 37).

Figure 26. Plot of the π-electron density for the degenerate S_0 and S_1 states at the conical intersection structure (**CI**). The arrows indicate the number of electrons migrated from the CH_2CHCH- allyl fragment to the -$CHCHNH_2$ fragment. (From Ref. 37.)

Figure 27. (a) The cyclohexadiene (**CHD**)/*cZc*-hexatriene (***cZc*-HT**) photoconversion problem involves the formation of a common excited state intermediate (***cZc*-HT***) and its decay via a conical intersection point ($\mathbf{CI_{CHD}}$). (b) Due to the tetraradical electronic nature of $\mathbf{CI_{CHD}}$, relaxation on S_0 may occur along three different routes (**a**, **b** and **c**) associated with different bond formation modes and different recouplings. (From Ref. 82).

Figure 28. Energy profiles of the three valleys located around the conical intersection $\mathbf{CI_{CHD}}$.

Figure 29. Energy profiles along the MEPs describing the competing excited state isomerization paths from the Franck-Condon point (**FC**) to the decay points $\mathbf{S_1/S_0\ CI_{C2\text{-}C3}}$ and $\mathbf{S_1/S_0\ CI_{C4\text{-}C5}}$ of *all-trans* $C_7H_8NH_2^+$ (the relaxed planar stationary point is labelled **SP**). Open squares define the S_1 ($1B_u$-like) energy. Open circles indicate the position of the conical intersections. The structures (geometrical parameters in Å and degrees) document the geometrical progression along the path. (From Ref. 112.)

Figure 30. Structure of the S_1 energy surface of *all-trans* $C_7H_8NH_2^+$. The initial part of the MEPs (see framed region in Figure 29) are indicated by full lines. The frequencies are computed at the points indicated with an open square and at the relaxed planar stationary point **SP** (full square). The frequencies along the modes leading to decay are given on the surface. The frequency along the **SP** mode which correlates with the initial gradient is given in parenthesis. The direction of the initial gradient is represented by arrows on the top structure. Torsional co-ordinates are indicated by curly arrows on the right and left structures. (From Ref. 112.)

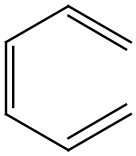

1

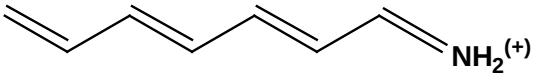

2

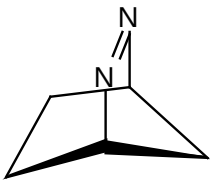

3

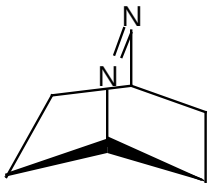

12

13

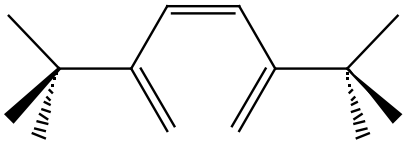

14

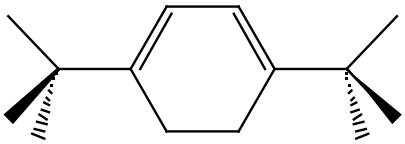

15

Structures

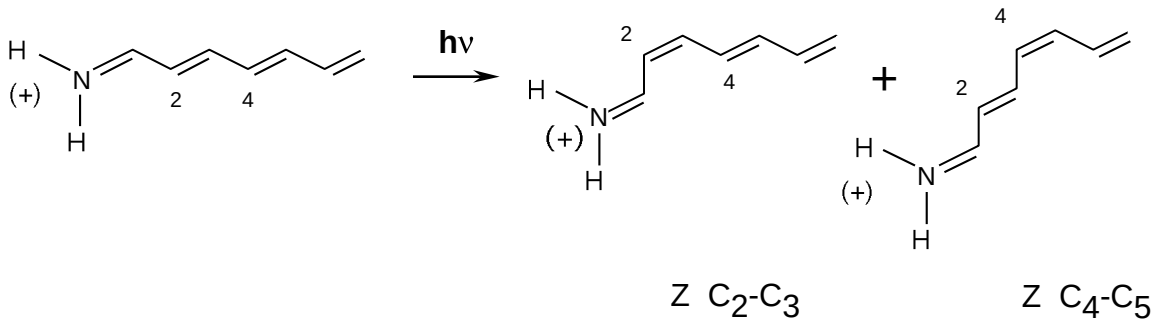

Scheme 1

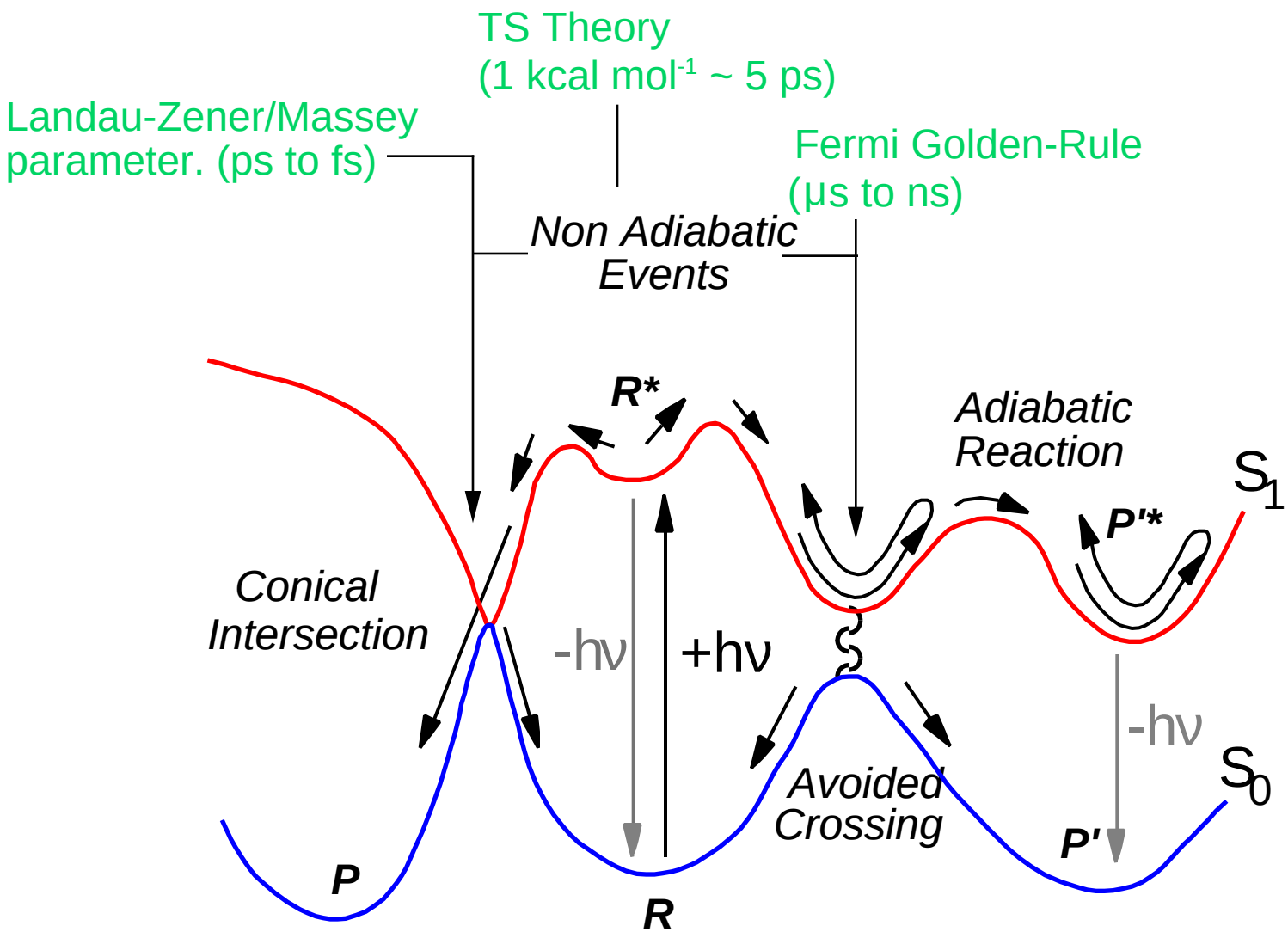
TS Theory
(1 kcal mol-1 ~ 5 ps)
Landau-Zener/Massey
parameter. (ps to fs)
Fermi Golden-Rule
(µs to ns)
Non Adiabatic
Events
R*
Adiabatic
Reaction
S1
P'*
Conical
Intersection
-hν
+hν
-hν
Avoided
Crossing
S0
P
R
P'

Figure 1

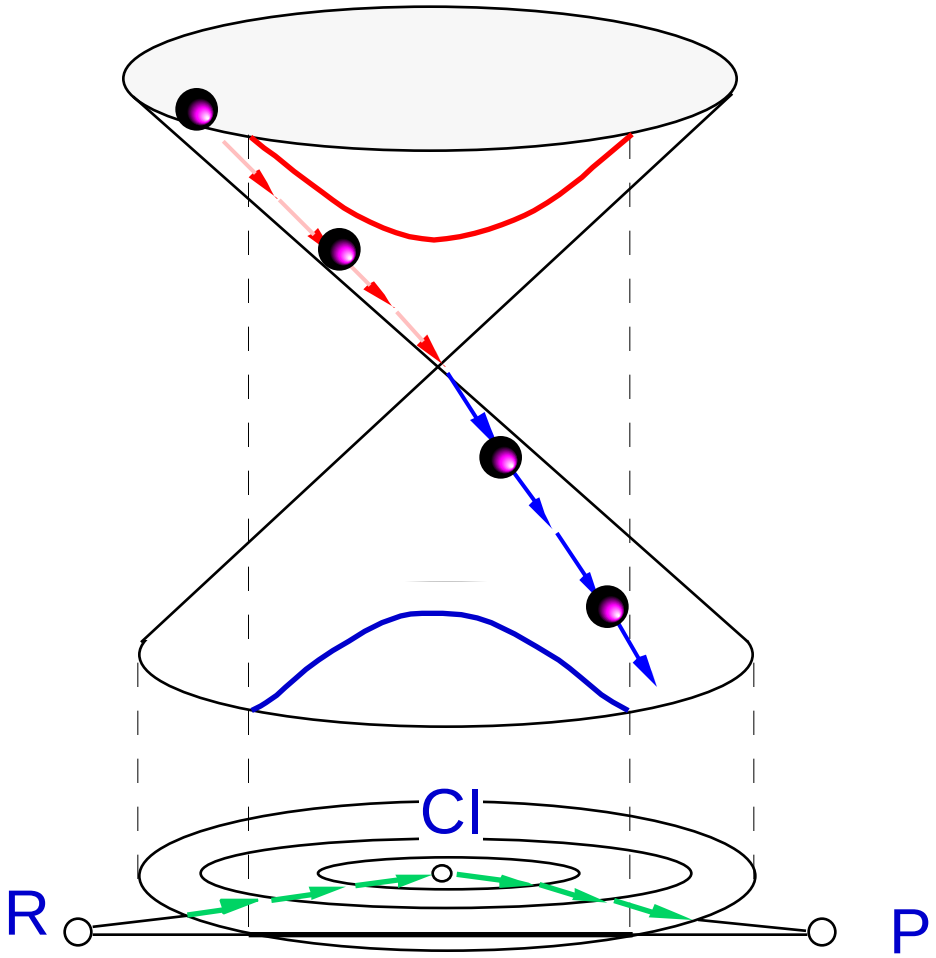

Figure 2

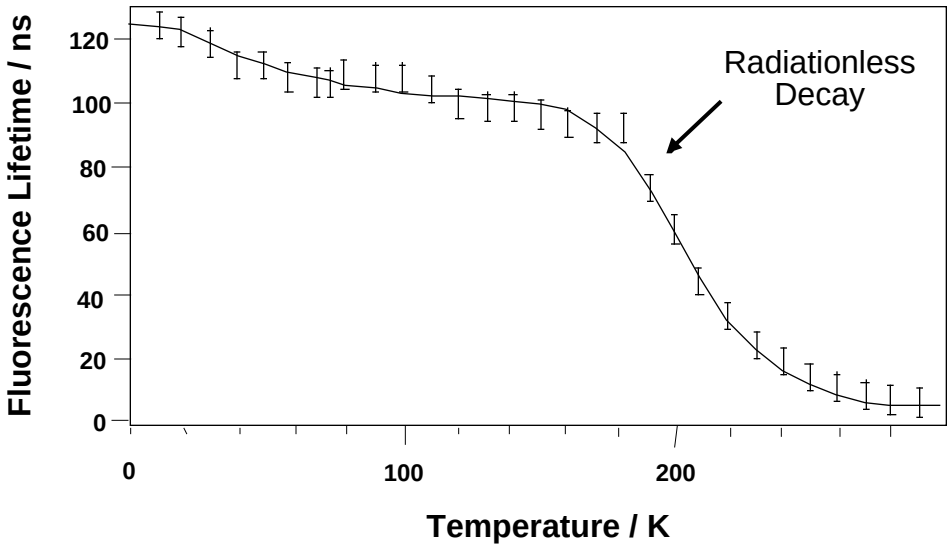
Fluorescence Lifetime / ns
120
100
80
60
40
20
0
0
100
200
Temperature / K
Radiationless
Decay

(a)

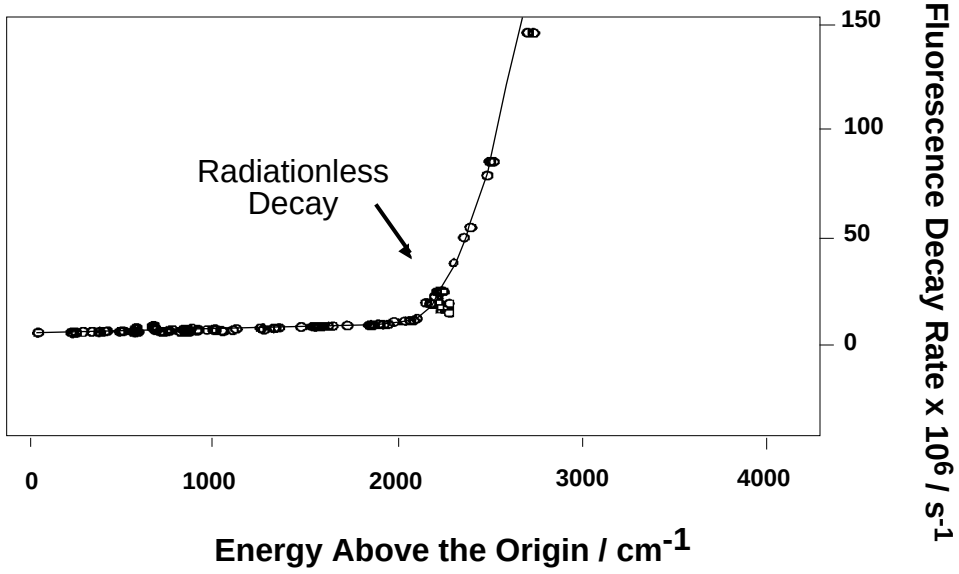
150
100
50
0
Fluorescence Decay Rate x 10⁶ / s⁻¹
Radiationless
Decay
0
1000
2000
3000
4000
Energy Above the Origin / cm⁻¹

(b)

Figure 3

- Photochemistry or emission depending on barrier

- Ultrafast Photochemistry

- Photophysics only

M*→TS→CI

FC→CI

M*→CI

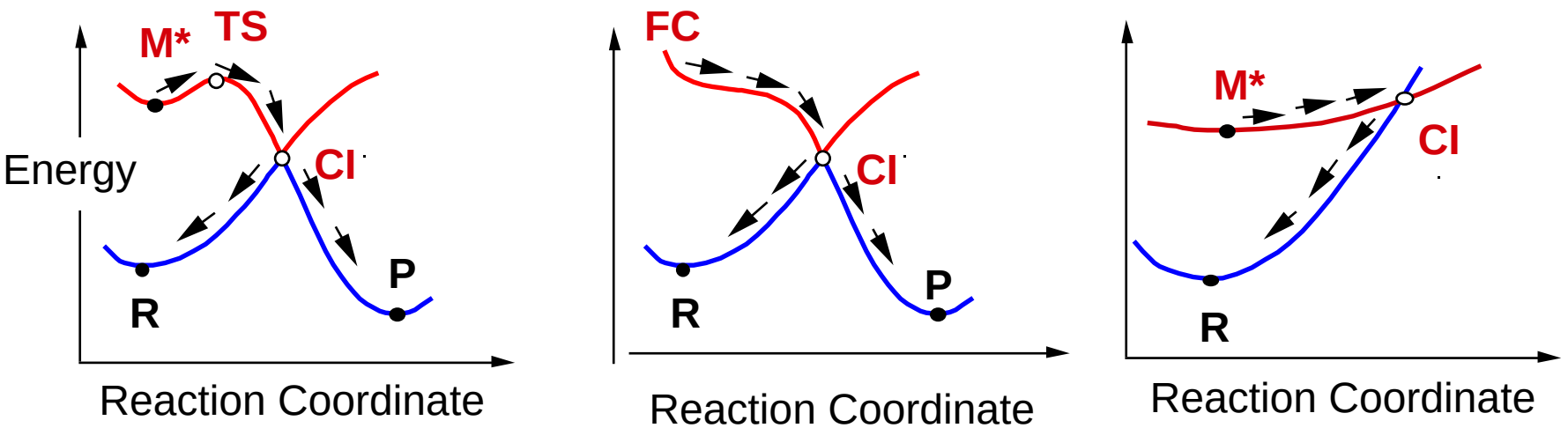

(a) **(b)** **(c)**

Figure 4

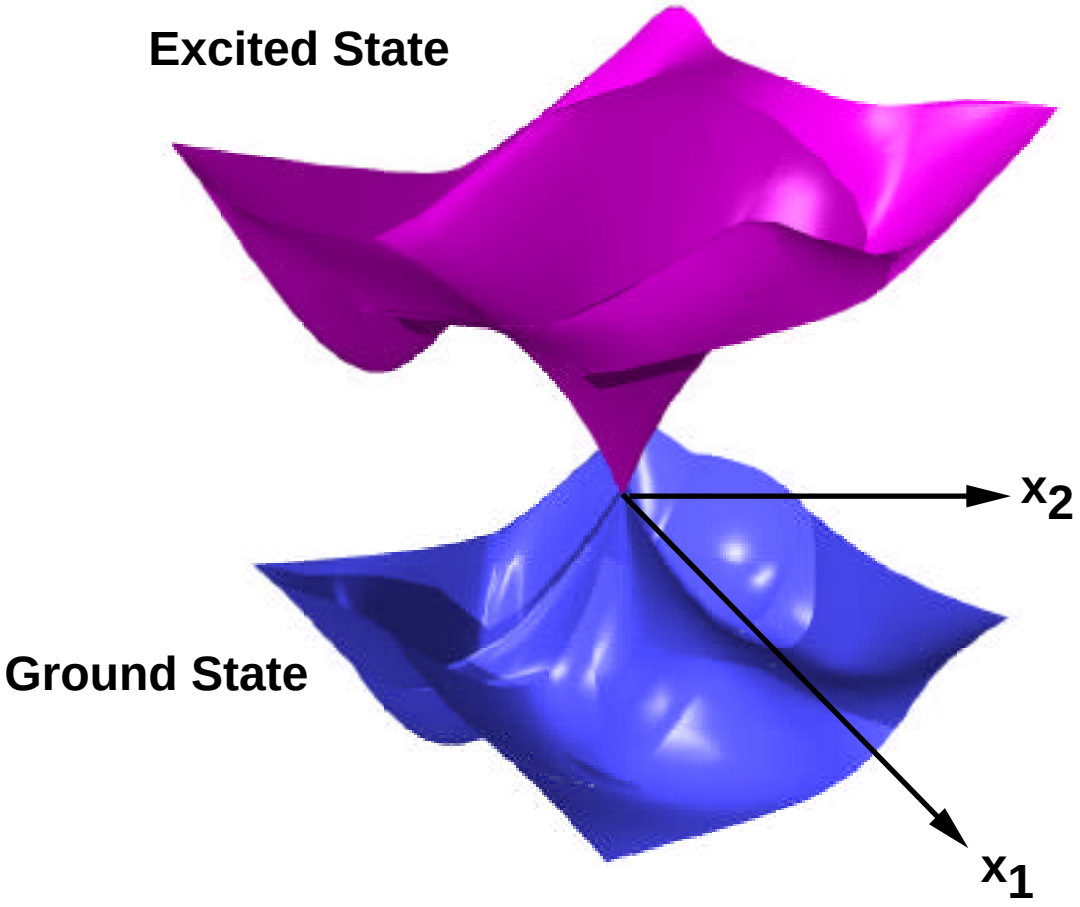
Excited State
Ground State
x2
x1

(a)

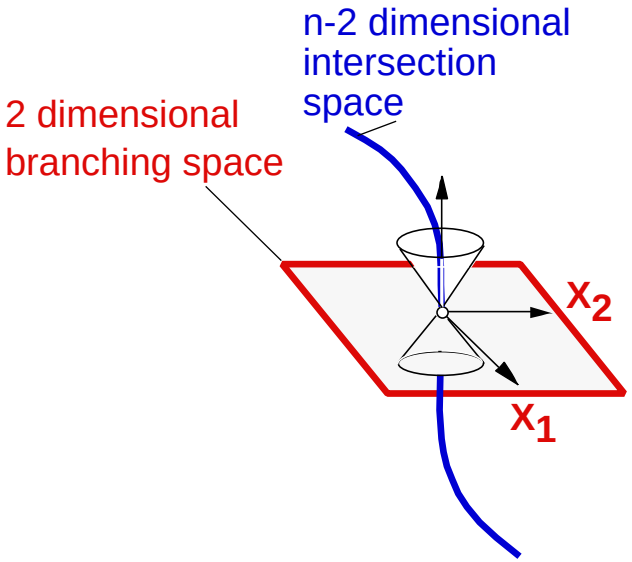
n-2 dimensional
intersection
space
2 dimensional
branching space
x2
x1

(b)

Figure 5

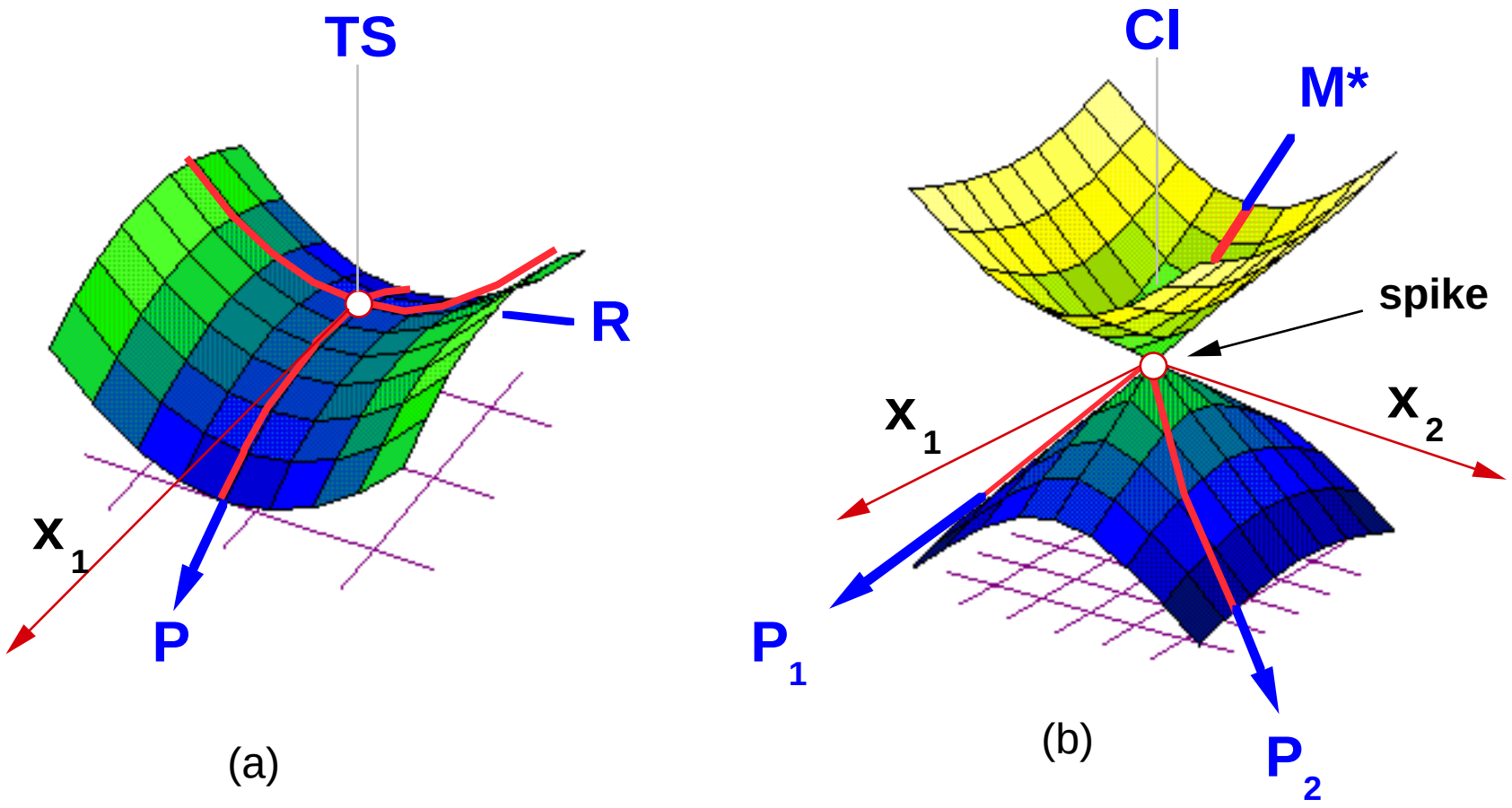

Figure 6

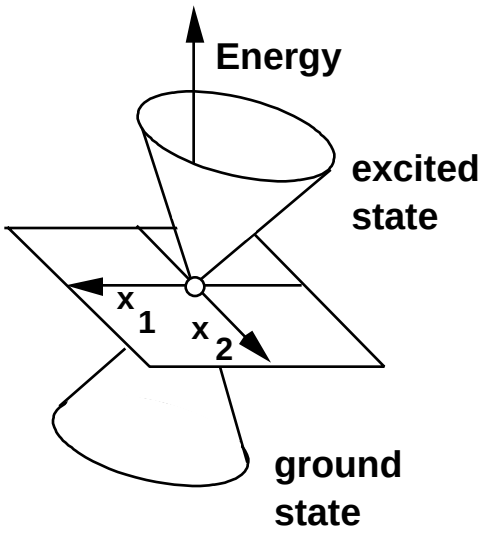

(a)

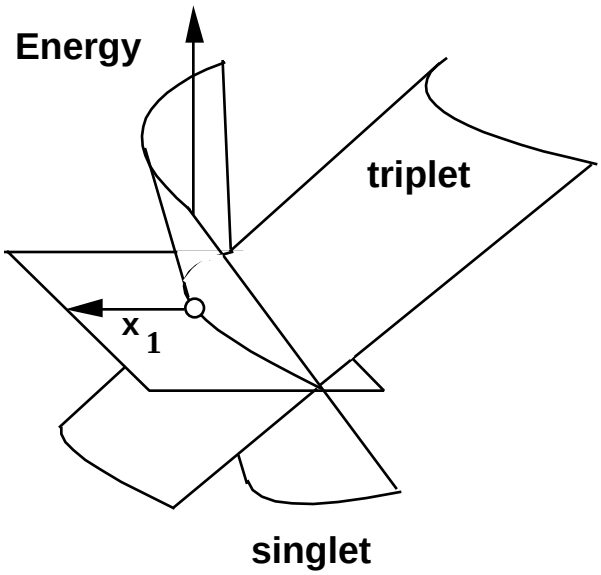

(b)

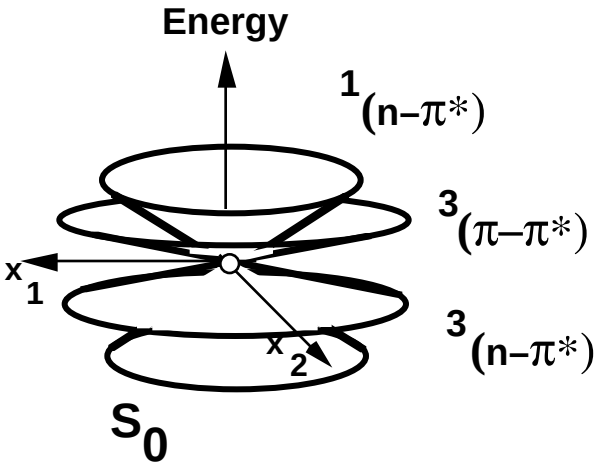

(c)

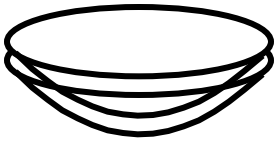

(d)

Figure 7

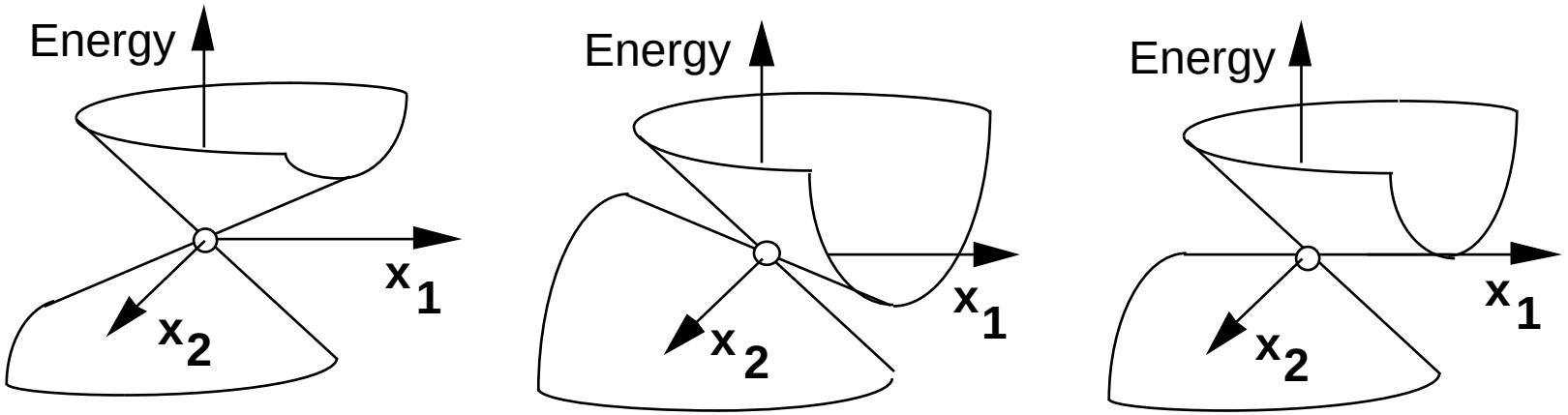

Peaked Conical Intersection

(a)

Sloped Conical Intersection

(b)

Intermediate Conical Intersection

(c)

Figure 8

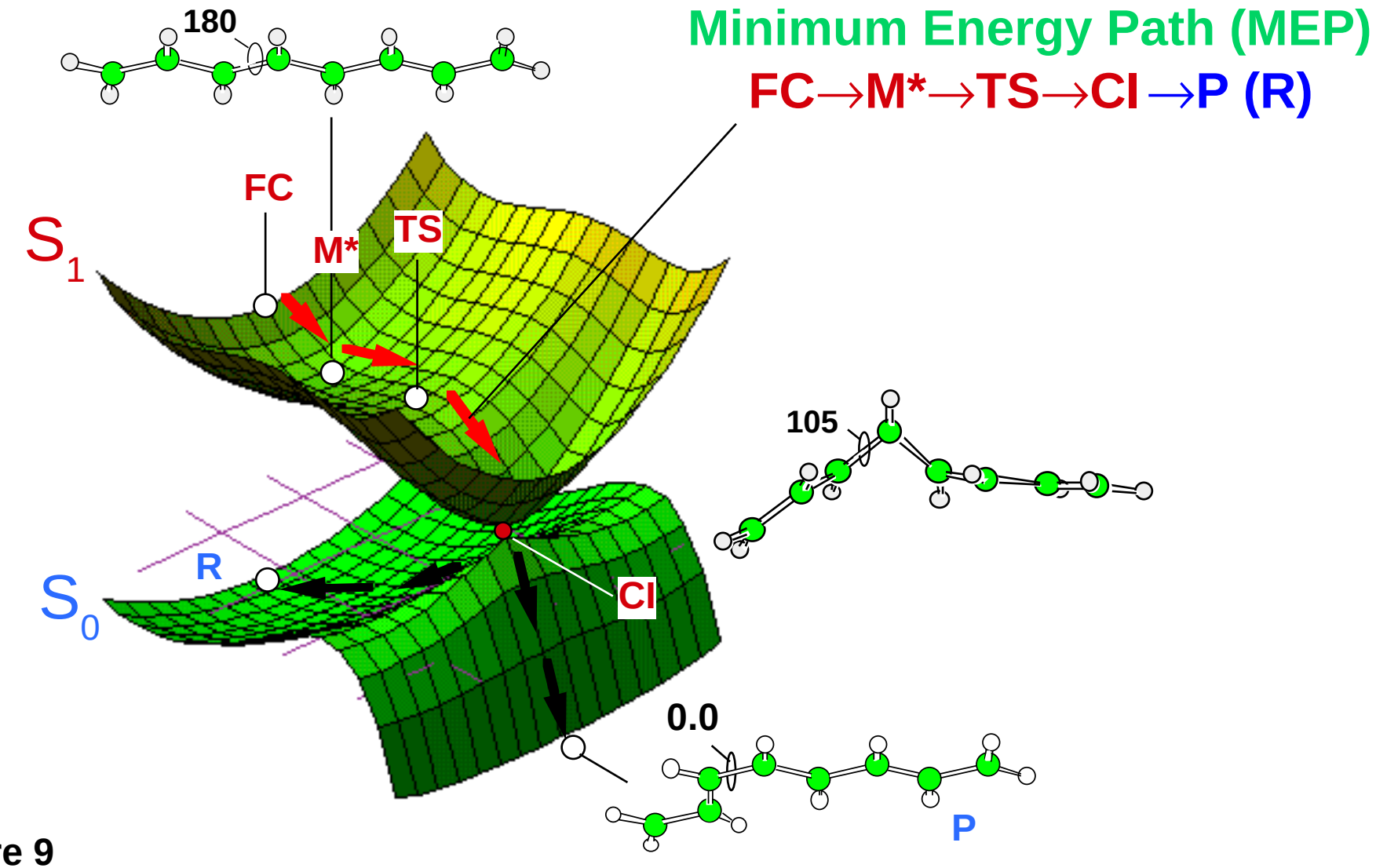
Minimum Energy Path (MEP)
FC→M*→TS→CI→P (R)
180
FC
M*
TS
S1
S0
R
CI
105
0.0
P

Figure 9

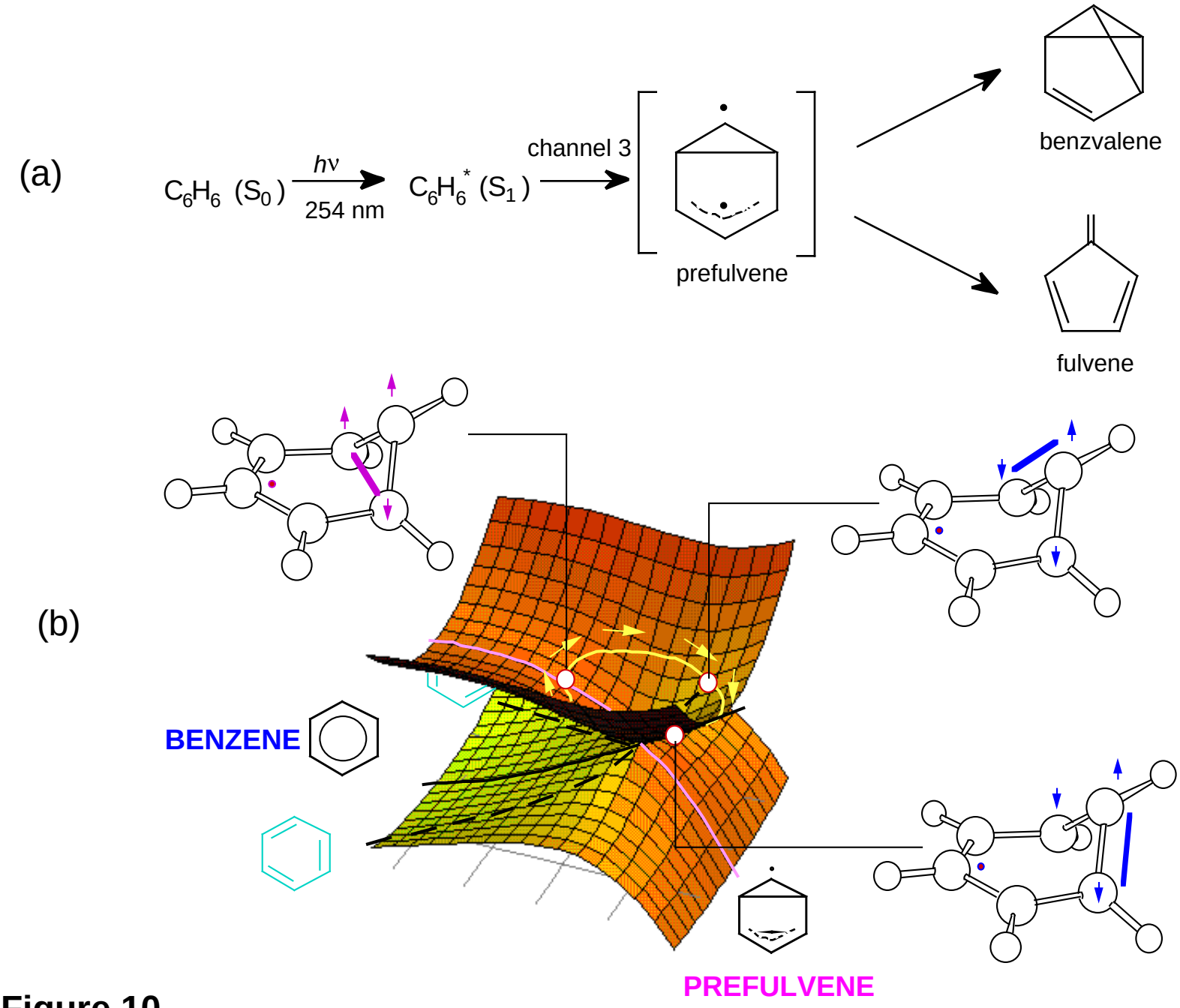
(a)
C_6H_6 (S_0)
hν
254 nm
$C_6H_6^*$ (S_1)
channel 3
prefulvene
benzvalene
fulvene
(b)
BENZENE
PREFULVENE

Figure 10

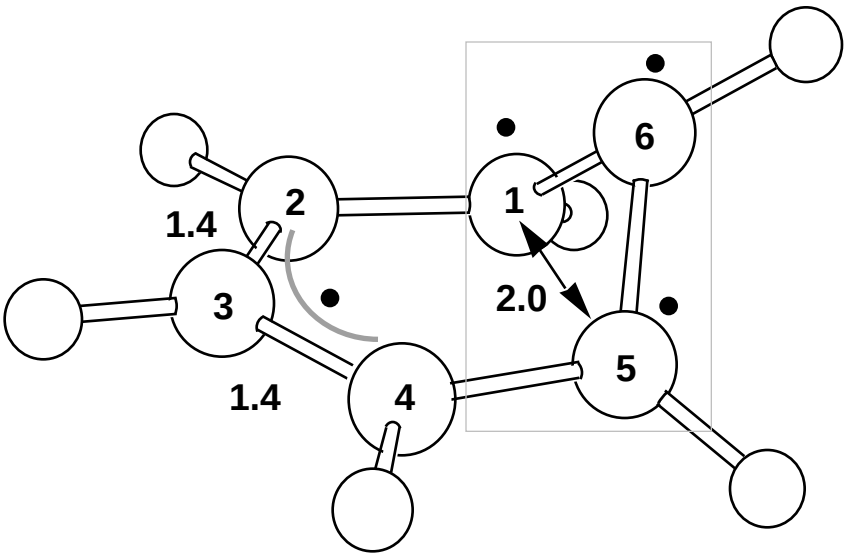

Figure 11

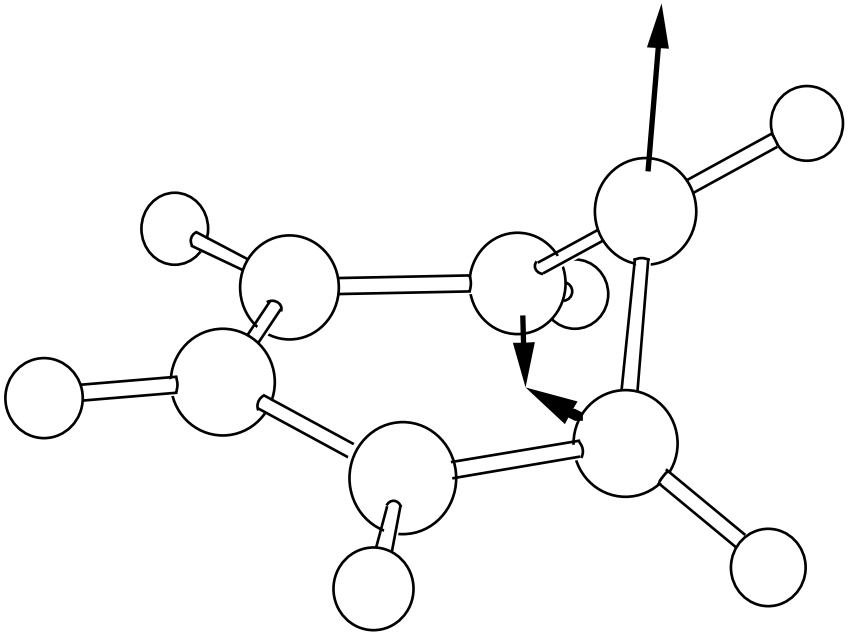

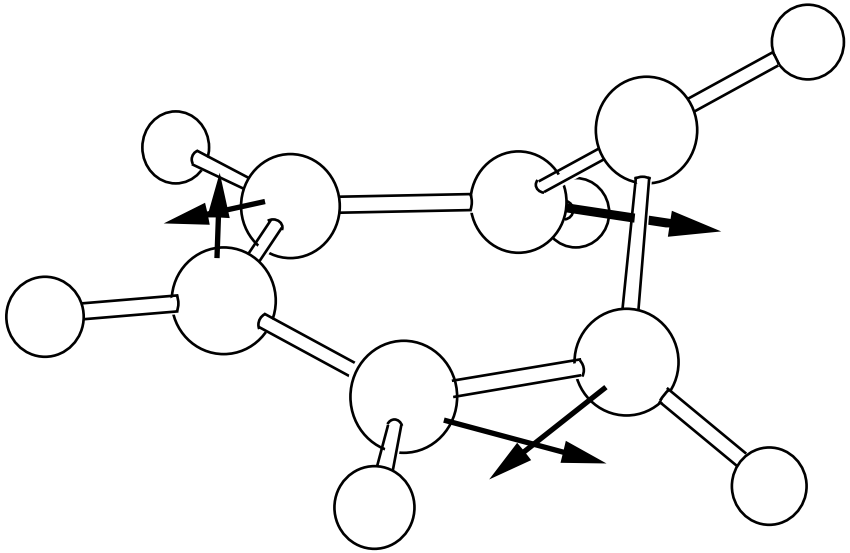

$$x_1 = \frac{\partial(E_1 - E_2)}{\partial Q}$$

$$x_2 = \left\langle \phi_1 \left| \frac{\partial}{\partial Q} \right| \phi_2 \right\rangle$$

Figure 12

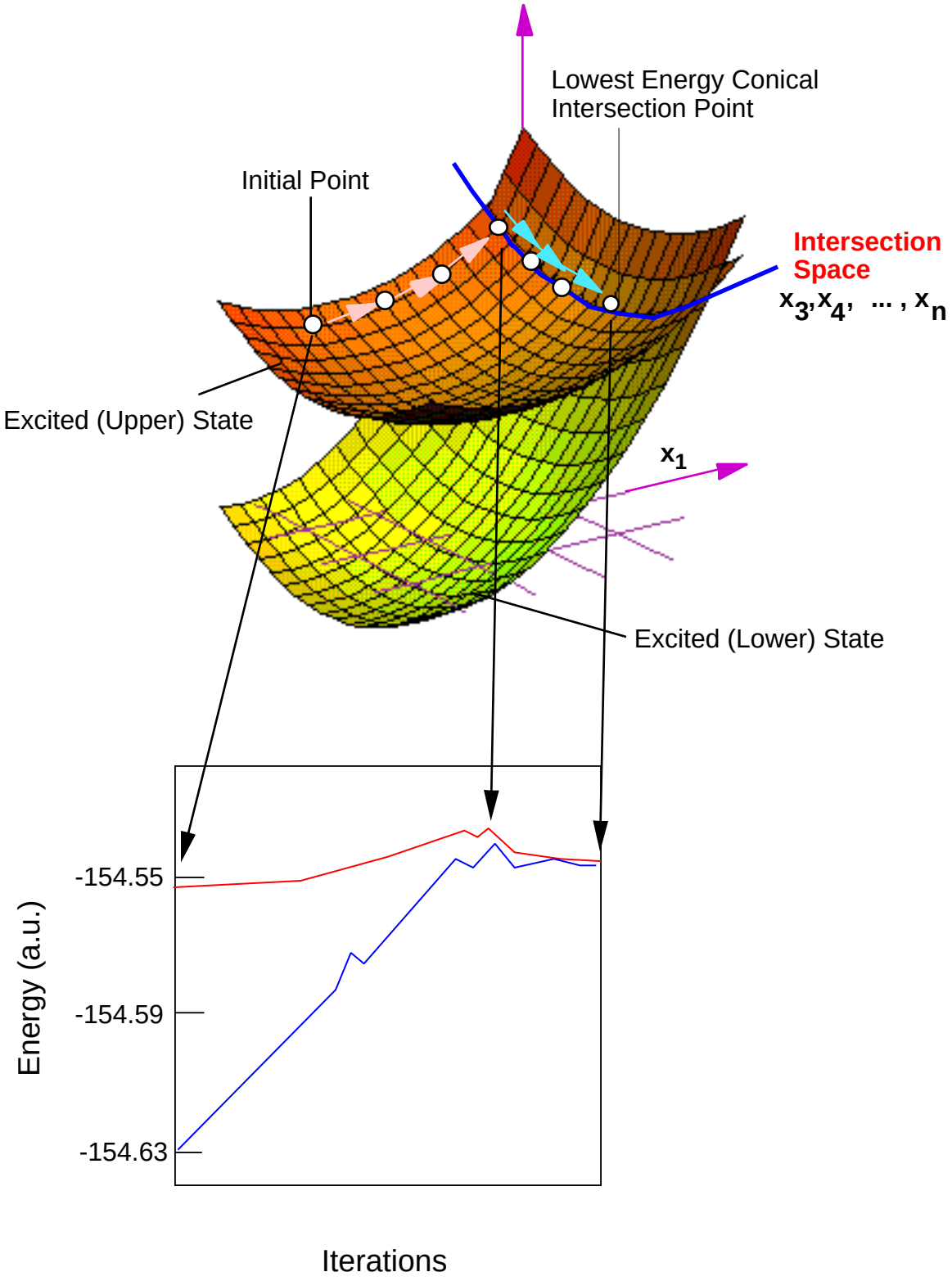
Lowest Energy Conical
Intersection Point
Initial Point
Intersection
Space
$x_3, x_4, \ldots, x_n$
Excited (Upper) State
x_1
Excited (Lower) State
-154.55
-154.59
-154.63
Energy (a.u.)
Iterations

Figure 13

Figure 14

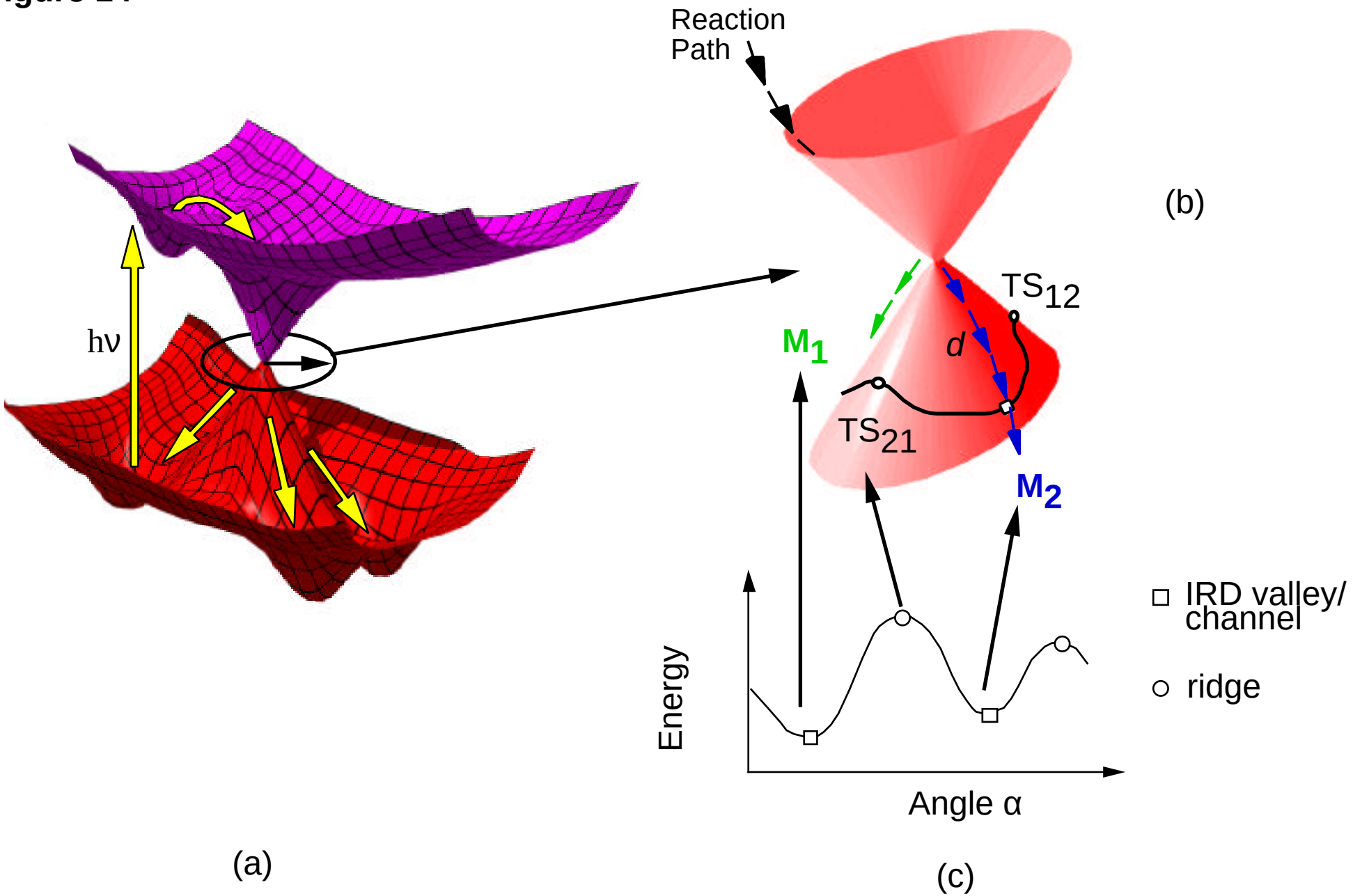
Reaction
Path
hν
(a)
(b)
M1
d
TS12
TS21
M2
Energy
Angle α
(c)
IRD valley/
channel
ridge

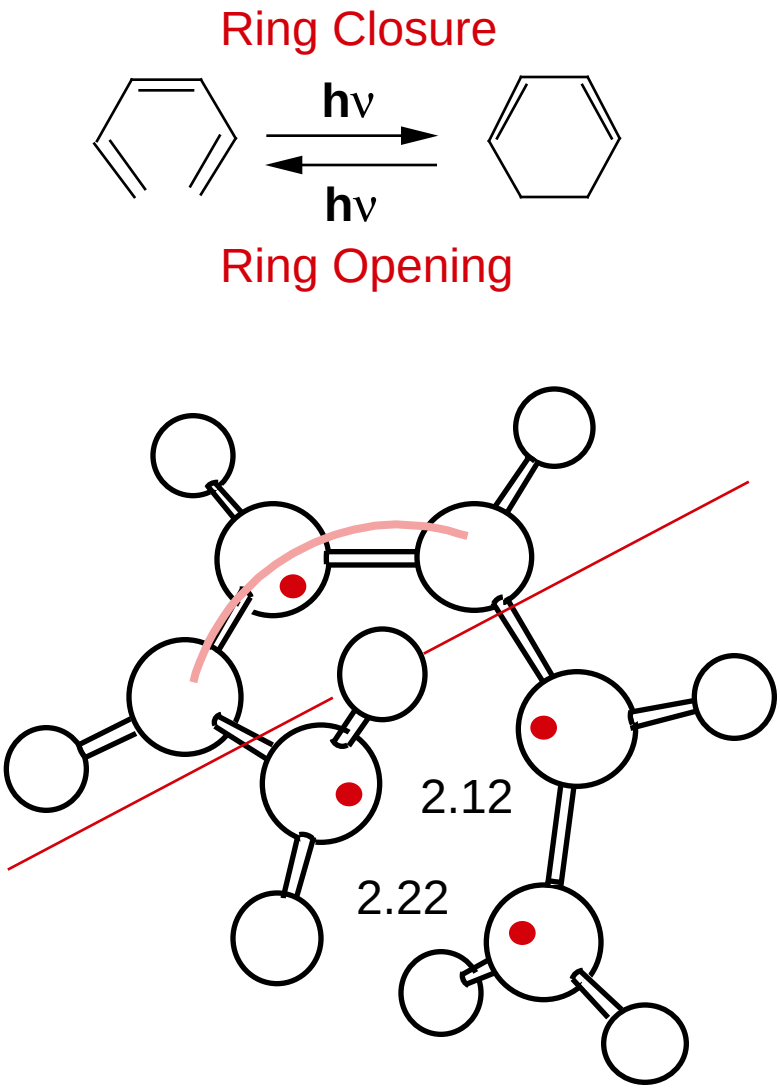

Figure 15

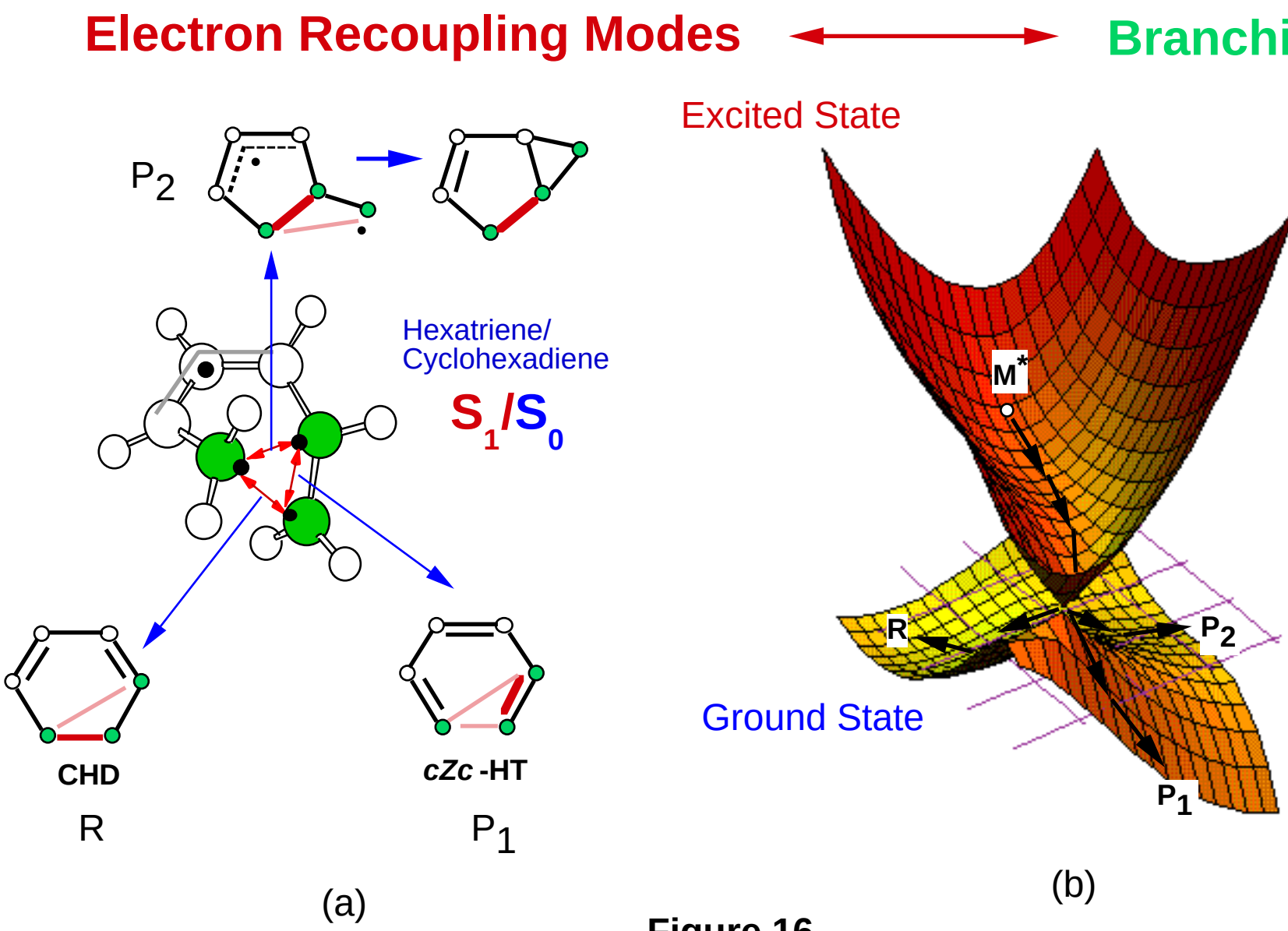
Electron Recoupling Modes
Branching
P2
Hexatriene/
Cyclohexadiene
S1/S0
CHD
R
cZc -HT
P1
(a)
Excited State
M*
R
P2
Ground State
P1
(b)

Figure 16

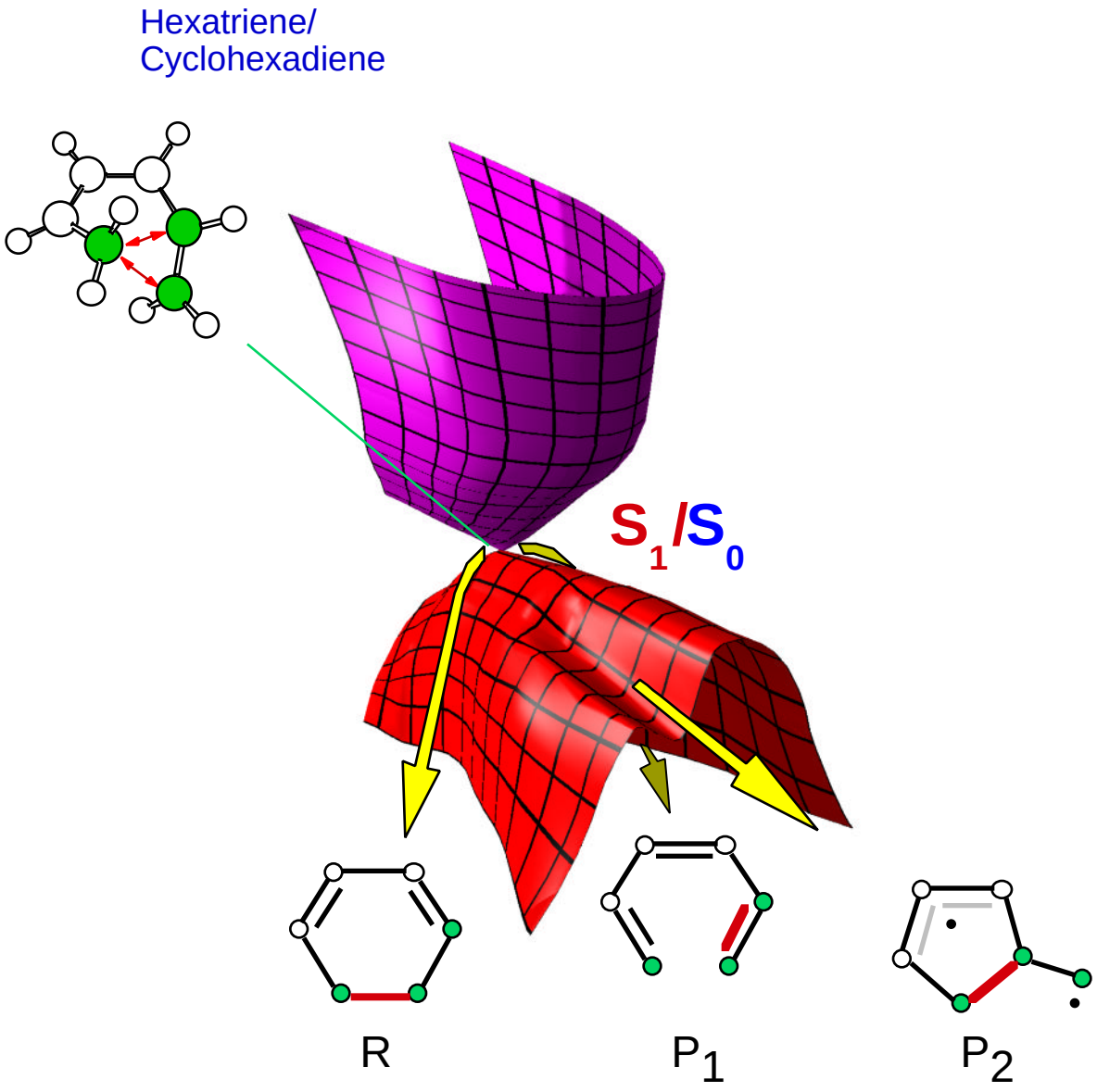

Figure 17

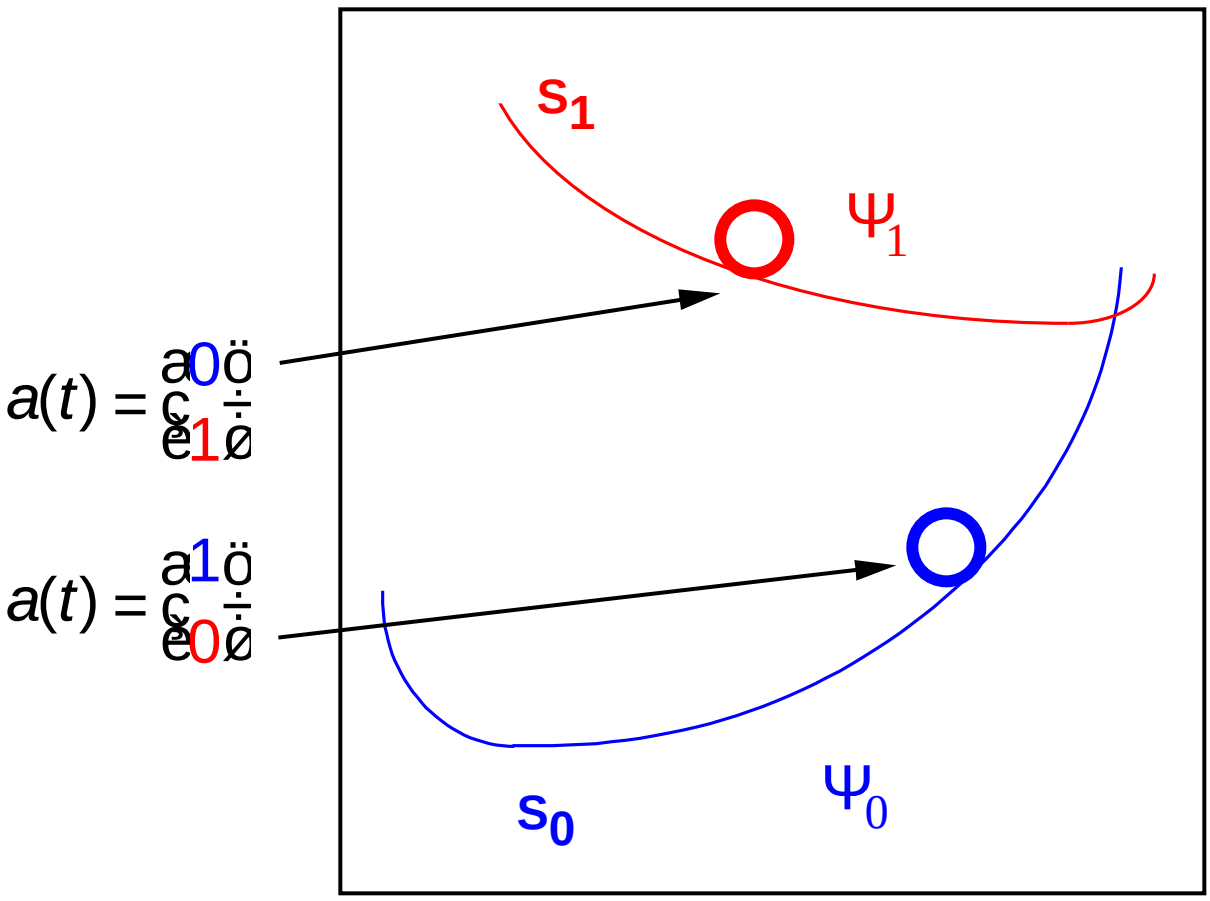

Figure 18

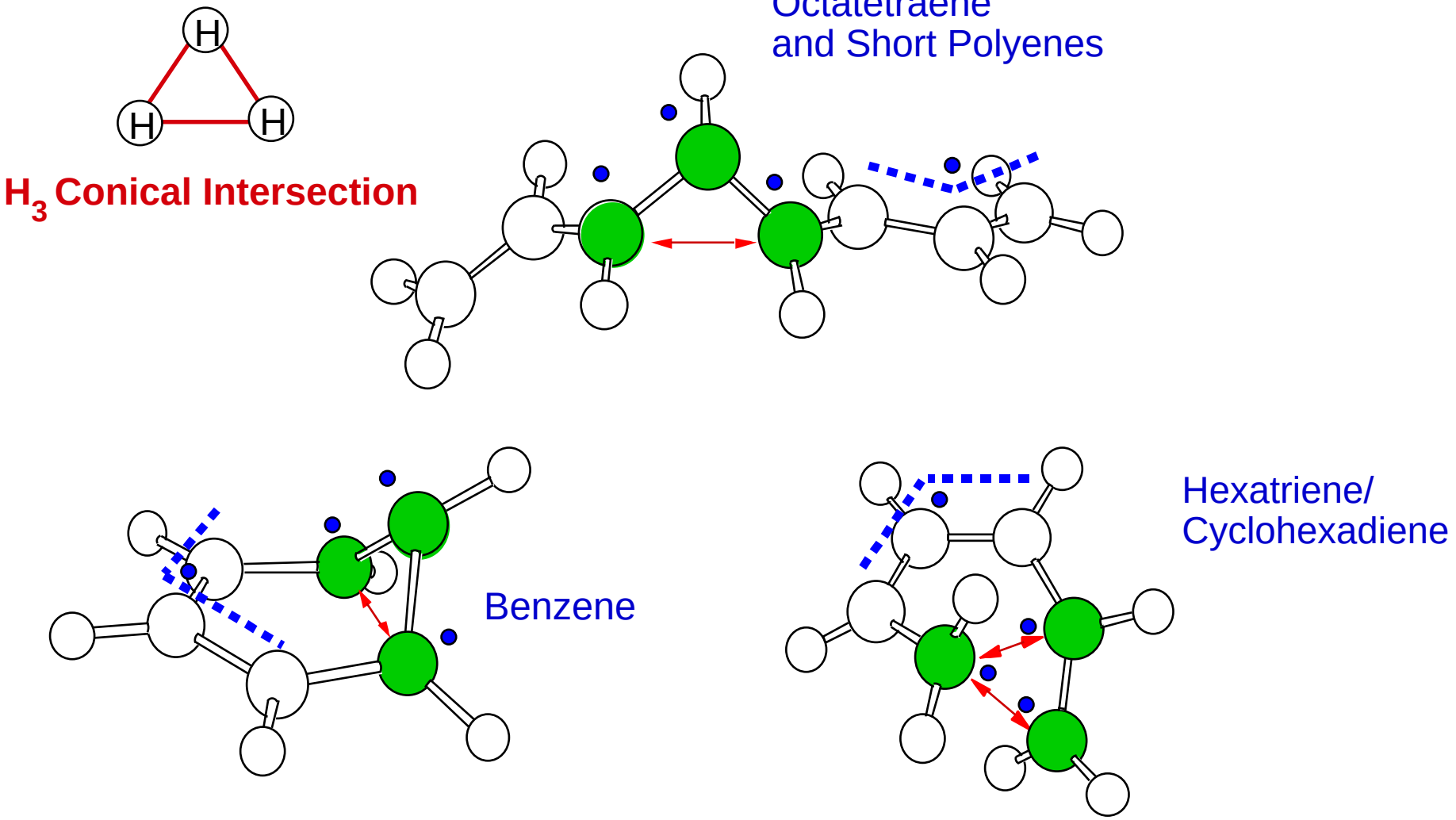
H
H
H
H3 Conical Intersection
Octatetraene
and Short Polyenes
Benzene
Hexatriene/
Cyclohexadiene

Figure 19

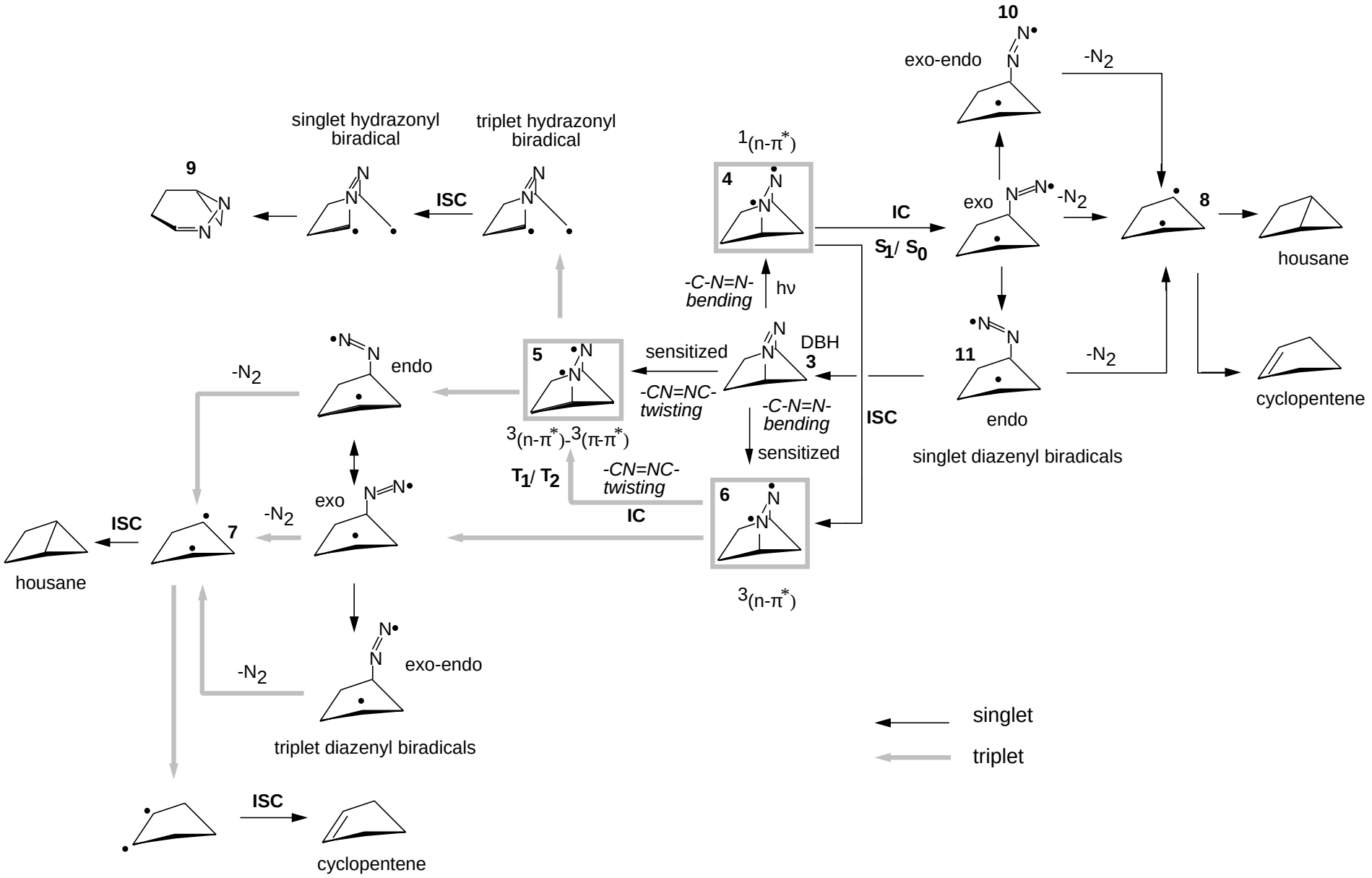
10
exo-endo
-N2
singlet hydrazonyl biradical
triplet hydrazonyl biradical
1(n-π*)
9
ISC
4
IC
S1/ S0
exo
-N2
8
housane
-C-N=N- bending
hν
-N2
endo
5
sensitized
DBH
3
11
-N2
cyclopentene
-CN=NC- twisting
-C-N=N- bending
ISC
endo
singlet diazenyl biradicals
3(n-π*)-3(π-π*)
T1/ T2
-CN=NC- twisting
sensitized
IC
ISC
exo
-N2
7
6
housane
3(n-π*)
-N2
exo-endo
triplet diazenyl biradicals
singlet
triplet
ISC
cyclopentene

Figure 20

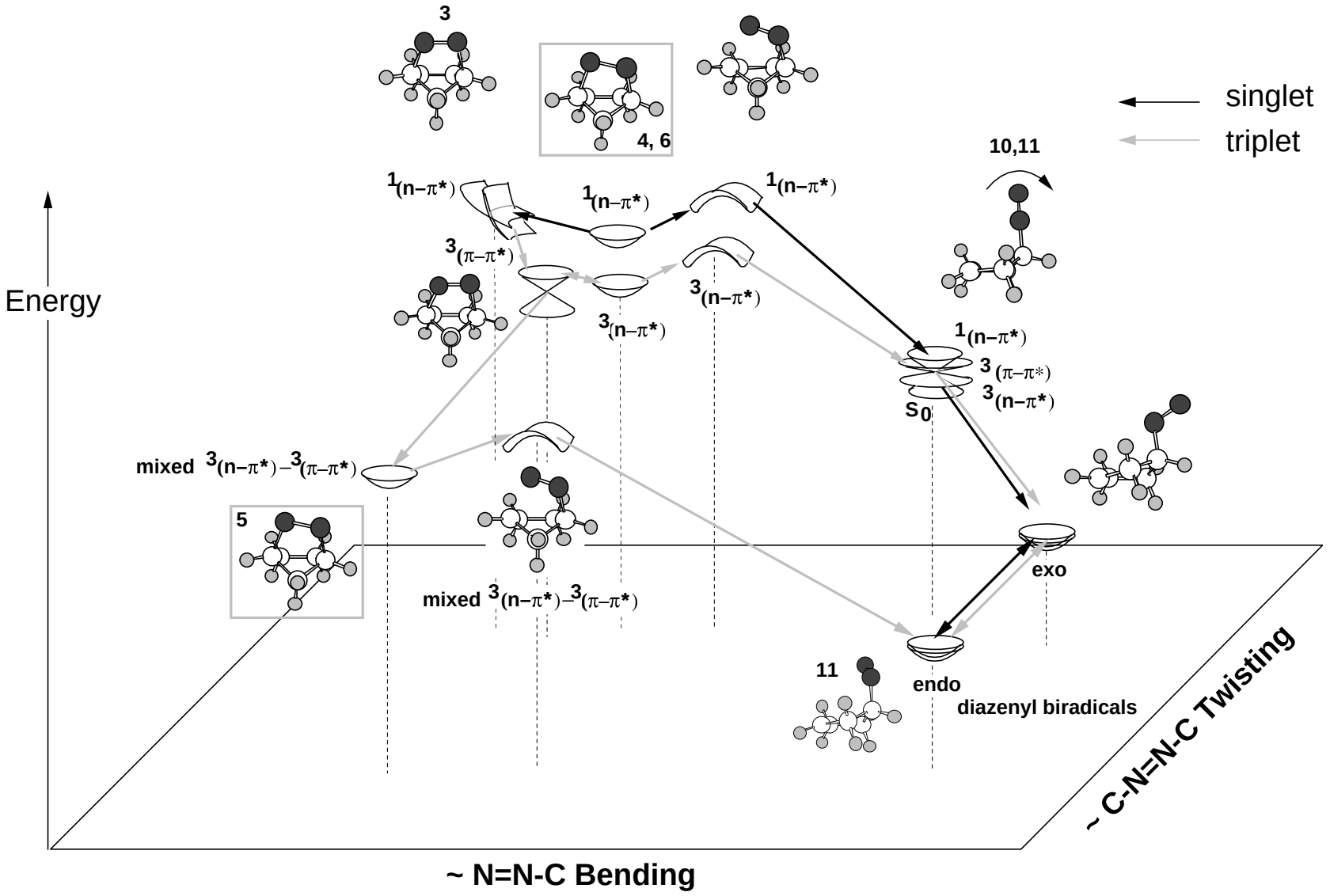
3
4, 6
singlet
triplet
10,11
Energy
$^1(n-\pi^*)$
$^1(n-\pi^*)$
$^1(n-\pi^*)$
$^3(\pi-\pi^*)$
$^3(n-\pi^*)$
$^3(n-\pi^*)$
$^1(n-\pi^*)$
$^3(\pi-\pi^*)$
$^3(n-\pi^*)$
S_0
mixed $^3(n-\pi^*)-^3(\pi-\pi^*)$
5
mixed $^3(n-\pi^*)-^3(\pi-\pi^*)$
exo
11
endo
diazenyl biradicals
~ C-N=N-C Twisting
~ N=N-C Bending

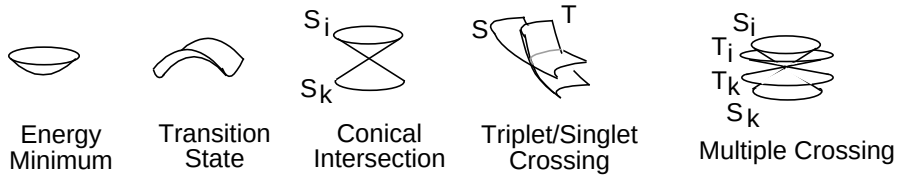
Energy Minimum
Transition State
S_i
S_k
Conical Intersection
S
T
Triplet/Singlet Crossing
S_i
T_i
T_k
S_k
Multiple Crossing

Figure 21

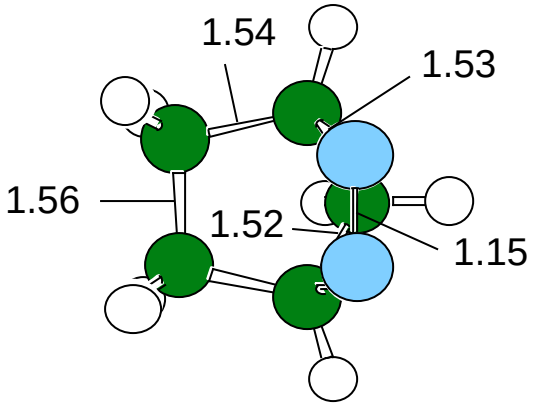

DBH equilibrium Struct.

3

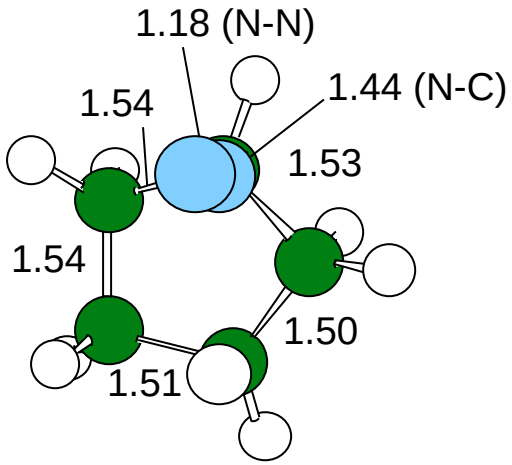

Crossing

10,11

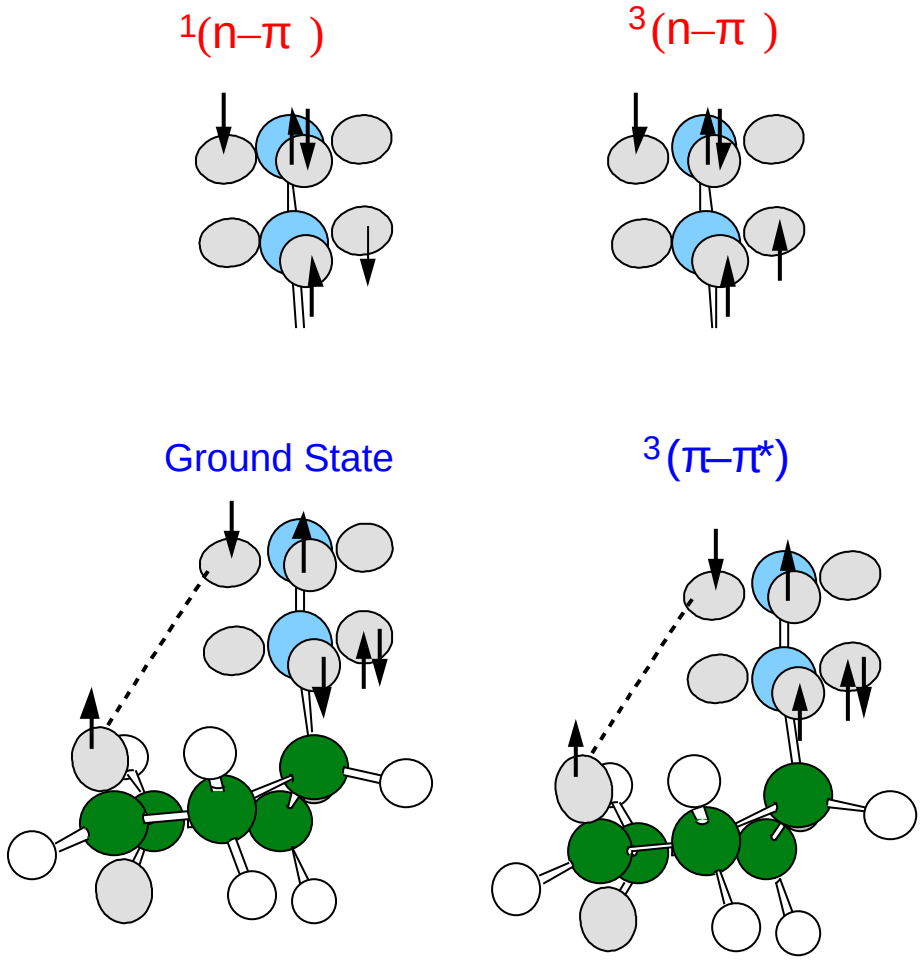

Crossing

10,11

Figure 22

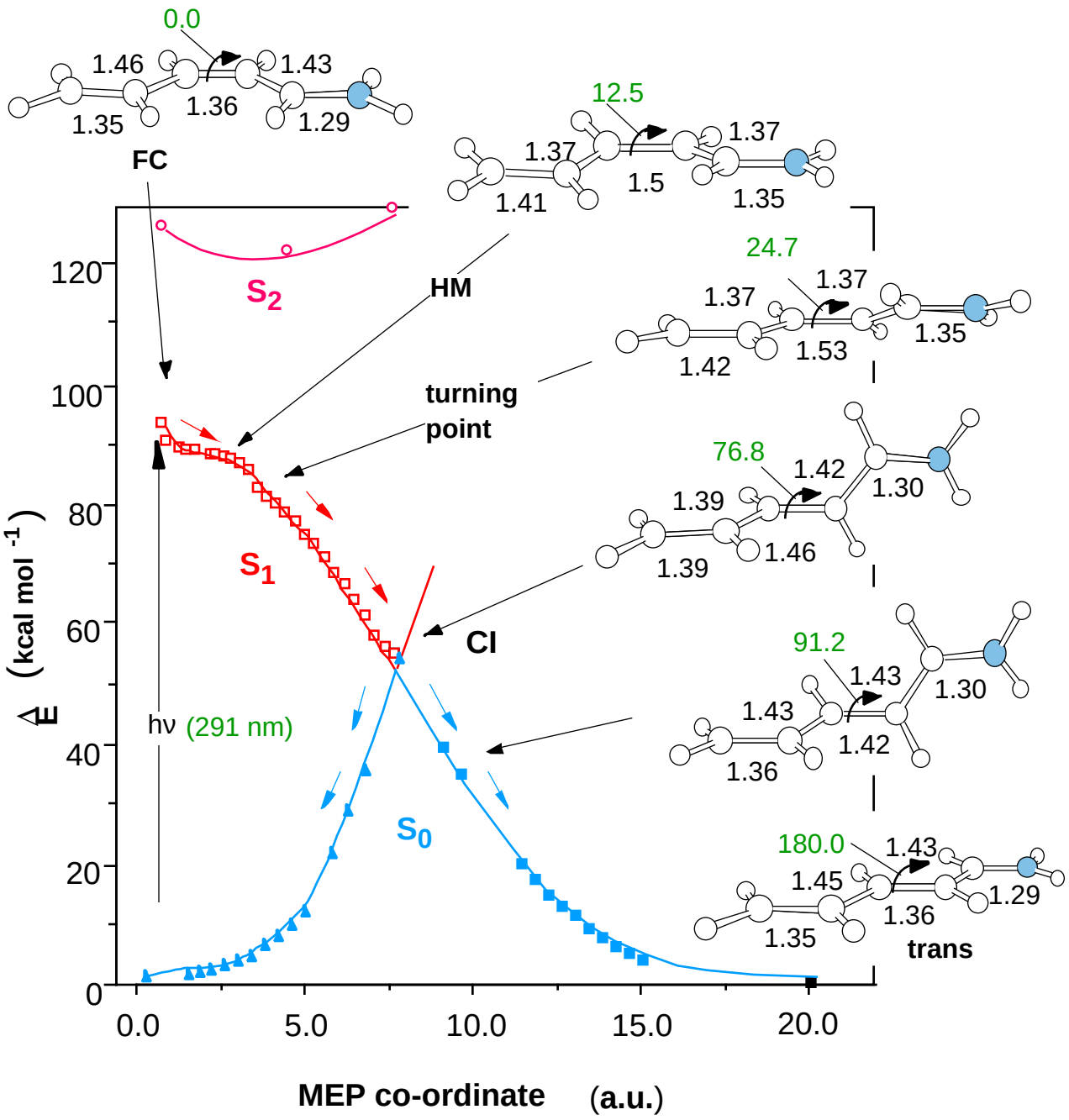
0.0
1.46
1.43
1.36
1.35
1.29
FC
12.5
1.37
1.37
1.41
1.5
1.35
24.7
1.37
1.37
1.35
1.42
1.53
HM
turning
point
76.8
1.42
1.30
1.39
1.39
1.46
S2
S1
CI
91.2
1.43
1.30
1.43
1.42
1.36
hν (291 nm)
S0
180.0
1.43
1.45
1.29
1.36
1.35
trans
ΔE (kcal mol -1)
120
100
80
60
40
20
0
0.0
5.0
10.0
15.0
20.0
MEP co-ordinate (a.u.)

Figure 23

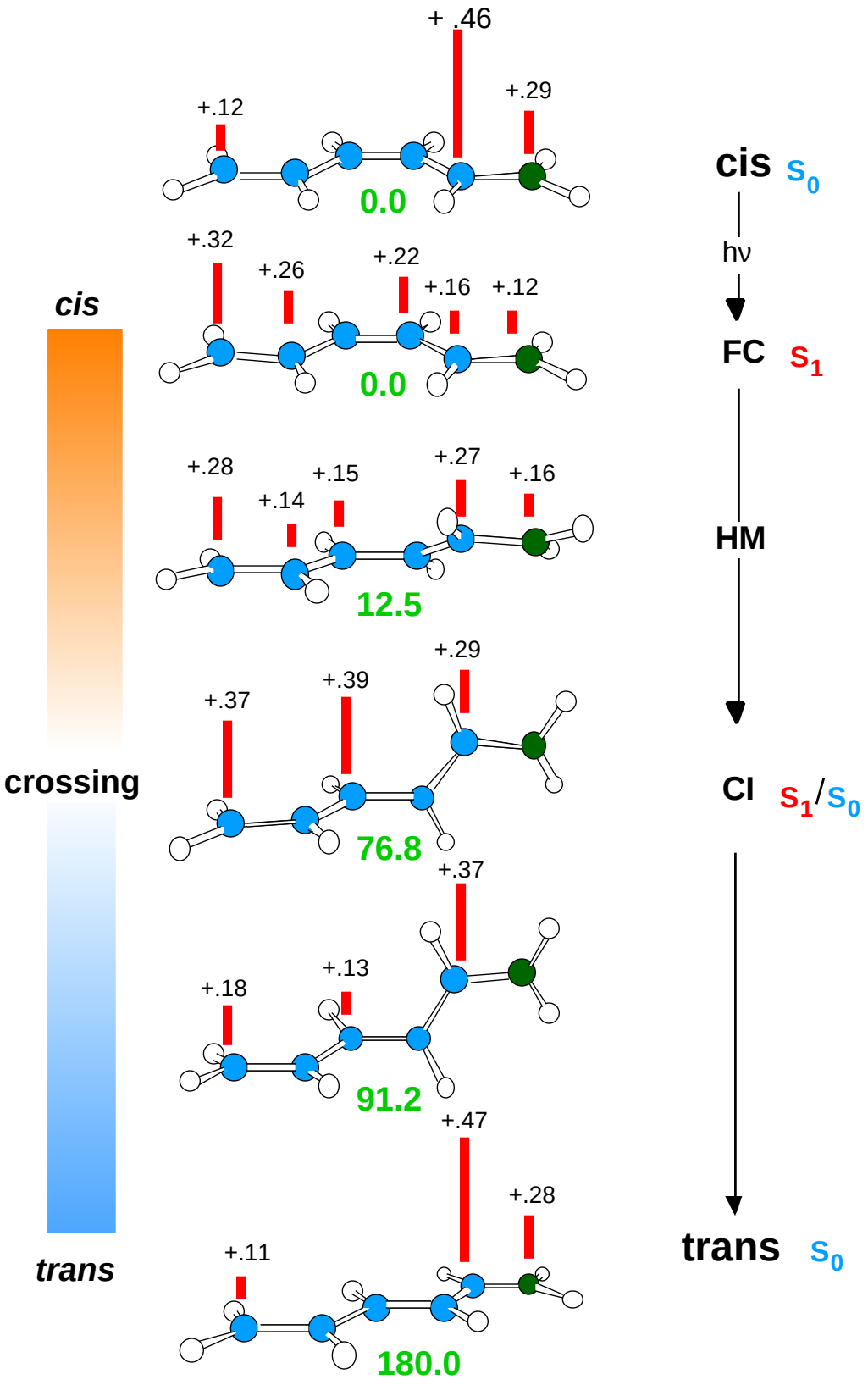
+ .46
+.12
+.29
0.0
cis S0
hν
+.32
+.26
+.22
+.16
+.12
cis
0.0
FC S1
+.28
+.14
+.15
+.27
+.16
12.5
HM
+.29
+.37
+.39
76.8
crossing
CI S1/S0
+.37
+.18
+.13
91.2
+.47
+.28
+.11
180.0
trans S0
trans

Figure 24

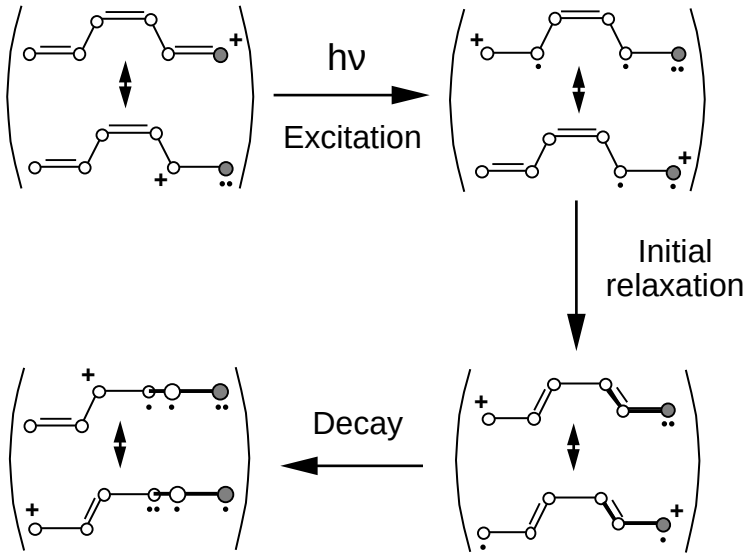

Figure 25

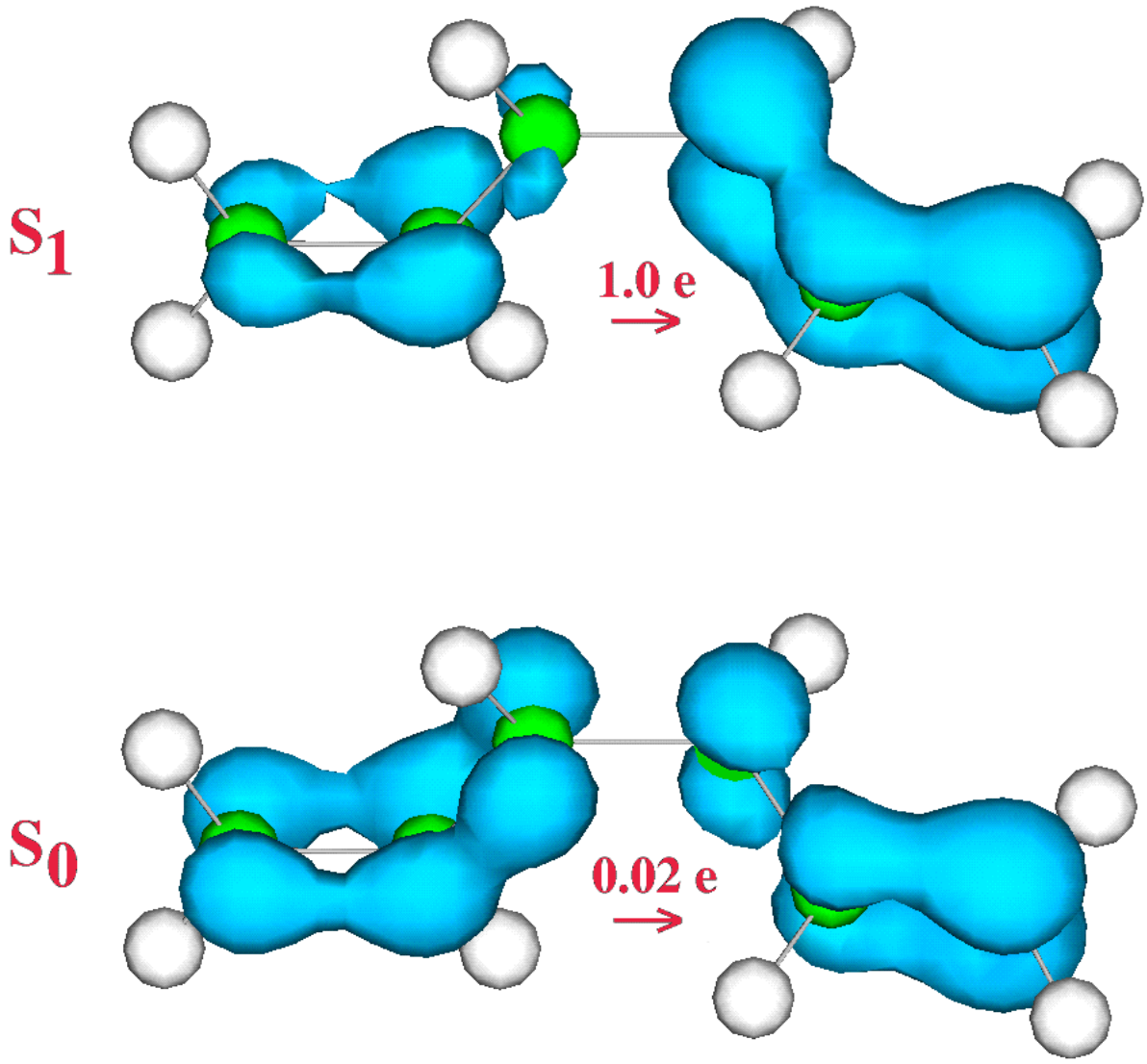

Figure 26

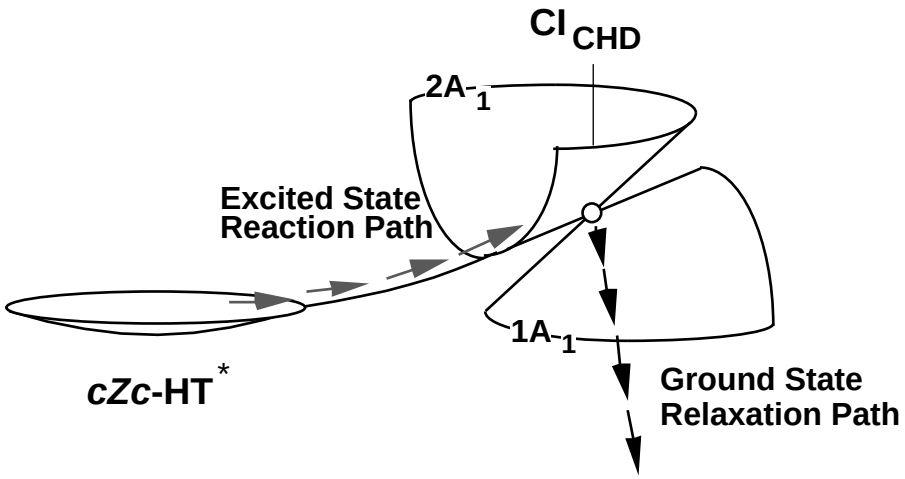
Cl CHD
2A-1
Excited State
Reaction Path
1A-1
cZc-HT*
Ground State
Relaxation Path

(a)

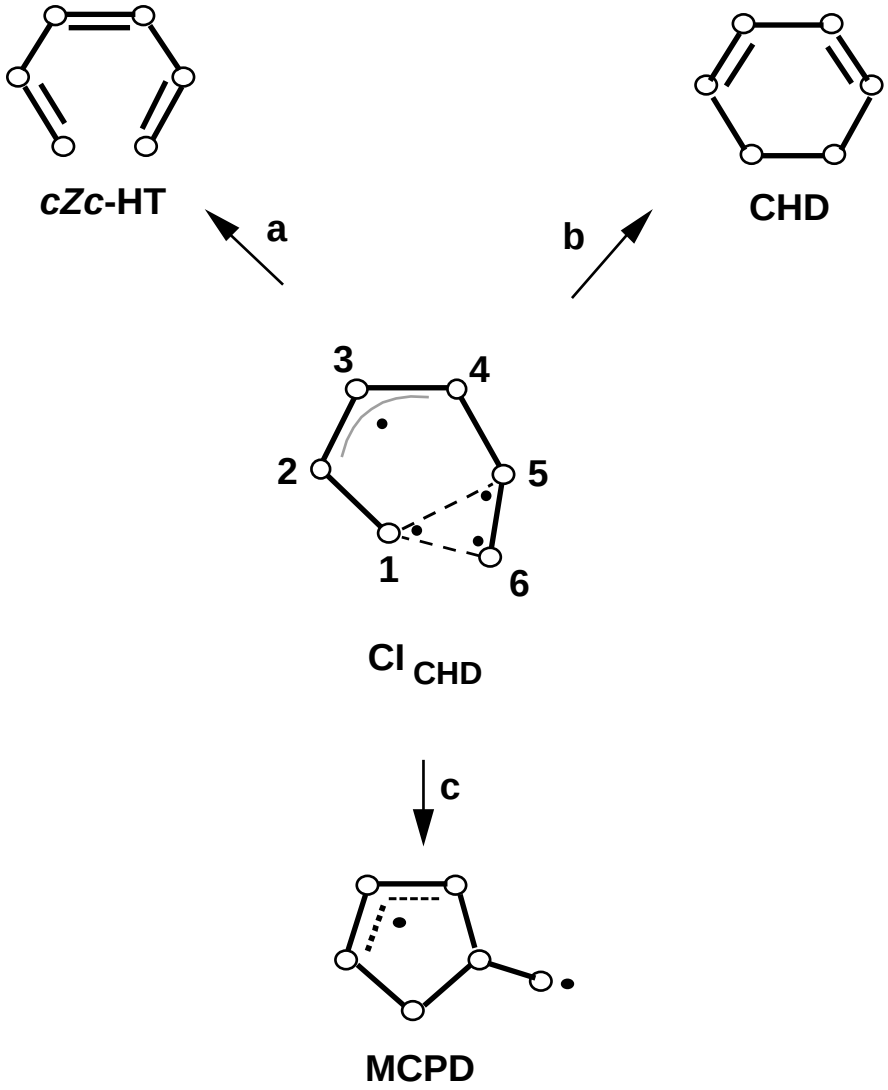
cZc-HT
a
b
CHD
3
4
2
5
1
6
Cl CHD
c
MCPD

(b)

Figure 27

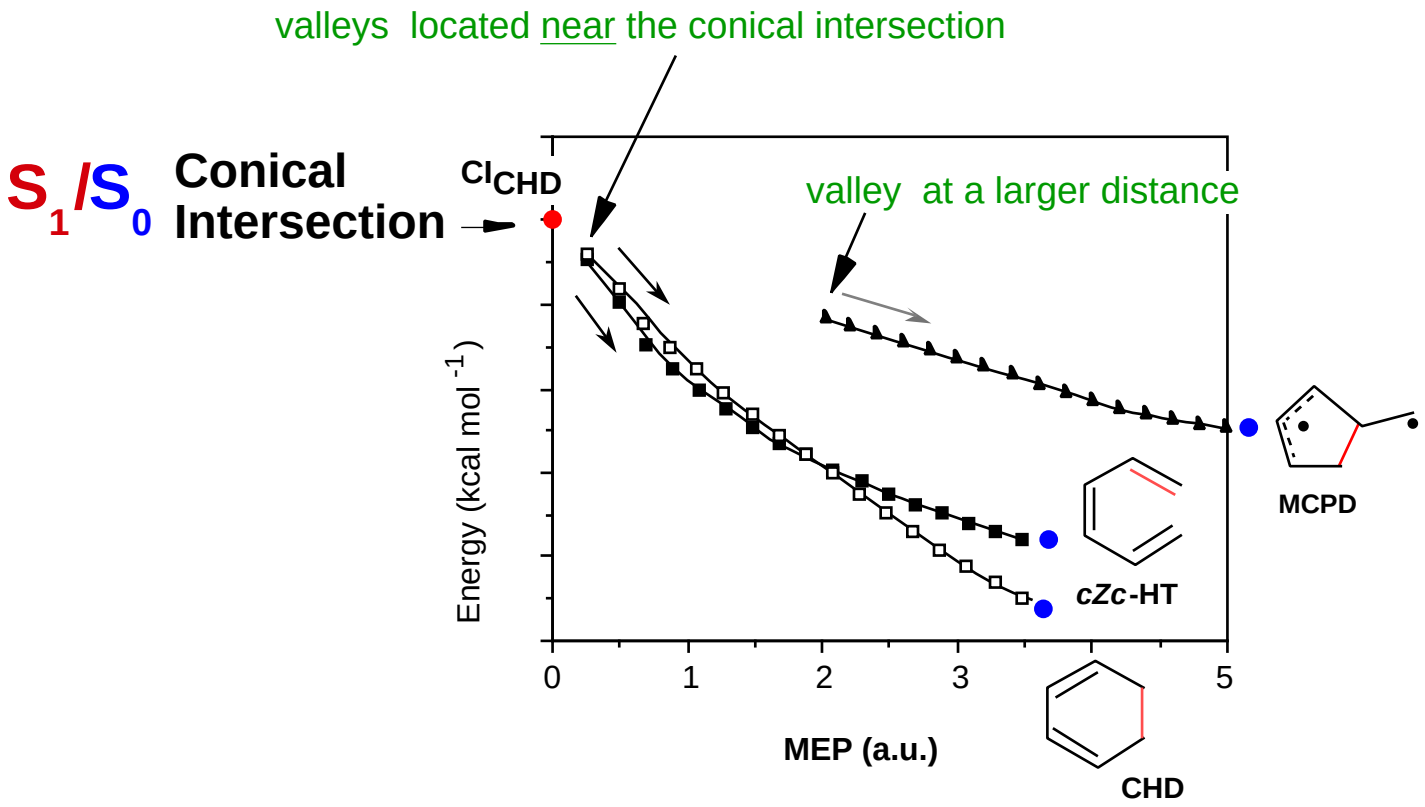
valleys located near the conical intersection
S1/S0 Conical Intersection
CICHD
valley at a larger distance
Energy (kcal mol-1)
MCPD
cZc-HT
0
1
2
3
5
MEP (a.u.)
CHD

Figure 28

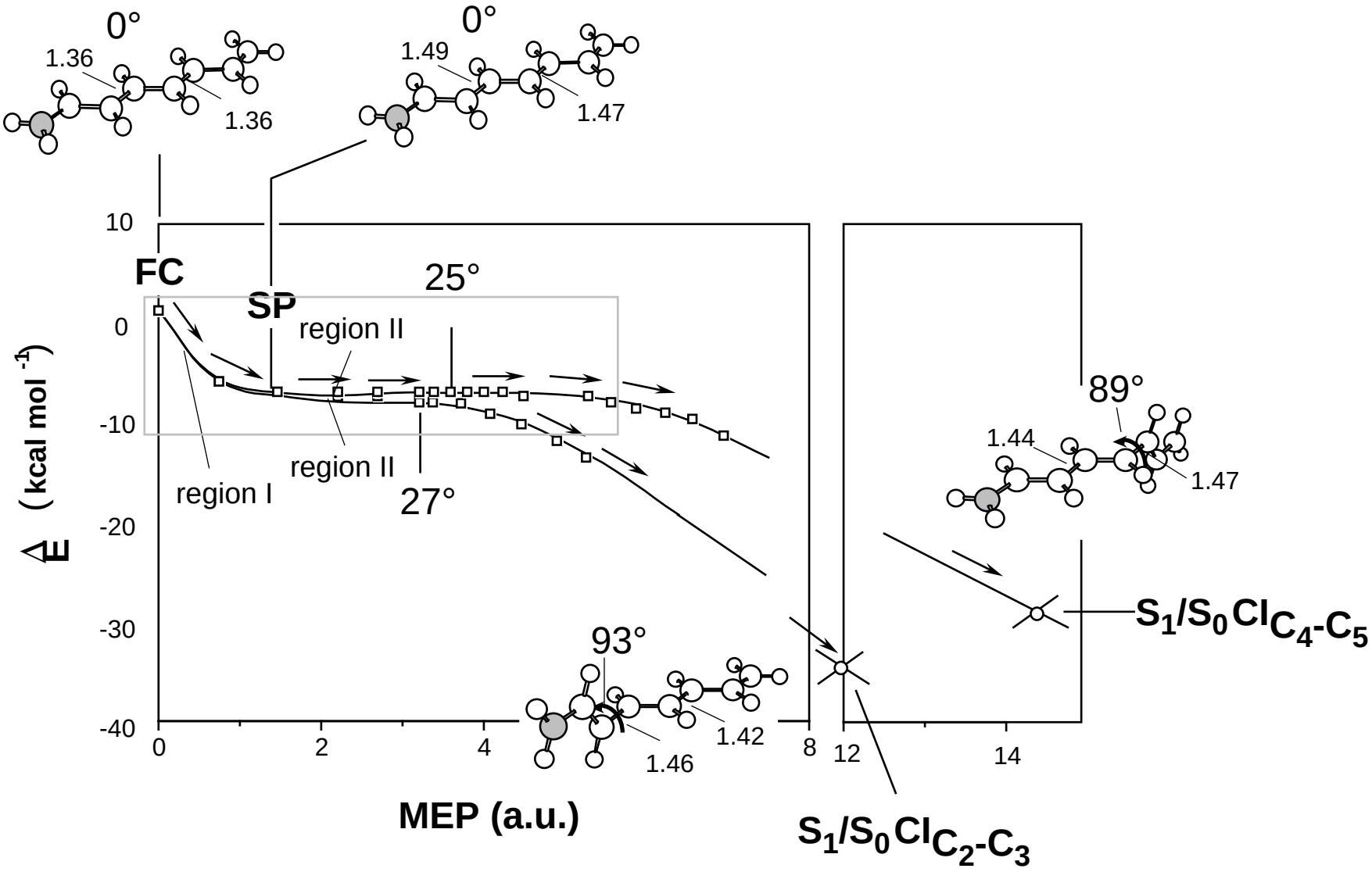
0°
1.36
1.36
0°
1.49
1.47
10
0
-10
-20
-30
-40
FC
SP
25°
region II
region I
region II
27°
ΔE (kcal mol-1)
89°
1.44
1.47
S1/S0 ClC4-C5
93°
1.42
1.46
0
2
4
8
12
14
MEP (a.u.)
S1/S0 ClC2-C3

Figure 29

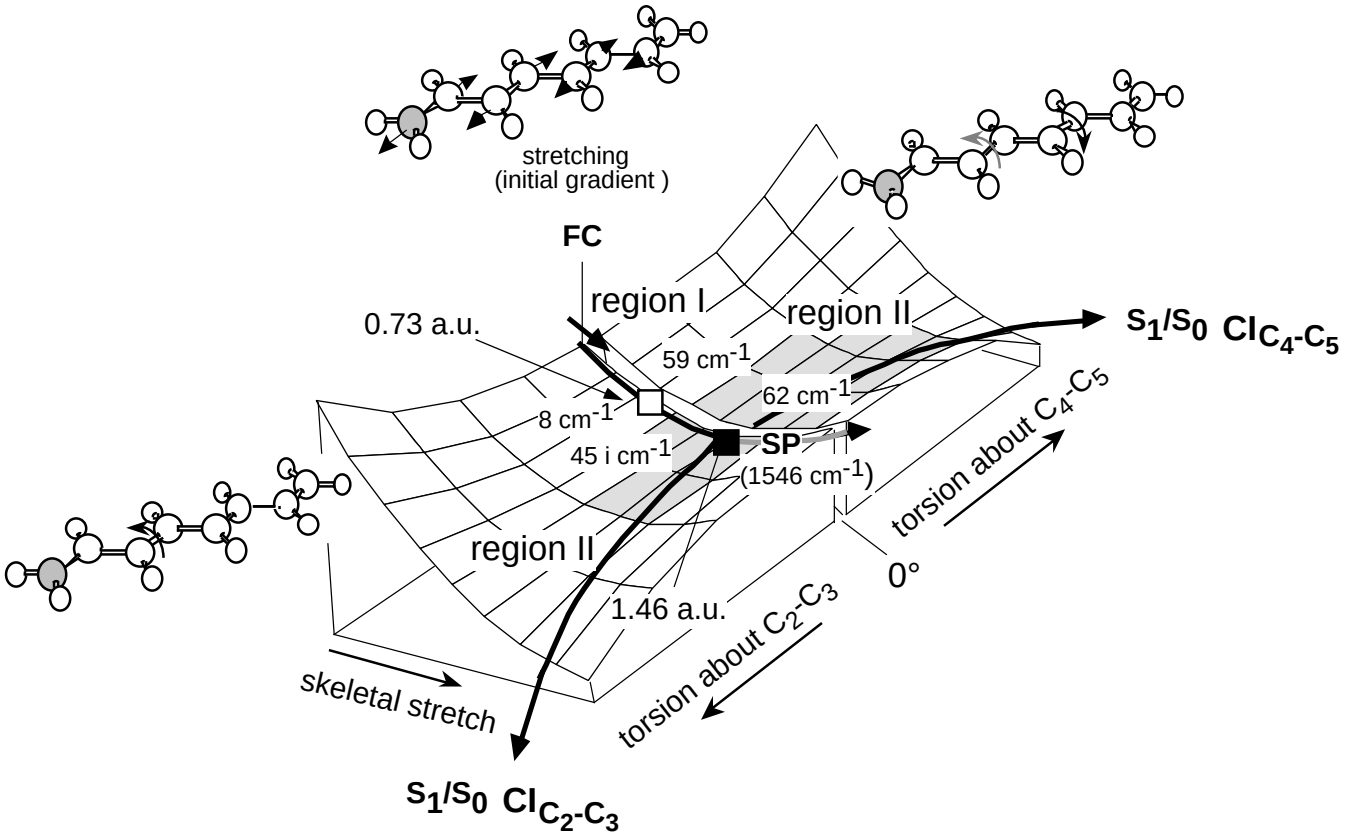
stretching
(initial gradient)
FC
region I
region II
0.73 a.u.
59 cm-1
62 cm-1
8 cm-1
45 i cm-1
SP
(1546 cm-1)
S1/S0 CIC4-C5
torsion about C4-C5
0°
region II
1.46 a.u.
skeletal stretch
torsion about C2-C3
S1/S0 CIC2-C3

Figure 30